Identification of chromate binding mechanisms in a hydrated cement paste

Diss. ETH No. 19 464   **Sabine Melanie Leisinger**

DISS. ETH NO. 19464

IDENTIFICATION OF CHROMATE BINDING MECHANISMS IN A HYDRATED CEMENT PASTE

A dissertation submitted to

ETH ZURICH

for the degree of

Doctor of Sciences

presented by

SABINE MELANIE LEISINGER

Dipl. Geol., University of Bern

born on April 17, 1977

citizen of Steffisburg (BE) and Davos (GR)

accepted on the recommendation of

Prof. Dr. B. Wehrli
Dr. A.C. Johnson
Dr. B. Lothenbach

2011

Für Nico und Carina

Die Arbeit läuft Dir nicht davon, wenn Du Deinem Kind den Regenbogen zeigst - aber der Regenbogen wartet nicht, bis Du mit der Arbeit fertig bist.

<div align="right">Autor unbekannt</div>

Die vergangenen 5 Jahre waren eine spannende Zeit, gespickt mit beruflichen und privaten Herausforderungen. Dank der Unterstützung zahlreicher Personen, konnte diese Arbeit erfolgreich zu Ende geführt werden.

An dieser Stelle möchte ich mich **herzlich bedanken** bei:

Annette Johnson für die Betreuung der Arbeit. Nebst fachlicher Unterstützung genoss ich grosse Freiheiten was die Arbeits- und Zeiteinteilung anbelangte. Dies erleichterte es mir enorm, Familie und Arbeit zu vereinbaren

Bernhard Wehrli für die Leitung der Doktorarbeit und die jeweils wertvollen Feedbacks und Tipps zu den verschiedenen Projekten.

Barbara Lothenbach für die intensive Unterstützung bei den GEMS Modellierungen und bei der Datenevaluation.

Gwenn Le Saout für die Hilfe bei der Auswertung der XRD Daten und seine Ausdauer und Geduld bei der intensiven Forschung an den AFm-Phasen.

Ralf Kägi für die Durchführung der Experimente am ESEM oder TEM. Besonders die Morphologieanalysen waren stets eine willkommene Abwechslung zur sonst zahlenlastigen Arbeit.

Markus Janousch für die Durchführung der Experimente an der Swiss Light Source und die spannenden Diskussionen über Kristallstrukturen.

Hermann Mönch für die verschiedensten Hilfeleistungen im Labor sowie die vielen frischen Köstlichkeiten aus seinem Garten.

Ann-Kathrin Leuz für die fachliche Unterstützung, ihre Hilfeleistungen beim Abschliessen der Doktorarbeit und nicht zuletzt auch für die gemeinsamen gemütlichen Abendessen.

Table of Contents

Zusammenfassung

Die vielseitige Verwendung von Chrom in der metallurgischen und chemischen Industrie führt zu großen Abfallmengen mit erhöhter Chromkonzentration (z.B. Schlacke, Flugasche), die entweder mit Zement verfestigt und in der Umwelt als Deponie deklariert werden oder sie finden Wiederverwendung als Sekundär- oder Ersatzbrennstoffe in der Zementproduktion. Zusätzlich führt der Chromgehalt geogenen Ursprungs aus den Rohmaterialien Kalk und Ton zu erhöhten Chromkonzentration in zementartigen Materialien.

In der Umwelt kommt Chrom in zwei stabilen Oxidationszuständen als Cr(III) und Cr(VI) vor. Cr(III) wird entweder durch Adsorptionsprozesse gebunden oder fällt als schwerlösliches $Cr(OH)_3$ aus und ist deshalb nur in geringen Konzentrationen in Lösung enthalten. Cr(VI) hingegen, ist toxisch, karzinogen und in oxidativem Milieu als Oxyanion (CrO_4^{2-}) sehr gut löslich und kann in die Umwelt ausgewaschen werden.

Vorhersagen zu langzeitlichen Auswaschungen von CrO_4 (Ladungen werden einfachheitshalber weggelassen) sind deshalb notwendig und ist Ziel dieser Arbeit. Aufgrund von thermodynamischen Daten zu CrO_4 bindenden Mineralien und der chemischen Zusammensetzung eines hydratisierten Portlandzements soll die CrO_4-Konzentration im Porenwasser vorhergesagt werden.

Es wird angenommen, dass CrO_4 in einer hydratisierten Zementmatrix als Mischkristall in Ettringit oder Monosulfat eingebaut und dadurch die Löslichkeit von CrO_4 erheblich verringert wird.

Das erste Projekt beinhaltete die Synthese reiner SO_4- und CrO_4-Ettringiten sowie deren Mischphasen ($3CaO \cdot Al_2O_3 \cdot 3Ca[(SO_4)_{1-X},(CrO_4)_X] \cdot 32H_2O$), wobei X den CrO_4-Anteil im Mineral beschreibt. Die Festphasen wurden mit verschiedenen mikroskopischen und spektroskopischen Methoden charakterisiert, und deren Löslichkeitskonstanten wurden bestimmt. Es zeigte sich, dass eine Mischkristallreihe zwischen CrO_4- und SO_4-Ettringit mit einer Mischungslücke für Proben mit einem CrO_4-Anteil ($XCrO_4$) zwischen $0.4 \leq XCrO_4 \leq 0.6$ existiert.

Im zweiten Projekt wurde die Mischkristallreihe zwischen Monosulfat und Monochromat ($3CaO \cdot Al_2O_3 \cdot Ca[(SO_4)_{1-x},(CrO_4)_x] \cdot 12H_2O$) untersucht. Analog zum ersten Projekt wurden

die Festphasen mit verschiedenen mikroskopischen und spektroskopischen Methoden charakterisiert und deren Löslichkeit bestimmt. Die Resultate zeigten, dass von einer Mischungslücke zwischen $0.15 < XCrO_4 < 0.85$ ausgegangen werden muss und dass der Prozess von Wasseraufnahme und -abgabe in AFm-Phasen schnell und reversibel ist.

Die thermodynamischen Daten (aus Projekt 1 und 2) wurden im dritten Projekt für die Vorhersage von CrO_4-Konzentrationen im Porenwasser aus CrO_4-versetzten Zementen angewandt. Gemessene Porenwasserkonzentrationen wurden mit den modellierten Werten verglichen wobei eine mögliche Mischkristallbildung zwischen $CaCrO_4$ und $CaSO_4$ als Degradationsprodukte bei tiefem pH in die Modellierung miteinbezogen wurde. Es zeigte sich, dass Portlandzement bis zu 0.1 mol CrO_4 / kg binden kann, während die CrO_4-Konzentration in Lösung stark anstieg bei Proben versetzt mit >0.1 mol CrO_4 / kg. Das Bindungsverhalten von CrO_4 in Abhängigkeit des pH zeigte auf, dass bei pH <10 um die 95 % vom totalen CrO_4-Gehalt im Zement in Lösung geht, respektive nicht gebunden ist. Die tiefsten CrO_4-Konzentrationen lagen zwischen pH 11 und 13. In diesem Bereich wurde die gelöste CrO_4-Konzentration durch die Bildung von Mischkristallen in Ettringit kontrolliert, wobei die modellierten Werte höher lagen als die gemessenen, was darauf hinweist, dass ein zusätzlicher CrO_4-Bindungsprozess existiert (z.Bsp. Mischphasenbildung mit Hydrotalkit oder Bindung an Calcium-Silikat-Hydrat), welcher nicht berücksichtig wurde.

Die neuen thermodynamischen Daten für CrO_4-Ettringit, Monochromat und $CaCrO_4$ sowie deren Mischkristalle mit SO_4 konnten für die Schätzung von Chromatkonzentrationen im Porenwasser aus einem hydratisierten Portlandzement erfolgreich angewandt werden. Mit der Weiterentwicklung dieser thermodynamischen Daten kann bei der Verfestigung von Abfällen mit Zement oder in der Produktion von zementhaltigen Materialien die langzeitliche CrO_4-Auswaschung genauer

vorhergesagt und berücksichtigt werden.

Abstract

The multifaceted use of chromium in chemical and metallurgical industries leads to large quantities of wastes (e.g. fly ash, slags) that are either stabilized with cement prior to disposal or used in cement production as secondary material or fossil fuel replacement. Additionally, the geogenic chromium source in the raw materials (limestone and clay) leads to enhanced Cr concentrations in cementitous materials.

In the environment chromium is stable as trivalent Cr(III) and hexavalent Cr(VI). In solution Cr(III) concentrations are low due to adsorption and incorporation processes in/on minerals and due to precipitation as $Cr(OH)_3$. Chromium(VI) is toxic, carcinogenic and highly soluble under oxidizing conditions since it is present as oxyanion (CrO_4^{2-}) - thus holding a high potential to be released to the environment.

The assessment of the long-term leaching of chromate is crucial and the aim of this study. Based on the thermodynamic database including chromate binding minerals and the bulk chemical composition of hydrated OPC (ordinary Portland cement) porewater concentrations can be predicted.

In a cementitous system, CrO_4 (charges are omitted for simplicity) is thought to be incorporated as a solid solution with SO_4 in ettringite or monosulfate. The formation of a solid solution could lower the soluble CrO_4 concentrations.

In a first project pure ettringite containing SO_4 or CrO_4 and mixtures thereof ($3CaO \cdot Al_2O_3 \cdot 3Ca[(SO_4)_{1-x},(CrO_4)_x] \cdot 32H_2O$) were synthesized with x representing chromate mole fraction in the mineral. The resulting solids were characterized by different microscopic and spectroscopic techniques and their solubility products were determined. It could be shown that a solid solution between SO_4- and CrO_4-ettringite with a miscibility gap for samples with chromate mole fraction ($XCrO_4$) between $0.4 \leq XCrO_4 \leq 0.6$ exists.

In a second project solid solutions between monosulfate and monochromate were investigated ($3CaO \cdot Al_2O_3 \cdot Ca[(SO_4)_{1-x},(CrO_4)_x] \cdot 12H_2O$). The synthesized solids were characterized by microscopic and spectroscopic techniques. The solubility products of were determined and a solid solution including a large miscibility gap $0.15 < XCrO_4 < 0.85$ was proposed. Furthermore

the process of water uptake and release into AFm phases was observed to be fast and reversible.

The third project addressed the applicability of determined thermodynamic data (in project 1 and 2) to predict CrO_4 porewater concentrations of a hydrated OPC doped with 0.01-0.8 mol/kg $CaCrO_4$. Doped cement pastes were hydrated for 28 days at a temperature of 20 °C. Chromate solubility was determined in cement pore waters and in re-equilibrated suspensions as a function of pH. Measured concentrations were compared to modeled data including potential solid solution formation with the degradation product $CaCrO_4$ - $CaSO_4$ at low pH. The hydrated cement paste was able to bind chromate up to 0.1 mol $CaCrO_4$ / kg cement. Solid-phase and porewater concentrations were directly correlated and the lowest chromate leaching concentrations were found between a pH of 11 and 13. It could be showed that chromate solubility was limited through solid solution formation in ettringite. However predicted chromate concentrations in solution were higher than measured concentrations for all cement samples indicating that an additional CrO_4 binding mechanism takes place (e.g. solid solutions with hydrotalcite or uptake by calcium-silicate-hydrates). Below pH 10, where cement minerals were degraded, 95 % of total CrO_4 in the system was released to solution.

The new thermodynamic data of CrO_4-ettringite, monochromate as well as solid solutions with sulfates have been successfully validated for the prediction of chromium solubility in cement matrices. The further development of thermodynamic data controlling chromate solubility will allow a more accurate prediction. Ultimately better choices in waste management and in the production of cementitous materials are possible by identifying minimal CrO_4 release conditions for long periods of time.

Chapter 1

Introduction

1.1 Chromium in the environment

Chromium is the 21th most frequent element in the earth's crust with an average concentration of around 100 ppm [1]. It is mainly found in ultramafic rocks and in serpentines. It is released by the weathering of ultramafic rocks and serpentinites and chromium-containing rocks including, enstatite $(Mg,Cr)SiO_3$, augite $(Ca,Na)(Mg,Fe,Al,Cr)(Si,Al)_2O_6$, chromite $FeCr_2O_4$, and magnetite $(Fe,Cr)_3O_4$ [2]. Chromium is also present in aerosols emitted through volcanic eruptions [3].

High chromium concentrations are found naturally in crocoite $PbCrO_4$ and the primary ore mineral chromite that is mined for commercial purposes. It is the first mineral that crystallizes during cooling and accumulates at the bottom of the magma body due to its high density (7.14 g/cm^3 at 20 °C) [3]. Chromite is resistant to high temperatures and pressures and because of its' high melting point of around 1900 °C and moderate thermal expansion it became important in industry in the production of refractory components in the bricks and linings of blast furnaces, and in metallurgy for the production of stainless steel, alloys and coatings. Chromium also plays an important role in the chemical industry as a catalyst and in dyeing and leather tanning processes [4]. Chromium is listed under the 10 most frequently mined metals of the world with a mining production of 3'750'000 tones per year [1]. The multifaceted industrial use of chromium leads to large quantities of liquid, solid, and gaseous wastes that are discharged in the environment. This can have significant adverse effects on biology and ecology. Table 1 lists the quite broad concentration ranges of chromium in different kind of wastes [5].

Table 1 Ranges of total chromium content of metallurgical slags, residues from municipal solid waste incineration and from fossil fuel combustion

		Cr (mg/kg)
Metallurgical slags	Blast furnace slag	30
	Steel slag	8000-30'000
	Non-ferrous slag	20-300
municipal solid waste incineration residues	Bottom ash	20-3000
	Fly ash	100-1000
	Air pollution control (APC) residues	70-700
fossil fuel combustion residues	Coal bottom ash	0.2-6000
	Coal fly ash	4-900
	Flue gas desulfurization (FGD) ash	2-200

Chromium is a redox-sensitive element. It can exist in several chemical forms in oxidation states from 0 to VI. In the environment only the trivalent Cr(III) and the hexavalent Cr(VI) are thermodynamically stable states. They exhibit a completely different behavior in terms of charge, physicochemical properties as well as chemical and biochemical reactivity [6]. The cation Cr(III) is the common form of naturally occurring chromium. It is largely immobile because of adsorption on clay minerals, and precipitation as homogeneous (hydr)oxides or with Al(III)/Fe(III)-hydroxides [7]. Formation of Cr(III)-containing organic complexes can increase Cr(III) solubility [6]. Chromium(III) is an essential nutrient that helps the body to remove glucose from blood and supports the regulation of the fat metabolism. The daily requirement for a 60 kg adult is estimated to be 0.5-2 μg of absorbable Cr(III). With an assumed fractional absorption value of 25 % from food this is provided by a daily dietary intake of 2-8 μg of Cr(III). This corresponds to 0.03-0.13 μg of Cr(III) per kg of body weight per day [8, 9]. Lack of chromium can cause diabetes type II and reduced cholesterol levels [4, 10]. The contrary is the case for the hexavalent Cr(VI)

which exerts carcinogenic and mutagentic effects on biological systems. Additionally, skin contact with Cr(VI) compounds can induce skin allergies and dermatitis [11, 12].

Chromium(VI) is highly soluble under oxidizing conditions since it is present as oxyanion (CrO_4^{2-}). Chromate can be sorbed to inorganic surfaces such as goethite, iron and aluminum oxides and other soil colloids with a positively charged surface [13]. The adsorption of Cr(VI) is pH dependent and decreases with increasing pH. Cr(VI) can be reduced to Cr(III) by organic matter or reduced inorganic species such as Fe(II) or S(-II). The oxidation of Cr(III) to Cr(VI) is observed within ultramafic- and serpentinite-derived soils and sediments. Birnessite, a Mn(IV/III)-oxide mineral, commonly forms surface coatings on weathered mineral grains in ultramafic rocks and serpentinites. Dissolved Cr(III) ions are transferred as soluble complexes to the surface of birnessite where adsorbed Cr(III) is oxidized to Cr(VI) and the Mn(IV/III)-oxide is reduced to Mn(II). [14] The Cr(VI)-oxidation rate is depended of pH, O_2 concentrations and also influenced by the nature and concentration of reducers, oxidation mediators and complexing agents. However, most elevated Cr(VI) concentrations occurring in soils and waters have anthropogenic sources [6].

Average chromium concentrations in rainwater is in the range of 0.2-1 g/l. Natural chromium concentrations in seawater lie at 0.04-0.5 µg/l. Rivers and lakes are usually limited to 0.03-5.2 µg/l, Surface waters affected by industrial activity can have higher chromium concentrations. Groundwater has generally low chromium concentrations (<1 µg/l). Naturally higher concentrations can be found in spring waters from ultramafic rocks for example in the coast ranges of California with Cr(VI) concentrations between 12-22 µg/l [2, 6]. The World Health Organization sets the limit for chromium concentrations in drinking water to 50 µg/l for Cr(III) and 0.05 µg/l for Cr(VI). The chromium concentrations in polluted areas caused by discharge of waste water can be much higher [3]. With the increasing contamination of the natural environment in

some part of the world, the problem of heavy metal immobilization generally and Cr(VI) specifically becomes more and more significant.

1.2   Chromium in cement and concrete production

In recent years the cement industry has made significant changes in cement production in terms of the improved of mechanical properties as well as increased sustainability in the production process. Since the middle of the 20th century significant quantities of industrial wastes including fly ash and different slags have been used as cement additives to lower the consumption of raw materials and to reduce CO_2 emissions [15]. Fossil fuels have been partially replaced with used tyres, sewage sludges, oil residues and matured timber in cement kilns. In Switzerland the amounts of wastes that are incinerated in cement plants: has increased from 570'000 t in 1990 to 1'462'000 t per year in 2002 [16]. Chromium, as well as other heavy metal concentrations, is increased in cement-based materials by recycling wastes as alternative raw material and fuel. The chromium contents in clinker produced in Switzerland is restricted to a concentration of maximum 150 ppm [16].

Waste additives are not the only source of chromium in cement. The main natural sources of chromium in ordinary portland cement (OPC) are limestone, sand and, in particular clay. As the clinkers are burnt at 1450 °C under oxidizing conditions, Cr(III) can be oxidized to Cr(VI). Cement with high chromium and especially Cr(VI) content may cause contact dermatitis to construction workers. Itching, redness and /or an eczema-like rash on the skin can be observed. Therefore the EU-legislation lowered the maximum allowed Cr(VI) content in cement from 20 ppm to 2 ppm. The cement industry solved this problem by adding chromate reducing agents, like iron(II) sulfate, to modern cements which efficiently reduces the soluble chromate content within short time [17].

1.3   Chromium in waste management

The use of cement to stabilize hazardous wastes prior to disposal is common worldwide and known as *solidification/stabilization* (S/S) technique. The cementitious matrix acts as both a physical barrier to water and subsequent leaching (*solidification*) and as geochemical barrier by lowering solubility and binding metallic and metalloid species to cement minerals (*stabiliziation*). The potential risk of toxic substances and high heavy metal concentrations that could be released to the environment can be greatly reduced. In the long-term, however, as the cementitious matrix weathers, contaminant species may be released [18, 19]. In the 1990's the importance of understanding heavy metal binding mechanisms in the cementitious matrix was recognized and this led to an increase in research activity [19]. A wide range of leaching experiments have been carried out on ground hydrated cement pastes doped with metal ions, on cement stabilized wastes and on cements and mortars containing elevated metal concentrations derived from wastes [20-23]. Apart from the difficulty of comparing results of leaching experiments due to the variable parameters defining these experiments (e.g. type of cement, hydration time, water : solid ratio, time for the leaching process) three basic binding mechanisms that contribute to the immobilization potential for toxic species could be discerned: precipitation, adsorption to the surfaces of minerals either by specific binding or electrostatically by ion exchange, and incorporation in cement hydrate minerals to form solubility-limiting phases [19, 20, 24].

1.4   Cement minerals present for chromium binding

A hydrated OPC consists mainly of calcium silicate hydrates (C-S-H), portlandite, ettringite and AFm-phases (see Table 2). These minerals make up

about 90 weight % in a hydrated OPC cement paste [25]. C-S-H, ettringite and AFm-phases are considered to play the most important role in heavy metal binding partly because of its structures and partly because of its abundance (e.g. [26-28]).

Ettringite is composed of main columns of $Al(OH)_6$ octahedra alternating with triangular groups of edge-sharing CaO_8 polyhedra in hexagonal array. In the inter channels water and SO_4^{2-} ions are present and balance the charge [29]. Several substituted ettringite phases have been synthesized for a variety of anions (e.g. CrO_4^{2-}, SeO_4^{2-}, CO_3^{2-}, BO_3^{3-}) and aluminum(III) was successfully was successfully substituted by Fe and Cr [30-33].

Table 2 General composition of a hydrated OPC [29].

		composition	weight %
calcium-aluminum-silicate	C-S-H	$1.7CaO \bullet SiO_2 \bullet 1.4H_2O$ (Ca:Si ratio varies)	40-60
portlandite		$Ca(OH)_2$	15-25
Aluminum-ferrite-tri (AFt)	ettringite	$3CaO \bullet (Al,Fe)_2O_3 \bullet 3CaSO_4 \bullet 32H_2O$	10-20
Aluminum-ferrite- mono (AFm)	monosulfate	$3CaO \bullet (Al,Fe)_2O_3 \bullet CaSO_4 \bullet 12H_2O$	
	monocarbonate	$3CaO \bullet (Al,Fe)_2O_3 \bullet CaCO_3 \bullet 10H_2O$	
	hydrocalumite	$4CaO \bullet Al_2O_3 \bullet 13-19H_2O$	
pore solution			10-20
minor components (calcite, Fe and Mg hydration products, unreacted phases)			0-5

AFm phases are based on a layered structure with alternating main layers composed of $[Ca_2Al(OH)_6]^+$ and inter layers where water molecules and anions balance the charge [29, 34]. The amount of water present in the inter layer is

extremely sensitive to the relative humidity. Monosulfate $3CaO \cdot Al_2O_3 \cdot CaSO_4 \cdot nH_2O$ contains one mole sulfate and a variable amount of water in the inter layer (n=16, 14, 12, 10.5, 10, 9 and 6) [35, 36]. Since the inter layer molecules are loosely bound to the main layers through hydrogen bonding, they are easily exchangeable and many isomorphic substitutions for SO_4-anions are known (e.g. OH^-, CO_3^{2-}, NO_3^- and Cl^-) [37]. Next to fully substituted AFt- and AFm-phases, solid solution formation is also observed [37-39].

While Cr(III) is known to substitute Al(III) in calcium aluminate hydrates, as well as in ettringite and monosulfate [40, 41], binding mechanism for the mobile CrO_4 is more complicated. Adsorption is low in the highly alkaline environment. Results from leaching experiments have shown that CrO_4 leaching concentrations are related to the occurence of ettringite and monosulfate [22, 39, 42]. Indeed, CrO_4-enriched ettringites and pure monochromate have been identified in a chromate containing cement [43]. Zhang investigated CrO_4 incorporation into hydrocalumite. At low concentrations (<10 ppm) of Cr added to hydrocalumite their concentrations are reduced to close to or below detection. This observation suggests that there are no structural constraints on the incorporation of the anions by OH-AFm. At higher concentrations Cr incorporation into hydrocalumite produces solid solutions that then control their solution concentration. The uptake capacity of OH-AFm in Cr-rich solutions showed that CrO_4 concentrations in solution could be drastically lowered by solid solution formation.

The identical charge, similar structure and comparable radii of SO_4^{2-} and CrO_4^{2-} ions (2.3 Å and 2.4 Å respectively) suggests that chromate should readily substitute in the crystal structure of ettringite and monosulfate to form solid solutions [39, 44]. Characterization of the solid solutions by XRD and SEM has been performed [45]. Perkins [46] connected results of the solid characterization with analysis of the solution. A continuous solid solution series between the

pure SO_4 and CrO_4 end members was suggested, even though difficulties in the calculations of the solubility products occurred.

C-S-H, the principal hydration product, is an amorphous or micro-crystalline calcium siliate hydrate. It has a variable composition with a Ca/Si ratio in the range of 0.8 to 2.0. Its morphology depends on the Ca/Si ratio, the setting conditions and water/solid ratio [29]. C-S-H has a large sorption potential due to its high specific surface area and the range of sorption sites. It has been shown that cations [47, 48] as well as anions can be taken up depending on the Ca/Si ratio causing either a positive or a negative surface charge. Sulfate sorption increases with the Ca/Si ratio of the C-S-H [49]. Since CrO_4^{2-} is comparable to SO_4^{2-} concerning the charge, the tetrahedral geometry and the ionic radius, CrO_4^{2-} sorption on C-S-H especially at high CrO_4^{2-} concentrations might be possible.

1.5   Scope of this study

Until now it has not possible to predict the solubility of chromate in hydrated cement pastes. The aim of the study is to determine the binding processes controlling the solubility of chromate in cementitious matrices and to obtain thermodynamic data in order to be able to model porewater concentrations from solid phase composition. Based on current research results the following hypothesis can be formulated:

The binding mechanism that controls chromate solubility in hydrated OPC porewater is solid solution formation in AFt and/or AFm phases.

Project 1

The solubility of pure CrO_4-ettringite and SO_4-ettingite has been published [31, 50]. However, since there is no thermodynamic solubility data to describe mixed systems, solid solutions between CrO_4- and SO_4-ettringite were investigated. The following questions were addressed:

- Does a solid solution series between CrO_4- and SO_4-ettringite exist?
- What are the solubility products of such solid solution phases?
- How can the solid-solution aqueous-solution system (SSAS) best be described in terms of ideality or non-ideality?

Solid solutions of CrO_4- and SO_4-ettringite were synthesized with varying chromate mole fractions of 0, 0.1, 0.2, 0.4, 0.6, 0.8, 1. Solids were characterized by scanning electron microscopy (SEM), thermogravimetric analysis (TGA), X-ray diffraction (XRD) and inductive coupled plasma optical emission spectroscopy (ICP-OES). Determined solubilities of solid solutions were illustrated as total solubility product in a Lippmann diagram. Resulting thermodynamic data of the solid solution series were added to the thermodynamic data base and were used for the modeling chromate porewater concentrations.

Project 2

Monosulfate is regarded to be the second important phase for chromate binding in a hydrated cement paste. The solid solution system between monosulfate and monochromate is investigated and these questions were asked:

- Is there a solid solution series between between monochromate and monosulfate?
- What are the solubility products of synthesized solid solution phases?

• Is there a continuous solid solution series?

Solid solutions with chromate mole fractions of 0, 0.1, 0.2, 0.4, 0.6, 0.8, 1 were synthesized. Solids were again characterized by SEM, TGA, XRD and ICP-OES. The solubility products were determined and implemented in the thermodynamic database.

Project 3

This project addresses the applicability of the thermodynamic data (from project 1 and 2) to hydrated OPC systems doped with Cr(VI). It also explores potential solid solution formation with the degradation product $CaSO_4$ - $CaCrO_4$ at low pH.

• What is the chromate solubility determining phase and what are the chromate binding mechanisms in a hydrated OPC respectively?

• What are the changes in chromate porewater concentrations if the pH varies?

Different sets of experiments on hydrated cement pastes doped with varying chromate concentrations ranging from 0 up to 0.8 mol $CaCrO_4$/kg were carried out. In a first series chromate doped samples were hydrated for 28 days and ion porewater concentrations were measured. Additionally, chromate solubility was determined in re-equilibrated suspensions using ground samples as a function of pH. These pH-dependent experiments showed that in the pH range between 8 and 10 solid solution formations between $CaCrO_4$ and $CaSO_4$ could be the chromate solubility limiting phase. Thus, solid solutions with varying chromate mole fraction were synthesized and characterized according to the solid solutions of the first and second project. Solubility products of the solid solutions were determined and added to the thermodynamic database.

Experimentally derived chromate concentrations in solution were compared to modeled data. Based on the thermodynamic stabilities of the three different chromate solid solution systems, chromate binding mechanisms in a hydrated OPC were determined and porewater concentrations were calculated.

The combination of the new thermodynamic data of chromate containing cement minerals with solid-solution modeling has been validated successfully for the prediction of chromium solubilities in cement matrices. This way lead to better choices in waste management by identifying minimal CrO_4 release conditions for long periods of time. Thermodynamic calculations are as well applicable in the field of new construction products (cement-based materials) since wastes are increasingly used in their production process.

1.6   References

[1] Emsley, J., Chromium. Nature's Building Blocks: an A-Z Guide to the Elements. . 2001, Oxford, England: Oxford University Press. 495-498.

[2] Oze, C., et al., Chromium geochemistry in serpentinized ultramafic rocks and serpentine soils from the Franciscan Complex of California. American Journal o Science, 2004. **304**: p. 67-101.

[3] Nriagu, J.O. and E. Nieboer, eds. Chromium in the natural and human environments. 1 ed. Advances in Environmental Science and Technology, ed. J.O. Nriagu. Vol. 20. 1988, John Wiley & Sons, Inc. 571.

[4] Sueker, J.K., D.R.D.M. Ph, and L.M. Brian, Chromium, in Environmental Forensics. 2005, Academic Press: Burlington. p. 81-95.

[5] Cornelis, G., et al., Leaching mechanisms of oxyanionic metalloid and metal species in alkaline solid wastes: A review. Applied Geochemistry, 2008. **23**(5): p. 955-976.

[6] Kotas, J. and Z. Stasicka, Chromium occurrence in the environment and methods of its speciation. Environmental Pollution, 2000. **107**(3): p. 263-283.

[7] Sparks, D.L., ed. Sorption, Metals. Encyclopedia of Soils in the environment, ed. D. Hillel. 2005, Elsevier Ltd. 2200.

[8] Trumbo, P., et al., Dietary Reference Intakes: Vitamin A, Vitamin K, Arsenic, Boron, Chromium, Copper, Iodine, Iron, Manganese, Molybdenum, Nickel, Silicon, Vanadium, and Zinc. Journal of the American Dietetic Association, 2001. **101**(3): p. 294-301.

[9] Fawell, J.K., U. Lund, and B. Mintz, Chromium in Drinking-water: Background document for development of WHO Guidelines for drinking-water quality. 1996, WHO: Geneva. p. 1-8.

[10] Langard, S. and M. Costa, eds. Chromium. Handbook on the Toxicology of Metals, ed. G. Nordberg, et al. 2007, Academic Press, Inc. 1024.

[11] Shelnutt, S.R. and P. Goad, Dermatological Toxicity of hexavalent chromium. Critical Review in Toxicology, 2007. **37**: p. 375-387.

[12] Wise, S.S., A.L. Holmes, and J.P. Wise Sr, Particulate and soluble hexavalent chromium are cytotoxic and genotoxic to human lung epithelial cells. Mutation Research/Genetic Toxicology and Environmental Mutagenesis, 2006. **610**(1-2): p. 2-7.

[13] Scheffer, F. and P. Schachtschabel, Lehrbuch der Bodenkunde. 15 ed. 2002, Heidelberg: Spektrum Akademischer Verlag GmbH. 593.

[14] Johnson, A. and A.G. Xyla, The oxidation of chromium(III) to chromium(VI) on the surface of manganite(y-MnOOH). Geochem. Cosmochim. Acta, 1991. **55**: p. 2861-2866.

[15] Malhotra, V.M., ed. Fly ash, silica fume, slag and other mineral by-products in concrete. 1983, American Concrete Society: Detroit.

[16] Richtlinie: Ensorgung von Abfällen in Zementwerken, W.u.L.B. Bundesamt für Umwelt, Editor. 2005, Bundesamt für Umwelt, Wald und Landschaft (BUWAL). p. 15.

[17] Opinion on risks to health from chromium VI in cement, E.c.d.-g.h.a.c. protection, Editor. 2002.

[18] Cocke, D., et al., Binding chemistry and leaching mechanisms in solidified hazardous wastes. Journal of Hazardous Materials, 1991. **28**(1-2): p. 193-194.

[19] Spence, R.D., Chemistry and microstructure of solidified waste forms. 1993, Boca Raton, Florida: Lewis Publishers. 276.

[20] Johnson, A., Cement stabilization of heavy-metal-containing wastes, in Energy, waste and the environment: a geochemical perspecitve, R. Grieré and P. Stille, Editors. 2004, The Geological Society: London. p. 595-606.

[21] van der Sloot, H.A., Leaching behaviour of waste and stabilized waste materials; characterization for environmental assessment purposes. Waste Management & Research, 1990. **8**(3): p. 215-228.

[22] van der Sloot, H.A., Characterization of the leaching behaviour of concrete mortars and of cement-stabilized wastes with different waste loading for long term environmental assessment. Waste Management, 2002. **22**(2): p. 181-186.

[23] van der Sloot, H.A., R.N.J. Comans, and O. Hjelmar, Similarities in the leaching behaviour of trace contaminants from waste, stabilized waste, construction materials and soils. Science of The Total Environment, 1996. **178**(1-3): p. 111-126.

[24] Glasser, F.P., Fundamental aspects of cement solidification and stabilisation. Journal of Hazardous Materials, 1997. **52**(2-3): p. 151-170.

[25] Hewlett, P.C., ed. Lea's chemistry of cement and concrete. fourth ed. 1998, Elsevier Butterworth Heinemann: Burlington, USA. 1057.

[26] Chrysochoou, M. and D. Dermatas, Evaluation of ettringite and hydrocalumite formation for heavy metal immobilization: Literature review and experimental study. Journal of Hazardous Materials, 2006. **136**(1): p. 20-33.

[27] Klemm, W.A., Ettringite and oxyanion-substituted ettringites - their characterization and applications in the fixation of heavy metals: a synthesis of the literature. 1998, Portland Cement Association Skokie, Illinois (USA). p. 68.

[28] Gougar, M.L.D., B.E. Scheetz, and D.M. Roy, Ettringite and C---S---H Portland cement phases for waste ion immobilization: A review. Waste Management, 1996. **16**(4): p. 295-303.

[29] Taylor, H.F.W., Cement Chemistry. Vol. 1. 1997, London: Thomas Telford Publishing. 459.

[30] Baur, I. and C.A. Johnson, The solubility of selenate-AFt ($3CaO \cdot Al_2O_3 \cdot 3CaSeO_4 \cdot 37.5H_2O$) and selenate-AFm

(3CaO·Al2O3·CaSeO4·xH2O) Cement and Concrete Research, 2003. **33**(11): p. 1741-1748.

[31] Perkins, R.B. and C.D. Palmer, Solubility of ettringite $(Ca_6[Al(OH)_6]_2(SO_4)_3 \cdot 26H_2O)$ at 5-75°C. Geochimica et Cosmochimica Acta, 1999. **63**(13-14): p. 1969-1980.

[32] McCarthy, G., D. Hassett, and J. Bender, Synthesis, crystal chemistry and stability of ettringite, a material with potential applications in hazardous waste immobilization. Mat. Res. Soc. Symp. Proc., 1992. **245**: p. 129-140.

[33] Möschner, G., et al., Solubility of Fe-ettringite $Ca_6[Fe(OH)_6]_2(SO_4)_3 \cdot 26H_2O$. Geochimica et Cosmochimica Acta, 2008. **72**(1): p. 1-18.

[34] Hartman, M.R. and R. Berliner, Investigation of the structure of ettringite by time-of-flight neutron powder diffraction techniques. Cement and Concrete Research, 2006. **36**(2): p. 364-370.

[35] Poellmann, H., Die Kristallchemie der Neubildungen bei Einwirkung von Schadstoffen auf hydraulische Bindemittel, in Naturwissenschaftliche Fakultät. 1984, Friedrich-Alexander-Universität: Erlangen-Nürnberg. p. 332.

[36] Dosch, W. and H. Zur Strassen, Untersuchungen in den Alkali enthaltenen Systemen, gebildet aus den Komponenten CaO, Al2O3, Fe2O3, SiO2, SO3, Na2O, K2O H2O. 1962, University of Mainz: Mainz (GER).

[37] Matschei, T., B. Lothenbach, and F.P. Glasser, The AFm phase in Portland cement. Cement and Concrete Research, 2007. **37**(2): p. 118-130.

[38] Möschner, G., et al., Solid solution between Al-ettringite and Fe-ettringite $(Ca_6[Al_1 - xFe_x(OH)_6]_2(SO_4)_3 \cdot 26H_2O)$. Cement and Concrete Research, 2009. **39**(6): p. 482-489.

[39] Zhang, M., Incorporation of oxyanionic B, Cr, Mo and Se into hydrocalumite and ettringite: application to cementitous systems, in Earth Science. 2000, University of Waterloo Ontario, Canada. p. 172.

[40] Evans, N.D.M., Binding mechanisms of radionuclides to cement. Cement and Concrete Research, 2008. **38**(4): p. 543-553.

[41] Kindness, A., A. Macias, and F.P. Glasser, Immobilization of chromium in cement matrices. Waste Management, 1994. **14**(1): p. 3-11.

[42] Park, J.-Y., W.-H. Kang, and I. Hwang, Hexavalent chromium uptake and release in cement pastes. Environmental Engineering Science, 2005. **23**(1): p. 133-140.

[43] Palmer, C.D., Precipitates in a Cr(VI)-contaminated concrete. Environ. Sci. Technol., 2000. **34**(19): p. 4185-4192.

[44] Zhang, M. and E.J. Reardon, Chromate and selenate hydrocalumite solid solutions and their application in waste treatment. Science in China, Ser.C Life Science, 2004. **1**: p. 165-173.

[45] Poellmann, H., et al., Solid solution of ettringites : Part II: Incorporation of $B(OH)_4^-$ and CrO_4^{2-} in $3CaO \cdot Al_2O_3 \cdot 3CaSO_4 \cdot 32H_2O$. Cement and Concrete Research, 1993. **23**(2): p. 422-430.

[46] Perkins, R.B., The solubility and thermodynamic properties of ettringite, its chromium analogs and calcium aluminum monochromate, in Environmental science and resources. 2000, Portland State University: Portland, USA. p. 200.

[47] Ziegler, F., R. Giere, and C.A. Johnson, The sorption mechanisms of zinc to calcium silicate hydrate: Sorption studies and microscopic investigations. Environ. Sci. Technol., 2001. **35**: p. 4556-4561.

[48] Ziegler, F., et al., Sorption mechanisms of zinc to calcium silicate hydrate: X-ray absorption fine structure (XAFS) investigation. Environmental Science & Technology, 2001. **35**(7): p. 1550-1555.

[49] Barbarulo, R., H. Peycelon, and S. Prene, Experimental study and modelling of sulfate sorption on calcium silicate hydrates. Ann. Chim. Sci. Mat. , 2003. **28**((Suppl. 1)): p. 5-10.

[50] Perkins, R.B. and C.D. Palmer, Solubility of $Ca_6[Al(OH)_6]_2(CrO_4)_3 \cdot 26H_2O$, the chromate analog of ettringite; 5-75°C. Applied Geochemistry, 2000. **15**(8): p. 1203-1218.

Chapter 2

Solid solutions between CrO_4- and SO_4-ettringite $Ca_6(Al(OH)_6)_2[(CrO_4)_x(SO_4)_{1-x}]_3*26\ H_2O$
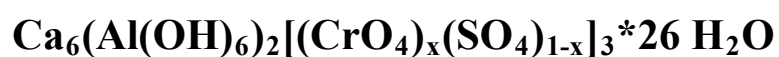
Sabine M. Leisinger, Barbara Lothenbach, Gwenn Le Saout, Ralf Kägi, Bernhard Wehrli, C. Annette Johnson

Abstract

Chromate is a toxic contaminant of potential concern as it is quite soluble in the alkaline pH range and could be released to the environment. In cementitous systems, CrO_4^{2-} is thought to be incorporated as a solid solution with SO_4^{2-} in ettringite. The formation of a solid solution (SS) could lower the soluble CrO_4^{2-} concentrations.

Ettringite containing SO_4^{2-} or CrO_4^{2-} and mixtures thereof have been synthesized. The resulting solids and their solubility after an equilibration time of 3 months have been characterized. For CrO_4-ettringite at 25 °C a solubility product log K_{S0} of -40.2 ± 0.4 was calculated:

$$\log K_{CrO_4-ettringite} = 6\log\{Ca^{2+}\} + 2\log\{Al(OH)_4^-\} + 3\log\{CrO_4^{2-}\} + 4\log\{OH^-\} + 26\log\{H_2O\}$$

X-ray diffraction and the analysis of the solution indicated the formation of a regular solid solution between SO_4- and CrO_4-ettringite with a miscibility gap between $0.4 \leq XCrO_4 \leq 0.6$. The miscibility gap of the SO_4- and CrO_4-ettringite solid solution could be reproduced with a dimensionless Guggenheim fitting parameter (a_0) of 2.03.

The presence of a solid solution between SO_4- and CrO_4-ettringite results in a stabilization of the solids compared to the pure ettringites and thus in an increased uptake of CrO_4^{2-} in cementitious systems.

2.1　Introduction

Cementituous materials are considered to be suitable for the containment of inorganic contaminants for both nuclear and non-nuclear applications because they act as physical and geochemical barriers to leaching *[1-4]*. Understanding the binding mechanisms of metal(loid) species to cement hydration phases *[3, 5, 6]* is crucial for the development of thermodynamic models that are used for the prediction of long-term leaching scenarios in the development and design of repositories.

Chromate is of particular interest in non-nuclear applications because it is a soluble anion present in cement clinkers and it is a common contaminant in wastes that is prone to leaching and, in addition, poses a health risk to workers (e.g. *[7-10]*. Chromium, mostly in the form of the trivalent Cr(III) cation, is present in the raw materials, such as limestone and clay, used for clinker manufacture. OPC clinker contains around 60 ppm chromium from geogenic sources *[11]*. The high temperatures (1450°C) encountered during clinker manufacture cause Cr(III) to be oxidized to Cr(VI) *[12]*. Chromate in the clinker or in added wastes can be released during hydration and then probably be incorporated into hydration products, resulting in lower solubility. Leaching tests on hydrated cement mortars support the hypothesis that chromate is bound in hydration products *[13, 14]*.

Ettringite-like minerals are important potential candidates for the immobilization of contaminant ions because substitutions are possible and because of its ease of formation from a wide range of starting materials. Indeed, it is generally accepted that the hydration product ettringite is a potential candidate for the incorporation of CrO_4^{2-} *[15]*. In cement nomenclature ettringite belongs to the group of AFt-phases (Al_2O_3-Fe_2O_3-tri) with the general constitutional formula $[Ca_3(Al,Fe)(OH)_6 \bullet 12H_2O]_2 \bullet A_3 \bullet xH_2O$ where x is, normally at least, ≤ 2 and A represents one formula unit of a doubly charged, or two formula units of a singly

charged anion *[16]*. Substituted ettringite phases have been synthesized for a variety of anions (e.g. CO_3^{2-}, CrO_4^{2-}, SeO_4^{2-}). Aluminum(III) can be substituted by Fe^{3+} and Cr^{3+} *[15-17]*. Perkins and Palmer [17] have determined the solubility product (Ksp) of chromate ettringite as logKsp = -41.46 +/- 0.3 based on the following reaction:
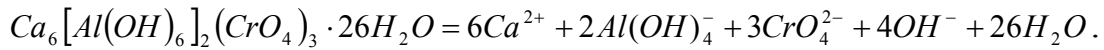
$$Ca_6\left[Al(OH)_6\right]_2\left(CrO_4\right)_3 \cdot 26H_2O = 6Ca^{2+} + 2Al(OH)_4^- + 3CrO_4^{2-} + 4OH^- + 26H_2O.$$

The identical charge, similar structure and comparable radii of SO_4^{2-} and CrO_4^{2-} ions suggest that chromate should readily substitute in the crystal structure of ettringite to form solid solutions *[18]*. Indeed Palmer *[19]* observed Cr(VI)-enriched ettringite in Cr(VI)-contaminated concrete. The rare investigations on the CrO_4-/SO_4-ettringite solid solution series have focused on solid composition analysis under different synthesis conditions, concluding that crystal morphology is dependent on the synthesis method *[20]*.

To date there are no published thermodynamic data for CrO_4-/SO_4-ettringite solid solutions. Solid solutions could stabilize CrO_4 by lowering the solubility product compared to the system without solid solution. The aim of this study is to investigate changes in solubilities and solid-phase characteristics resulting from partial SO_4^{2-} and CrO_4^{2-} substitutions in the ettringite structure. The results of this study will be useful in modeling the potential for ettringite to control CrO_4^{2-} concentrations.

2.2 Experimental Methods

2.2.1 Materials

All chemicals were at least of pro analysis (p.a.) grade. The following substances were used: $CaCrO_4$, $CaCO_3$, $CaSO_4 \cdot 2H_2O$ and Al_2O_3- powder. The following liquids were purchased: KOH solution (1M, Titrisol), nitric acid (HNO_3) Suprapur 65%, ICP-OES multi-elements standard solution IV and SO_4-anion standard solution.

To prevent possible CO_2 contamination, all handling of material, the sampling, and the pH measurements were carried out in a glovebox (Mecaplex) equipped with a CO_2 scrubber (pCO_2 < 1 ppm, DMP Ltd., Switzerland). Ultrapure water (resistivity >18MΩ.cm) was used for the preparation of solutions and rinsing processes. All polyethylene bottles, tubes and glassware were leached in acid solutions (0.3 M HCl, Merck) for at least 24 h and rinsed with ultrapure water three times.

2.2.2 Mineral synthesis and experiments

Solid solution phases were synthesized according to the following precipitation reaction:

$$(1) \quad \begin{array}{l} 6Ca^{2+} + 2Al(OH)_4^- + 3xCrO_4^{2-} + (3-3x)SO_4^{2-} + 4OH^- + 26H_2O \\ = Ca_6[Al(OH)_6]_2[(CrO_4)_x(SO_4)_{1-x}]_3 * 26H_2O \end{array}$$
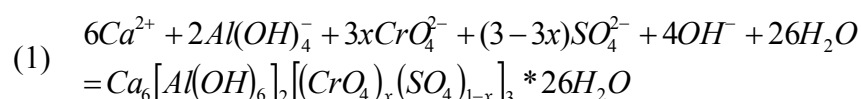
Tricalcium aluminate clinker (C_3A) was prepared by burning $CaCO_3$ and Al_2O_3 at 1400 °C for 24 hours *[21]*. Solid solution phases were synthesized by adding stoichiometric amounts of freshly burned C_3A (2 mmol), $CaCrO_4$ and $CaSO_4 \cdot 2H_2O$ (totally 6 mmol) to ultrapure water (50 ml) to obtain different chromate mole fractions ($XCrO_4$ = [CrO_4^{2-}]/([CrO_4^{2-}]+[SO_4^{2-}])) of 0, 0.1, 0.2, 0.4, 0.5, 0.8 and 1. The liquid/solid ratio was held constant at 20. All mixtures were

equilibrated in sealed HDPE bottles of 50 ml at 25 °C on a rotary shaker at 125 rpm. For each solid solution phase between 8 and 15 samples were synthesized to show the reproducibility. Dissolution and precipitation experiments showed that pure CrO_4- and SO_4-ettringite equilibration time is reached within a couple of days *[17, 22]*. However, for the solid solutions to reach equilibrium a much longer equilibration time is expected according to Perkins *[23]*. In this study an equilibration time of 90 days was used. The samples were then centrifuged for 20 min at 4000 rpm. The supernatant was separated, filtered with 0.45 μm nylon membrane filters (Titan), and acidified with concentrated HNO_3 Suprapur (1:100). All samples were stored at 4 °C. Solid phases were washed with acetone after filtration and stored in desiccators over silica gel and soda lime. The CrO_4-ettringite solubility was determined from precipitation and dissolution experiments with varying pH ranging from 11 to 12 with 0.25 steps using KOH and in a serie without pH adjustment. These experiments were carried out the way described above for the mineral synthesis. Dissolution experiments started as precipitation experiments just with the half water content (only 25 ml). After one month 25 ml water was added and equilibrated for further 2 month.

2.2.3   Characterization of the solid phase

After drying the samples were ground by hand with an agate mortar to <63 μm and analyzed by X-ray diffraction (XRD), environmental scanning electron microscope (ESEM), thermogravimetric analysis (TGA), and inductive coupled plasma optical emission spectroscopy (ICP-OES). XRD analysis was used to determine the purity and crystallinity of the phases using CuKα radiation. Elemental silicon was mixed to the powder samples as internal standard or the determination of the unit cell parameters. Raw data were evaluated by X'Pert

HighScore Plus. The following evaluation steps were carried out: 1) the background was set manually, 2) second a peak search was performed and 3) a profile fitting followed. The indexing of the reflections was done using the McMaille method *[24]*. Unit cell parameters were then refined by a least squares algorithm *[25]*. TGA was carried out on a TGA/SDTA 851 apparatus by Mettler Toledo. The samples (8 - 12 mg) were heated under N_2 over a temperature range of 30 - 980 °C at a rate of 20 °C/min. TGA was carried out to observe mass changes in relation to change in temperature/time. The determined mass losses were used to estimate fractions of the solid that were water or CO_2. Morphology of the samples was controlled by SEM using a Philips ESEM FEG XL 30 in high vacuum mode. Solid stoichiometry was determined using ICP-OES. A solid sample (0.1 g) was dissolved in 500 μl HNO_3 Suprapur in a 50 ml HDPE bottle and filled with ultrapure water to 50 ml. Samples were diluted 1:10 and 1:100 prior to measurement. Multi-element standard solution was used for calibration of Ca, Al and Cr. Anion standard solution was used for the SO_4 calibration.

2.2.4 Characterization of the liquid phase

Part of the liquid phase was used for pH-measurement, which was carried out with a Aquatrode Plus Pt 1000 electrode from Metrohm. Prior to the measurements the pH electrode was calibrated by titration with fresh KOH-solutions (0.001-1 M) to minimize the alkali error. The voltage reading was correlated to the calculated target pH-value of the respective KOH-solution considering ionic strength as well as the measured temperature of the solution. Dissolved concentrations of Ca, Al, Cr and SO_4, were determined by ICP-OES with the same method described for solid phases. Charge balance errors of all samples lay within 1 to 10 %.

2.2.5 Thermodynamic modeling

Aqueous activities, solubility and stability calculations were carried out with the broad-purpose geochemical modeling code GEMS-PSI (Gibbs Energy Minimization Selector). The principle of GEM method is the minimization of the Gibbs energy of a complex chemical system. It computes mass balances, based on equilibrium phase assemblages and speciation in a complex chemical system from its total bulk elemental composition. Chemical interactions involving solids, solid solutions, gas mixture and aqueous electrolyte are considered simultaneously *[26]*. A built-in thermodynamic database *[27]* is provided and with a graphical user interface for easy extension of the thermodynamic database to user-defined "projects" missing data can be added. Initially this database was designed in "log *K* format" for application to codes such as PHREEQC. These codes use law of mass action algorithms at standard conditions (1 bar and 25°C). The log *K* values were converted into standard molar Gibbs energies and merged with *slop98.dat* database (originally developed for the SUPCRT92 code *[28]*) to include it in GEMS *[29]*. For aqueous species this dataset is based on the Helgeson-Kirkham-Flowers (HKF) equation of state which is used to calculated temperature and pressure corrections up to 1000°C and 5kbar *[30, 31]*. The thermodynamic data used are compiled in Supporting Information.

Activity coefficients of aqueous species y_i were computed with the built-in expanded extended Debye-Hückel equation in Truesdell-Jones form (equation 2).

$$(2) \quad \log \gamma_i = \frac{-A_y z_i^2 \sqrt{I}}{1 + B_y a_i \sqrt{I}} + b_y I$$

where z_i denotes the charge of species i, I the effective molal ionic strength, a_i is a parameter   dependent on the size of ion i, b_y is a semi-empirical parameter (˜

0.64 at 25°C), and A_y and B_y are P,T-dependent Debye-Hückel solvent parameters. This activity correction should be applicable up to 1-2 m ionic strength [26],[27].

All solubility products were calculated based on the measured ion concentrations and pH values and refer to zero ionic strength. Since measured pH values are lower than the theoretically expected values, the presence of small quantities of CO_2 was considered such that measured and calculated pH values agreed.

The temperature dependence of the solubility product for CrO_4-ettringite was computed using the measured concentrations from 5-75 °C from Perkins and Palmer [22] and the solubilities at 25° from the current study. Methods and results can be found in Supporting Information.

2.3 Results and discussion

2.3.1 Solid phases of the solid solution series

The solids had rather constant Ca and Al ratios at variable SO_4:CrO_4 ratios (Table 1). Ettringite has an ideal stoichiometry of 6Ca:2Al:3(SO_4+CrO_4). However, due to the synthesis method and the amount of water present, deviations from ideal stoichiometry were observed. Calculated molar ratios of SO_4:CrO_4 revealed that each sample was more enriched in SO_4 than the suspension from which it was synthesized. This was expected, since SO_4-ettringite has a lower solubility than the CrO_4-endmember. Excess of Al, Ca and SO_4 in some samples are reasoned by the existence of secondary phases, such as amorphous Al-hydroxide and gypsum.

Table 1 Results of solid digest analyses of synthesized
$Ca_6(Al(OH)_6)_2[(CrO_4)_x(SO_4)_{1-x}]_3 * 26\ H_2O$

$XCrO_4$[a] in reagents	measured solid digest concentrations in (mM/l) (measurement precision $^+/.10\%$)				molar ratios Ca:Al:(CrO4+SO4) normalized to 6 Ca					solid CrO4 mole fraction
	Ca	**Al**	**SO₄**	**CrO₄**	**Ca**	**Al**	**CrO₄+SO₄**	**SO₄**	**CrO₄**	**XCrO₄**
1	8.5	4.4	0	4.9	6	3.1	3.5	0	3.5	**1**
0.8	8.7	4.4	2.0	3.3	6	3	3.6	1.4	2.2	**0.6**
0.5	9.0	4.2	3.3	2.2	6	2.8	3.7	2.2	1.5	**0.4**
0.4	9.4	4.5	3.8	1.6	6	2.9	3.5	2.4	1.1	**0.3**
0.2	9.2	4.0	5.3	0.7	6	2.6	3.9	3.4	0.5	**0.1**
0.1	9.3	3.8	6.2	0.12	6	2.4	4.1	4	0.1	**0.03**
0	9.9	3.6	6.3	0	6	2.2	3.8	3.8	0	**0**

[a] chromate mole fractions
$XCrO_4 = CrO_4^{2-}/(SO_4^{2-}+CrO_4^{2-})$

Sharp peaks in the XRD patterns indicate well crystallized solids with peak positions belonging to ettringite (Figure 1). Peak positions and unit cell parameters of both end members are consistent to the values of the powder diffraction in the database of the International Center for Diffraction Data (ICDD) for CrO_4-ettringite and SO_4-ettringite respectively. Solid solutions at low $XCrO_4$ contained gypsum (indicated with gy in Figure 1). No other additional phases were detected.

The observed peak shift from sulfate end member (Cr0) to the chromate end member (Cr1) is due to the larger ionic radius of the CrO_4^{2-} molecule (2.4 Å) compared to the SO_4^{2-} molecule (2.3 Å, *[32]*) (Figure 2). This causes an increase of the lattice distances (d-spacings) in the crystal. Solid solutions with increasing $XCrO_4$ have increasing lattice distances and the peak shifts continuously from the SO_4-ettringite to the CrO_4-ettringite. This was the case for all phases except samples Cr0.4 and Cr0.6 where clear peak splitting was observed. Two distinct peaks indicate a mixture of two ettringite phases instead of one solid solution phase. Hence a miscibility gap in the solid solution series exists for samples with $0.4 \leq XCrO_4 \leq 0.6$. The peaks of these samples lie somewhere between the peaks

of the pure end-members indicating mixed phases. Solid solutions within a miscibility gap of a solid solution series are called secondary solid solutions.

The unit cell parameters show an increase of a-axis values for samples with increasing $XCrO_4$ (Figure 3). In samples Cr0.4 and Cr0.6 two values indicate that two separate ettringite-phases are present. The same was observed for the unit cell volume. The volume increased up to the miscibility gap where peak splitting caused two values for the two existing samples. Calculated c-axes stayed constant within the measurement error at a value of 21.47 Å +/- 0.01.

ESEM and TEM analysis showed the typical acicular structure of ettringite. Crystallite sizes became smaller and thinner with increasing chromate content. This corresponds to the observed lower crystallinity in XRD diagram (Figure 1).
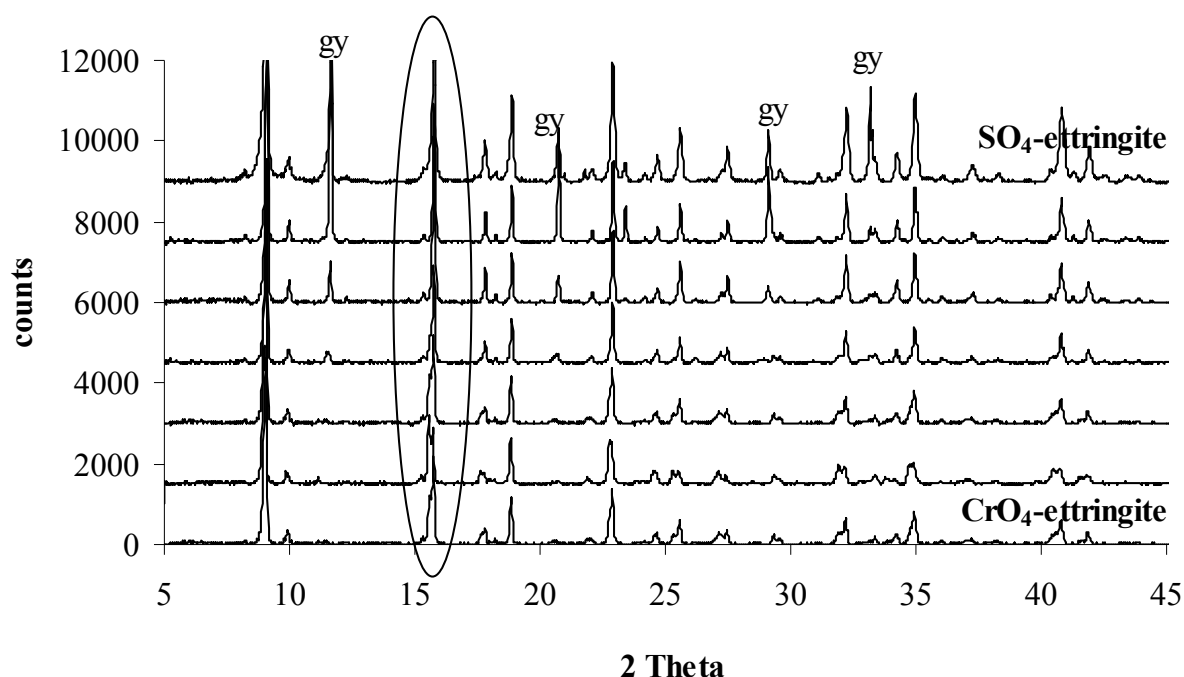
Figure 1 XRD scans of the solid solution series of CrO_4- and SO_4-ettringites. The additional phase is gypsum - (gy). Samples closer to the CrO_4-endmember show a slight peak broadening due to smaller crystals. A zoom at the 2 theta value of 22.8 is shown in Figure 2.
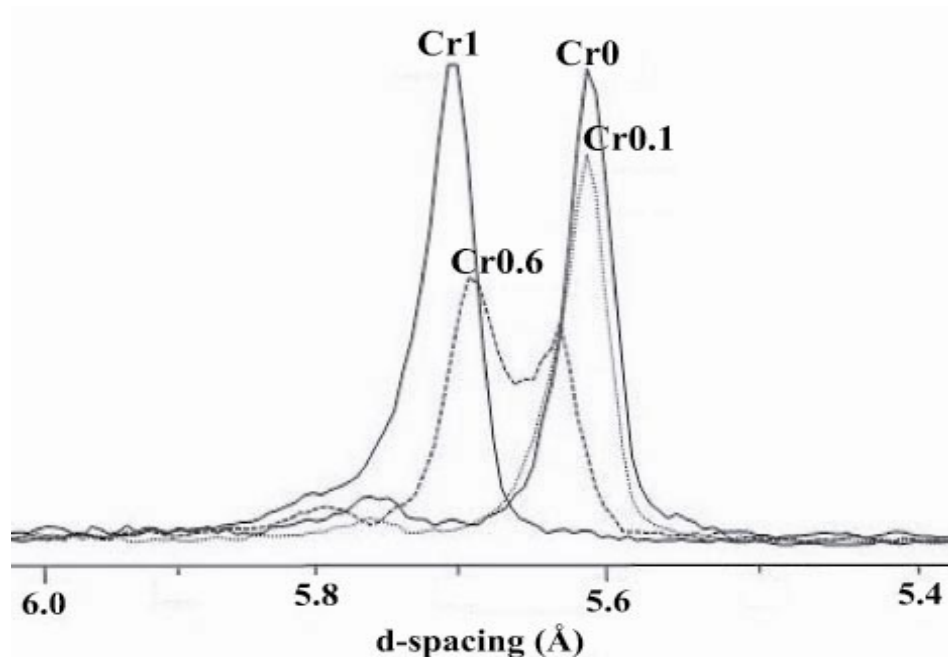
Figure 2 Peak shift for SO_4-ettringite (Cr0) to pure CrO_4-ettringite (Cr1) in the XRD peaks close to $2\Theta = 22.8$. Lattice distances increase with increasing CrO_4 content in the samples. Peak splitting is clearly observed for sample Cr0.6 indicating two co-existing phases.
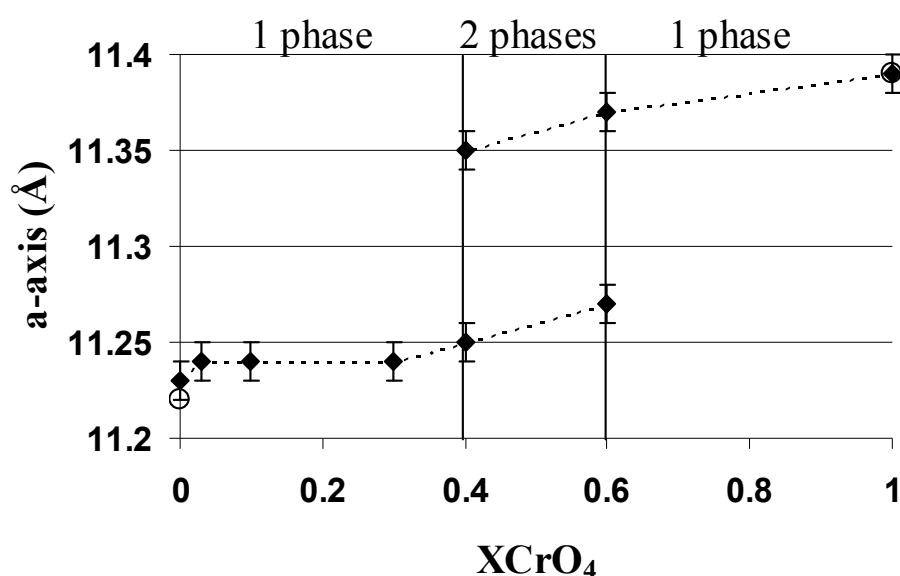
Figure 3 Unit cell a-axis as a function of chromium content. At $XCrO_4 = 0.4$ peak splitting indicates the presence of two phases. Black circles at $XCrO_4=1$ and 0 show values from powder diffraction files 041-0218 and 037-1476 for the CrO_4- and the SO_4-ettringites respectively.

Results of thermal analysis displayed that dehydration of all samples proceeds in mainly three steps as characteristic for ettringite *[33]*. Solid solutions close to the SO_4-ettringite end member showed an additional peak at around 150 °C that can be identified to the water loss of gypsum. Solid solutions closer to the CrO_4-ettringite end member revealed small mass losses between 250 °C and 300 °C. This is an evidence for the presence of amorphous $Al(OH)_3$. Since no crystalline $Al(OH)_3$ was observed in TGA the phase must be amorphous or the amount of this phase is smaller than the detection limit of the XRD analysis (<5 weight %). In all samples small amounts of CO_2 was observed at a temperature between 625-700 °C indicating calcite precipitations.

2.3.2 Characterization of the liquid phase

The $Ca:Al:SO_4:CrO_4$ ratios in solution differed from those of the solid, implying incongruent dissolution (Table 2). The presence of secondary phases (gypsum and Al-hydroxide) caused a lowering of dissolved Ca, Al and SO_4 concentrations in solution. Measured CO_2 content in the samples lowered the pH as well as Ca concentrations in solutions due to calcite precipitation.

Decreasing ion concentrations with decreasing $XCrO_4$ content in the samples are expected due to the lower solubility of SO_4-ettringite compared to CrO_4-ettringite. We can observe a positive correlation between the measured calcium and chromate concentrations due to the fact that aqueous $CaCrO_4^0$ complexes form ($Ca^{2+} + CrO_4^{2-} = CaCrO_4^o$; logK = 2.77), while the total solubility product is not affected.

Table 2 Determined total solubility products of the solid solution series are calculated based on the measured ion concentrations in solution.

Sample	Ion concentrations in solution (mmol/l)				calculated solubility products		
	Ca	**Al**	**SO$_4$**	**CrO$_4$**	**log $\sum\prod$[a]**	**log K$_{CrO4}$**	**log K$_{SO4}$**
Cr1	35.0 ± 9.0	0.2 ± 0.1	-	28.6 ± 12.8	**-40.2 ± 0.4**	*-40.2 ± 0.4*	-
Cr0.6	26.3 ± 4.4	0.2 ± 0.1	0.7 ± 0.1	20.0 ± 5.1	**-40.7 ± 0.4**	*-40.8 ± 0.4*	*-44.5 ± 0.4*
Cr0.4	18.0 ± 1.5	0.8 ± 0.2	0.2 ± 0.2	12.0 ± 1.6	**-40.8 ± 0.2**	*-40.8 ± 0.3*	*-46.0 ± 0.7*
Cr0.3	12.5 ± 1.9	1.3 ± 0.5	0.4 ± 0.1	7.5 ± 2.6	**-40.5 ± 0.4**	*-40.6 ± 0.4*	*-43.9 ± 0.4*
Cr0.1	16.2 ± 8.9	1.3 ± 1.1	3.9 ± 5.5	12.4 ± 6.4	**-41.2 ± 0.9**	*-41.2 ± 0.9*	*-43.8 ± 0.8*
Cr0.03	24.1 ± 1.3	0.01[b]	16.6 ± 0.9	9.3 ± 0.6	**-43.1 ± 0.2**	*-45.0 ± 0.1*	*-43.5 ± 0.1*
Cr0					**-44.9 ± 0.7[c]**	-	*-44.9 ± 0.7[c]*

[a] $\log \Sigma\Pi = 2\log\{Ca^{2+}\} + \frac{2}{3}\log\{Al(OH)_4^-\} + \log[\{CrO_4^{2-}\} + \{SO_4^{2-}\}] + \frac{4}{3}\log\{OH^-\} + 26\log\{H_2O\}$;
after all calculations were done, results are again multiplied by 3.
[b] average value of 3 measurements by ICP-MS
[c] due to analytical problems with Al concentrations below the ICP-OES detection limit, the published solubility value of log K$_{S0}$ = -44.9 [34] is used for further calculations.

2.3.3 Determination of CrO$_4$-ettringite solubility

The solubility of CrO$_4$-ettringite was calculated according to the reaction

(3) $\log K_{CrO_4-ettringite} = 6\log\{Ca^{2+}\} + 2\log\{Al(OH)_4^-\} + 3\log\{CrO_4^{2-}\} + 4\log\{OH^-\} + 26\log\{H_2O\}$

Solubility calculations of all precipitation and dissolution experiments resulted in a mean log K = -40.2 ± 0.4 (Figure 4). Data points of the dissolution experiments resulted in a slightly higher solubility products (-39.9 ±0.4) compared to the precipitation experiments (-40.4 ±0.4). The calculated solubility products varied since the system is very sensitive to CO$_2$ intrusion. Already a small CO$_2$ amount in the system lowers the pH.

The solubility of CrO$_4$-ettringite at 25°C was determined by Perkins [22] to be logK$_{S0}$ = -41.5 ± 0.3. Using the concentrations measured by *[22]* and the thermodynamic dataset used in this paper resulted in a logK$_{S0}$ of -41.2 ± 0.6 resulted. The solubility product of CrO4-ettringite calculated from the measurements of *[22]* of -41.2 ± 0.6 is one log lower than the solubility product measured in the paper (-40.2 ±0.4).
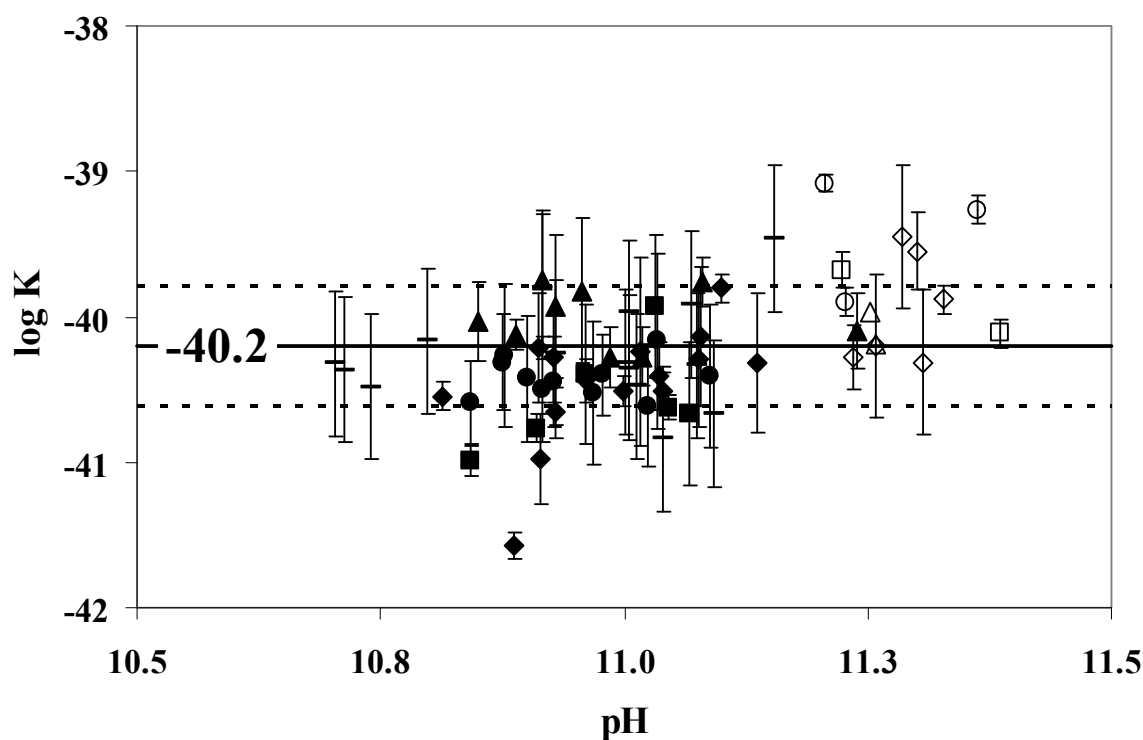

Figure 4 Precipitation and dissolution experiments at different pH values were carried out to determine the solubility product of CrO$_4$-ettringite (black filled symbols = precipitation exp.; open symbols = dissolution exp.; black small line = precipitation exp. without pH adjustment). A mean log K$_{S0}$ of -40.2 ± 0.4 was calculated as CrO$_4$-ettringite solubility product.

2.3.4   Solid solution solubility products

The calculated CrO_4- and SO_4-ettringite solubility products change as a function of $XCrO_4$ for mixed phases (Table 2). This indicates that solid solutions exist. Solubility data of the binary solid-solution system SO_4- and CrO_4-ettringites were illustrated by the Lippmann diagram (Figure 5) *[35, 36]*. The total solubility product, $\Sigma\Pi$ (equation 4) equals the sum of the partial solubility products of each end member, if the system has reached thermodynamic equilibrium and is called solidus (equation 5).

$$(4) \quad \Sigma\Pi = \{Ca^{2+}\}^2 \{Al(OH)_4^-\}^{\frac{2}{3}} [\{CrO_4^{2-}\} + \{SO_4^{2-}\}] \{OH^-\}^{\frac{4}{3}} \{H_2O\}^{\frac{26}{3}}$$

$$(5) \quad \Sigma\Pi_{eq} = \{Ca^{2+}\}^2 \{Al(OH)_4^-\}^{\frac{2}{3}} [\{SO_4^{2-}\} + \{CrO_4^{2-}\}] \{OH^-\}^{\frac{4}{3}} \{H_2O\}^{\frac{26}{3}} = K_{CrO_4} \cdot X_{CrO_4} \cdot f_{CrO_4} + K_{SO_4} \cdot X_{SO_4} \cdot f_{SO_4}$$

the waved brackets $\{\ \}$ are aqueous activities, K_{SO4} and K_{CrO4} represent the end member solubility products of pure SO_4- and CrO_4-ettringite, X_{SO4} and X_{CrO4} are the chromate mole fractions ($X_{SO4} + X_{CrO4} = 1$) in the solid   and f_{SO_4}, f_{CrO_4} are solid activity coefficients ($f_{CrO_4}, f_{SO_4} = 1$ for ideal solid solutions). To model solid solutions with GEMS the default model of simple ideal mixing demands that one ion can be substituted by another ion on one crystallographic site per end member formula unit. To fulfil this condition the stoichiometries of both end members were downscaled by the factor 3 as well as the logK values and the G° in the database (equation 5). Solid solution compositions are strongly related to their solution compositions described by the solutus curve (equation 6)

$$(6) \quad \Sigma\Pi_{eq} = \cfrac{1}{\left(\cfrac{x_{CrO_4,aq}}{K_{CrO_4} f_{CrO_4}} + \cfrac{x_{SO_4,aq}}{K_{SO_4} f_{SO_4}} \right)}$$

with aqueous activity fractions *$XCrO_4$, aq* and *XSO_4, aq* defined as:

(7) $\quad x_{CrO_4,aq} = \dfrac{\{CrO_4\}}{\{CrO_4\}+\{SO_4\}}$ and $\quad x_{SO_4,aq} = \dfrac{\{SO_4\}}{\{CrO_4\}+\{SO_4\}}$

In a Lippmann diagram there are two superimposed x-axes. The total solubility products of the solidus are drawn as a function of the solid chromate mole fractions, $XCrO_4(s)$ whereas the total solubility products of the solutus are drawn as a function of the chromate activity fractions in solution, $XCrO_4(aq)$. Solidus and solutus give the solid-phase and aqueous-phase compositions for the solid solution series of possible thermodynamic equilibrium states [36-38].

The excess free energy of mixing of a non-ideal solid solution model (equation 8) can be expressed by the Guggenheim expansion series modified by the Redlich and Kister expressions (equation 9 and 10) *[39]*. Regular non-ideal solid solutions only need one Guggenheim fitting parameter (a_0) which was determined by the MBSSAS code *[40]* and based on the experimentally observed symmetric miscibility gap $0.4<XCrO_4<0.6$. A value of $a_0 = 2.03$ resulted and was used to determine SO_4- and CrO_4-ettringite end member activity coefficients (equation 11 and 12).

(8) $\quad \Delta G_E = RT\left(X_{CrO_4}\ln\gamma_{CrO_4} + X_{SO_4}\ln\gamma_{SO_4}\right)$

(9) $\quad \ln\gamma_{CrO_4} = X^2_{SO_4}\left[a_0 - a_1\left(3X_{CrO_4} - X_{SO_4}\right) + a_2\left(X_{CrO_4} - X_{SO_4}\right)\left(5X_{CrO_4} - X_{SO_4}\right) + ...\right]$

(10) $\quad \ln\gamma_{SO_4} = X^2_{CrO_4}\left[a_0 - a_1\left(3X_{SO_4} - X_{CrO_4}\right) + a_2\left(X_{SO_4} - X_{CrO_4}\right)\left(5X_{SO_4} - X_{CrO_4}\right) + ...\right]$

(11) $\quad \ln\gamma_{CrO_4} = X^2_{SO_4}a_0$

(12) $\quad \ln\gamma_{SO_4} = X^2_{CrO_4}a_0$

The calculated $\sum\prod$ of the solid solution series fit best to the non-ideal model including the miscibility gap $0.4\leq XCrO_4\leq 0.6$ (Figure 5). The existence of a miscibility gap in the graph can be observed by the horizontal line of the solidus within the compositional boundaries of the miscibility gap. This result of solution analysis supports the findings of the solid analysis.
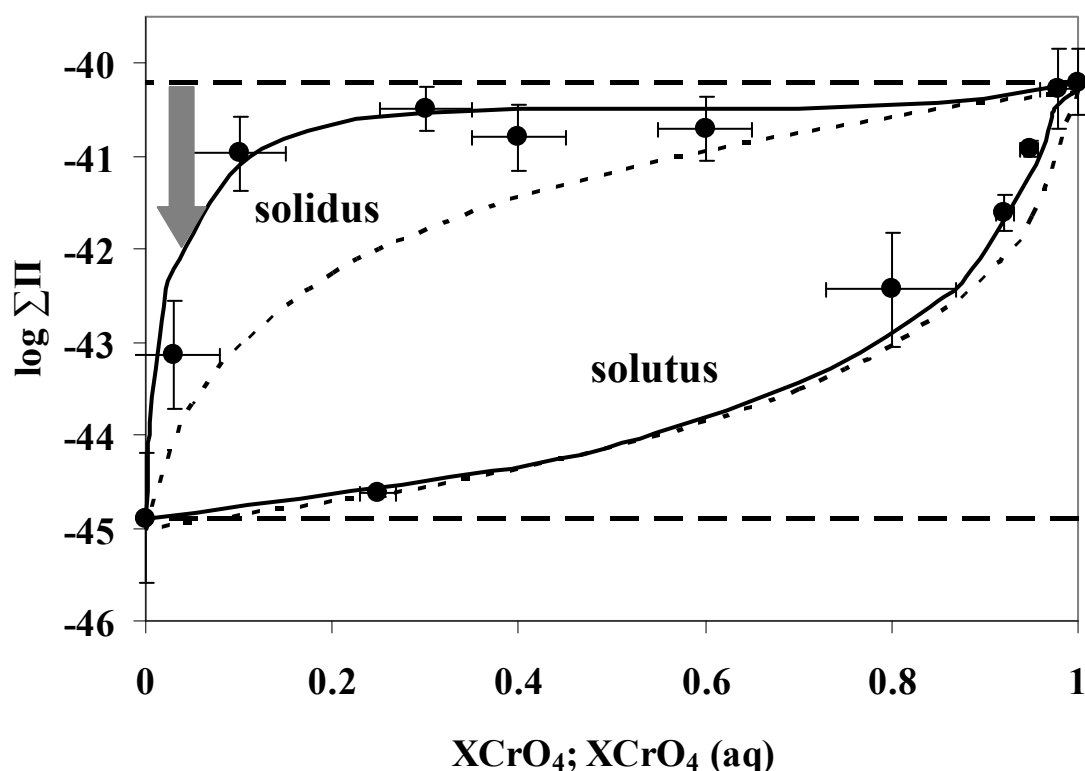
Figure 5 Lippmann diagram illustrating total solubility products of the CrO_4-/SO_4-ettringite solid solution series (dots) and the models without solid solution formation (dashed lines), with ideal solid solution (pointed lines) and the case for a non-ideal solid solution with a miscibility gap between $0.4 < XCrO_4 < 0.6$ (straight line). X-axis represents either solid chromate mole fractions, $XCrO_4$ or aqueous chromate activity fractions, $XCrO_4$ (aq). A gray arrow indicates the possible CrO_4 stabilization of the solid phase by lowering the solubility product through solid solution formation, compared to the system if no solid solution would exist. The lowering of the solubility is higher for solid solutions with a low chromate mole fraction.

These are the first published thermodynamic data of CrO_4- and SO_4-ettringite solid solutions. It could be shown that solid solutions exist and that this solid solution formation can stabilize solids and increase uptake of CrO_4^{2-} in SO_4-ettringite and vice versa (arrow in Figure 5). Pure CrO_4-ettringite formed at CrO_4^{-2} concentrations of 28 mmmol/l; solid solution can be formed at up to a four times lower chromate concentrations, depending on the composition (Table 2). In addition to ettringite (AFt-phase), AFm-phases (e.g. monosulfate) may

play an important role in CrO_4^{2-} binding mechanisms [41] in the cement matrix and should be taken into account in CrO_4^{2-} leaching modeling projects.

2.4   Acknowledgments

2.5   References

[1]   Spence, R.D., Chemistry and microstructure of solidified waste forms. 1993, Boca Raton, Florida: Lewis Publishers. 276.

[2]   Glasser, F.P., Properties of cement waste composites. Waste Management, 1996. **16**(1-3): p. 159-168.

[3]   Glasser, F., et al., Mechanisms and modeling of waste/cement interactions: International Workshop, May 8 to 12, 2005, Meiringen, Switzerland. Waste Management, 2006. **26**(7): p. 687-688.

[4]   Glasser, F.P., Progress in the immobilization of radioactive wastes in cement. Cement and Concrete Research, 1992. **22**(2-3): p. 201-216.

[5]   Atkins, M. and F.P. Glasser, Application of portland cement-based materials to radioactive waste immobilization. Waste Management, 1992. **12**(2-3): p. 105-131.

[6]   Cocke, D.L., The binding chemistry and leaching mechanisms of hazardous substances in cementitious solidification/stabilization systems. Journal of Hazardous Materials, 1990. **24**(2-3): p. 231-253.

[7]   Wang, S. and C. Vipulanandan, Solidification/stabilization of Cr(VI) with cement: Leachability and XRD analyses. Cement and Concrete Research, 2000. **30**(3): p. 385-389.

[8]   Evans, N.D.M., Binding mechanisms of radionuclides to cement. Cement and Concrete Research, 2008. **38**(4): p. 543-553.

[9]   Moulin, I., et al., Lead, zinc and chromium (III) and (VI) speciation in hydrated cement phases, in Waste Management Series. 2000, Elsevier. p. 269-280.

[10]   Langard, S. and M. Costa, eds. Chromium. Handbook on the Toxicology of Metals, ed. G. Nordberg, et al. 2007, Academic Press, Inc. 1024.

[11]   Stephan, D., et al., High intakes of Cr, Ni, and Zn in clinker: Part I. Influence on burning process and formation of phases. Cement and Concrete Research, 1999. **29**(12): p. 1949-1957.

[12]   Fregert, S. and B. Gruvberger, Factors decreasing the content of water-soluble chromate in cement. Acta Dermatovener, 1973. **53**: p. 267.

[13]   van der Sloot, H.A., Comparison of the characteristic leaching behavior of cements using standard (EN 196-1) cement mortar and an assessment of their long-term environmental behavior in construction products during service life and recycling. Cement and Concrete Research, 2000. **30**(7): p. 1079-1096.

[14]   Park, J.-Y., W.-H. Kang, and I. Hwang, Hexavalent chromium uptake and release in cement pastes. Environmental Engineering Science, 2005. **23**(1): p. 133-140.

[15]   Chrysochoou, M. and D. Dermatas, Evaluation of ettringite and hydrocalumite formation for heavy metal immobilization: Literature review and experimental study. Journal of Hazardous Materials, 2006. **136**(1): p. 20-33.

[16]   Taylor, H.F.W., Cement Chemistry. Vol. 1. 1997, London: Thomas Telford Publishing. 459.

[17]   Perkins, R.B. and C.D. Palmer, Solubility of ettringite ($Ca_6[Al(OH)_6]_2(SO_4)_3 \cdot 26H_2O$) at 5-75°C. Geochimica et Cosmochimica Acta, 1999. **63**(13-14): p. 1969-1980.

[18]   Zhang, M., Incorporation of oxyanionic B, Cr, Mo and Se into hydrocalumite and ettringite: application to cementitous systems, in Earth Science. 2000, University of Waterloo Ontario, Canada. p. 172.

[19]   Palmer, C.D., Precipitates in a Cr(VI)-contaminated concrete. Environ. Sci. Technol., 2000. **34**(19): p. 4185-4192.

[20]   Goetz-Neunhoeffer, F., J. Neubauer, and P. Schwesig, Mineralogical characteristics of Ettringites synthesized from solutions and suspensions. Cement and Concrete Research, 2006. **36**(1): p. 65-70.

[21]   Atkins, M., F.P. Glasser, and A. Kindness, Cement hydrate phases. Solubility at 25°C. Cement and Concrete Research, 1992. **22**(2-3): p. 241-246.

[22]   Perkins, R.B. and C.D. Palmer, Solubility of $Ca_6[Al(OH)_6]_2(CrO_4)_3 \cdot 26H_2O$, the chromate analog of ettringite; 5-75°C. Applied Geochemistry, 2000. **15**(8): p. 1203-1218.

[23]   Perkins, R.B., The solubility and thermodynamic properties of ettringite, its chromium analogs and calcium aluminum monochromate, in Environmental science and resources. 2000, Portland State University: Portland, USA. p. 200.

[24]   Le Bail, A., Monte Carlo indexing with McMaille. Powder Diffraction, 2004. **19**(3): p. 249-254.

[25]   Smith, G.S. and R.L. Snyder, A criterion for rating powder diffraction atterns and evaluating the reliability o powder indexing. J. Appl. Cryst., 1979. **12**: p. 60-65.

[26]   Kulik, D.A., U. Berner, and E. Curti, Modelling chemical equilibrium partitioning with the GEMS-PSI code, in PSI Scientific Report. 2003, PSI: Villigen. p. 109-122.

[27]   Hummel, W., et al., Nagra/PSI Chemical Thermodynamic Data Base 01/01. 2002, Parkland, Florida, USA: Universal Publishers/uPUBLISH.com.

[28]   Johnson, J.W., E.H. Oelkers, and H.C. Helgeson, SUPCRT92: a software package or calculating the standard molal thermodynamic properties of minerals, gases, aqueous species, and reactions from 1 to 5000 bar and 0 to 1000°C. Comput. Geosci., 1992. **18**(7): p. 899-947.

[29]   Thoenen, T. and D. Kulik, Nagra/PSI chemical thermodynamic database 01/01 for the GEM-Selektor (V.2-PSI) geochemical modeling code, PSI, Editor. 2003: Villigen.

[30]   Shock, E.L., et al., Inorganic species in geologic fluids: correlation among standard molal thermodynamic properties of aqueous ions and hydroxide complexes. Geochim. Cosmochim. Acta, 1997. **61**: p. 907-950.

[31]   Sverjensky, D., E.L. Shock, and H.C. Helgeson, Prediction of the thermodynamic properties of aqueous metal complexes to 1000°C and 5 kbar. Geochim. Cosmochim. Acta, 1997. **61**: p. 1359-1412.

[32]   Waddington, T.C. and H.J.E.a.A.G. Sharpe, Lattice Energies and their Significance in Inorganic Chemistry, in Advances in Inorganic Chemistry. 1959, Academic Press. p. 157-221.

[33]   Poellmann, H., Die Kristallchemie der Neubildungen bei Einwirkung von Schadstoffen auf hydraulische Bindemittel, in Naturwissenschaftliche Fakultät. 1984, Friedrich-Alexander-Universität: Erlangen-Nürnberg. p. 332.

[34]   Lothenbach, B., et al., Thermodynamic modelling of the effect of temperature on the hydration and porosity of Portland cement. Cement and Concrete Research, 2008. **38**(1): p. 1-18.

[35]   Lippmann, F., The solubility products of complex minerals, mixed minerals, and three-layer clay minerals. N.JB.Miner.Abh., 1977. **130**(3): p. 243-263.

[36]   Lippmann, F., Phase diagrams depicting aqueous solubility of binary mineral systems. N.JB.Miner.Abh., 1980. **139**(1): p. 1-25.

[37]   Glynn, P.D. and E.J. Reardon, Solid-Solution Aqueous-Solution Equilibria - Thermodynamic theory and representation. American Journal of Science, 1990. **290**(2): p. 164-201.

[38]   Prieto, M., Thermodynamics of solid solution-aqueous solution systems, in Thermodynamics and Kinetics of Water-Rock Interaction, E.H. Oelkers and J. Schott, Editors. 2009, Mineralogical Society of America and Geochemical Society. p. 47-85.

[39]   Redlich, O. and A.T. Kister, Algebraic representation of the thermodynamic properties and the classification of solutions. Ind. Eng. Chem., 1948. **40**: p. 345-348.

[40]   Glynn, P.D., MBSSAS: A code for the computation of Margules parameters and equilibrium relations in binary solid-solution aqueous-solution systems. Computers and Geoscience, 1991. **17**(7): p. 907-966.

[41]   Perkins, R.B. and C.D. Palmer, Solubility of chromate hydrocalumite (3CaO·Al$_2$O$_3$·CaCrO$_4$·nH$_2$O) 5-75°C. Cement and Concrete Research, 2001. **31**(7): p. 983-992.

[42]   Ball, J.W. and D.K. Nordstrom, Critical evaluation and selection of standard state thermodynamic properties for chromium metal and its aqueous ions, hydrolysis species, oxides, and hydroxides. J. Chem. Eng. Data, 1998. **43**(6): p. 895-918.

2.6   Supporting information

Table S1 Measured ion concentrations in solution (in mmol/l) of the solid solution series, including the calculated solubility products

XCrO4	pH	Ca	Al	SO$_4$	CrO$_4$	1/3 log K$_{S0}$	log K$_{S0}$
Cr1_1	11.0	23.0	0.3		14.2		-40.7
Cr1_2	11.0	27.4	0.3		16.9		-40.3
Cr1_3	11.1	48.6	0.1		46.8		-40.2
Cr1_4	10.8	50.3	0.1		49.1		-40.3
Cr1_5	10.7	45.6	0.1		41.9		-40.5
Cr1_6	10.8	22.6	0.3		14.4		-40.8
Cr1_7	11.0	32.5	0.2		25.2		-40.2
Cr1_8	10.9	53.1	0.1		52.1		-40.4
Cr1_9	10.7	31.2	0.2		23.8		-39.9
Cr1_10	11.0	30.3	0.2		21.6		-40.4
Cr1_11	11.0	30.6	0.2		22.3		-40.3
Cr1_12	10.9	33.8	0.2		26.3		-40.0
Cr1_13	10.9	32.0	0.2		24.5		-39.5
Cr1_14	11.0	27.2	0.3		18.1		-40.5
Cr1_15	10.8	37.5	0.3		32.2		-39.8
average	10.9	35.0	0.2		28.6		-40.2
std.dev.	0.1	9.8	0.1		12.8		0.3
Cr0.6_1	11.0	25.2	0.3	0.7	17.8	-13.4	-40.2
Cr0.6_2	10.9	23.8	0.3	0.6	16.4	-13.5	-40.6
Cr0.6_3	10.9	22.7	0.3	0.6	15.2	-13.5	-40.6
Cr0.6_4	10.9	21.1	0.3	0.6	15.7	-13.6	-40.9
Cr0.6_5	10.8	36.5	0.2	0.9	31.7	-13.4	-40.3
Cr0.6_6	10.8	26.1	0.2	0.7	21.1	-13.5	-40.6
Cr0.6_7	10.9	23.9	0.3	0.6	16.1	-13.5	-40.5
Cr0.6_8	10.8	29.2	0.3	0.7	24.1	-13.6	-40.8
Cr0.6_9	10.9	29.1	0.1	0.7	22.2	-13.7	-41.0
Cr0.6_10	10.8	25.0	0.1	0.7	20.2	-13.8	-41.4
average	10.9	26.3	0.2	0.7	20.0	-13.6	-40.7
+/-	0.1	4.4	0.1	0.1	5.1	0.1	0.4
Cr0.4_1	10.8	19.9	0.9	0.2	15.4	-13.5	-40.5
Cr0.4_2	10.9	16.3	1.0	0.1	10.2	-13.6	-40.8
Cr0.4_3	10.8	18.2	0.9	0.2	12.1	-13.6	-40.8
Cr0.4_4	10.9	17.4	1.0	0.1	11.1	-13.5	-40.5
Cr0.4_5	10.8	17.0	0.9	0.1	10.9	-13.7	-41.1
Cr0.4_6	10.8	18.1	0.8	0.2	13.2	-13.6	-40.9

Cr0.4_7	10.9	20.5	0.3	0.7	11.2	-13.7	-41.1
Cr0.4_8	10.9	16.8	0.8	0.1	11.8	-13.5	-40.6
average	**10.9**	**18.0**	**0.8**	**0.2**	**12.0**	**-13.6**	**-40.8**
+/-	**0.1**	**1.5**	**0.2**	**0.2**	**1.6**	**0.1**	**0.2**
Cr0.3_1	11.0	10.4	2.5	0.3	4.1	-13.6	-40.7
Cr0.3_2	11.1	11.0	1.5	0.3	5.8	-13.5	-40.5
Cr0.3_3	11.1	11.4	1.3	0.3	5.1	-13.5	-40.5
Cr0.3_4	11.0	12.7	1.0	0.4	8.2	-13.5	-40.6
Cr0.3_5	10.9	15.4	0.9	0.5	11.4	-13.4	-40.2
Cr0.3_6	10.9	11.1	1.4	0.4	6.6	-13.6	-40.7
Cr0.3_7	11.0	14.1	1.2	0.4	9.0	-13.3	-39.8
Cr0.3_8	10.9	15.1	0.7	0.5	11.1	-13.7	-41.1
Cr0.3_9	11.0	11.5	1.4	0.3	6.4	-13.4	-40.3
average	**11.0**	**12.5**	**1.3**	**0.4**	**7.5**	**-13.5**	**-40.5**
+/-	**0.1**	**1.9**	**0.5**	**0.1**	**2.6**	**0.1**	**0.4**
Cr0.1_1	11.1	8.8	2.1	0.3	6.4	-13.4	-40.1
Cr0.1_2	10.6	27.4	0.0	12.6	19.0	-14.4	-43.2
Cr0.1_3	10.8	13.5	1.5	0.6	11.9	-13.5	-40.5
Cr0.1_4	11.0	9.1	1.9	0.4	6.7	-13.6	-40.9
Cr0.1_5	11.0	8.7	2.8	0.3	5.1	-13.6	-40.7
Cr0.1_6	10.6	31.7	0.1	12.5	22.2	-13.8	-41.3
Cr0.1_7	10.8	18.9	0.1	3.9	17.6	-13.9	-41.7
Cr0.1_8	10.6	12.0	1.6	0.6	10.6	-13.9	-41.6
average	**10.8**	**16.2**	**1.3**	**3.9**	**12.4**	**-13.7**	**-41.2**
+/-	**0.2**	**8.9**	**1.1**	**5.5**	**6.4**	**0.3**	**0.9**
Cr0.03_1	10.8	25.41	0.008[1]	17.6	9.4	-14.3	-42.9
Cr0.03_2	10.8	25.26		17.5	9.0	-14.3[2]	-43.0
Cr0.03_3	10.8	23.71		16.2	9.5	-14.4[2]	-43.2
Cr0.03_4	10.8	23.15		16.9	8.0	-14.4[2]	-43.2
Cr0.03_5	10.8	24.10		16.5	9.3	-14.4[2]	-43.1
Cr0.03_6	10.8	22.12	0.007[1]	15.0	9.3	-14.5	-43.4
Cr0.03_7	10.8	25.65	0.007[1]	17.6	9.8	-14.3	-43.0
Cr0.03_8	10.8	23.17		15.8	10.2	-14.4[2]	-43.3
average	**10.8**	**24.1**	**0.01**	**16.6**	**9.3**	**-14.4**	**-43.1**
+/-	**0.0**	**1.3**		**0.9**	**0.6**	**0.1**	**0.2**

[1]Al-values measured by ICP-MS

[2] calculated with Al-average of 0.01

Table S2 Thermodynamic data used for speciation calculations

Reaction		$log\ K_{298}$	Ref.
Aqueous Species			
$H_2O = OH^- + H^+$		-14 .0	(1)
$Ca^{2+} + SO_4^{2-} = CaSO_4^0$		2.3	(1)
$Ca^{2+} + HCO_3^- = CaHCO_3^+$		1.11	(1)
$Ca^{2+} + HCO_3^- = CaCO_3 + H^+$		-7.11	(2)
$CrO_4^{2-} + 2H^+ = H_2CrO_4^0$		6.31	(2)
$CrO_4^{2-} + H^+ = HCrO_4^-$		6.55	(2)
$2CrO_4^{2-} + 2H^+ - H_2O = Cr_2O_7^{2-}$		4.7	[42])
$K^+ + CrO_4^{2-} = KCrO_4^-$		0.78	(3)
$K^+ + H_2O = KOH^0 + H^+$		-14.46	[42])
$K^+ + SO_4^{2-} = KSO_4^-$		0.85	[42])
$Ca^{2+} + CrO_4^{2-} = CaCrO_4^0$		2.77	[22])
$Ca^{2+} + H_2O = CaOH^+ + H^+$		-12.78	[27])
$Al^{3+} H_2O = AlOH^{2+} + H^+$		-4.96	[27])
$Al^{3+} + 2H_2O = Al(OH)^+_2 + 2H^+$		10.59	[27])
$Al^{3+} + 3H_2O = Al(OH)_3^0 + 3H^+$		$^-$16.43	[27])
$Al^{3+} + 4H_2O = Al(OH)_{4-}^- + 4H^+$		-22.88	[27])
$Al^{3+} + SO_4^{2-} = AlSO_4^+$		3.9	[27])
$Al^{3+} + 2SO_4^{2-} = Al(SO_4)_2^-$		5.9	[27])
Solid phases			
Portlandite	$Ca(OH)_2 = Ca^{2+} + 2H_2O - 2H^+$	22.8	[27])
Gypsum	$CaSO_4 * 2H_2O = Ca^{2+} + SO_4 + 2H_2O$	-4.58	[27])
Calcite	$CaCO3(s) + H^+ = CaHCO^{3+}$	1.85	[27])
Al-hydroxide am.	$Al(OH)_{3,\ amph} = Al(OH)_4^- - 1OH^-$	0.24	[27])
SO$_4$-ettringite	$Ca_6(Al(OH)_6)_2(SO_4)_3 * 26H_2O =$		
	$6Ca^{2+} + 2Al(OH)_4^- + SO_4^{2-} + 4OH^- + 26H_2O$	-44.9 $_{+/- 0.7}$	[27])
CrO$_4$-ettringite	$Ca_6(Al(OH)_6)_2(CrO_4)_3 * 26H_2O =$		
	$6Ca^{2+} + 2Al(OH)_4^- + CrO_4^{2-} + 4OH^- + 26H_2O$	-40.2 $_{+/-0.4}$	[27])

(1) Hummel, W., U. Berner, E. Curti, F.J. Pearson, T. Thoenen (2002) Nagra/PSI Chemical Thermodynamic Data Base 01/01, Universal Publishers/uPublish.com., Parkland, Florida.
(2) Ball, J.W., D.K. Nordstrom (1998) Critical evaluation and selection of standard state thermodynamic properties for chromium metal and its aqueous ions, hydrolysis species, oxides, and hydroxides. *J.Chem.Eng*. Data **43, 6**, 895-918.
(3) Allison J.D., Brown D.S., Novo-Gradac K.J. (1990) *MINTEQA2/PRODEFA2*, a geochemical assessment model or environmental systems: version 3.0 U.S. Environmental Protection Agency, Athens, GA.
(4) Perkins, R.B., C.D. Palmer (2000) Solubility of $Ca_6[Al(OH)_6]_2(CrO_4)_3$-$26H_2O$, the chromate analog of ettringite; 5-75 °C. *Appl. Geochem.*, **15**, 1203-1218.
(5) Lothenbach, B., Matschei, Th., Möschner, G., Glasser, F.P. Thermodynamic modeling of the effect of temperature on the hydration and porosity of Portland cement. Cement and Concrete Research **2008**, *38*, 1-18.

Temperature dependent solubility products of CrO$_4$-ettringite

The temperature dependence of the solubility product for CrO$_4$-ettringite was computed using the measured solubilities from 5-75 °C from Perkins and Palmer (1) and solubilities at 25° from the current study. The thermodynamic properties of the reaction (E1)

E1 $\quad Ca_6[Al(OH)_6]_2(CrO_4)_3 \cdot 26H_2O = 6Ca^{2+} + 2Al(OH)_4^- + 3CrO_4^{2-} + 4OH^- + 26H_2O$
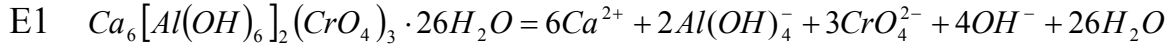
were calculated with GEMS using the built-in three-term temperature extrapolation (2,3) as given by equation E2-E5:.

E2 $\quad \log K_T = A_0 + \dfrac{A_2}{T} + A_3 \ln T$

E3 $\quad A_0 = \dfrac{0.4343}{R} \cdot \left[\Delta_r S_{T_0}^0 - \Delta_r Cp_{T_0}^0 \left(1 + \ln T_0 \right) \right]$

E4 $\quad A_2 = -\dfrac{0.4343}{R} \cdot \left(\Delta_r H_{T_0}^0 - \Delta_r Cp_{T_0}^0 T_0 \right)$

E5 $\quad A_3 = \dfrac{0.4343}{R} \cdot \Delta_r Cp_{T_0}^0$

where A_0, A_2, and A_3 are empirical coefficients of the heat capacity equation and T_0 stands for the reference temperature 298.15 K. $\Delta_r S_{T_0}^0$, $\Delta_r H_{T_0}^0$ and $\Delta_r Cp_{T_0}^0$ are the standard entropy change, standard enthalpy change and standard molar heat capacity change at T_0 and log K_T the solubility product at the temperature of interest T as given in E1. The heat capacity of the reaction $\Delta_r Cp_{T_0}^0 = \Delta_r Cp_T^0 = -1565$ J K^{-1} mol^{-1} is assumed to be constant. The value of $\Delta_r C_p^0$ has in the temperature range 0-100 °C little influence on the calculated log K$_{S0}$ value in equation (E2), which makes it insensitive to the fitting procedure. Thus, the heat capacity of reaction $\Delta_r C_p^0$ = -1565 J K^{-1} mol^{-1} was not fitted but calculated from the heat capacity $\Delta_f C_p°$ of CrO$_4$-ettringite according to reaction E1 using the values given in Table S3. The heat capacity $\Delta_f C_p°$ of

42

CrO_4-ettringite was estimated based on the heat capacity of the structural similar SO_4-ettringite according to equation E6.

E6 $\Delta_f C_p°$ (CrO_4-ettringite) = $\Delta_f C_p°$ (SO_4-ettringite) - 3 $\Delta_f C_p°$ ($CaSO_4$) + 3 $\Delta_f C_p°$ ($CaCrO_4$) = 2215 J K^{-1} mol^{-1} (see table S3).

To describe the solubility product of CrO_4-ettringite as a function of temperature, the entropy of reaction $\Delta_r S_{T_0}^0$ was adjusted to obtain the best visual fit between the experimental data given in Figure S1 and the extrapolated solubility curves using equation E2. The enthalpy of reaction $\Delta_r H_{T_0}^0$ was than obtained from equations E7 and E8 using the experimentally derived solubility product K_{S0} $10^{-40.2}$.

E7 $\Delta_r G_{T_0}^0 = \Delta_r H_{T_0}^0 - T \Delta_r S_{T_0}^0$

E8 $\Delta_r G_{T_0}^0 = -R T_0 \ln K_{T_0}$.

The fitted entropy of reaction $\Delta_r S_{T_0}^0$ of -571 ± 100 J K^{-1} mol^{-1} is in the same range as the value obtained in the paper of Perkins and Palmer (1) of -533 ± 83 J K^{-1} mol^{-1}, the values of $\Delta_r G_{T_0}^0$ = 229.2 kJ/mol and $\Delta_r H_{T_0}^0$ = 59.3 kJ/mol are lower than the respective values of Perkins and Palmer (1) (236.6 and 77.5 kJ/mol) as they calculated with log K_{S0} = -41.4 at 25 °C a lower solubility product than obtained in the present study (log K_{S0} = -40.2).

(1) Perkins, R.B., C.D. Palmer Solubility of $Ca_6(Al(OH)_6)_2(CrO_4)_3 * 26\ H_2O$, the chromate analog of ettringite; 5-75 °C. *Applied Geochemistry* **2000**, *15*, 1203-1218.
(2) Kulik, D. Minimizing uncertainty induced by temperature extrapolations of thermodynamic data: a pragmatic view on the integration of thermodynamic databases into geochemical computer codes. *Proceedings the use of thermodynamic databases in performance assessment*. Barcelona, OECD, **2002**, 125-137.
(3) Kulik, D. Thermodynamic properties of surface species at the mineral-water interface under hydrothermal conditions: a Gibbs energy minimization

single-site 2pKA triple-layer model of rutile in NaCl electrolyte to 250°C. *Geochimica et Cosmichimica Acta*, **2000**, *64*, 3161-3179.
(4) Kulik, D. GEMS-PSI 2.1, PSI-Villigen, Switzerland, 2005 available at http://les.web.psi.ch/Software/GEMS-PSI/.

Table S3 Thermodynamic data at standard conditions (25 °C, 1 atm)

Species	$\Delta_f G°$ kJ/mol	$\Delta_f H°$ kJ/mol	$\Delta_f S°$ J/(molK)	$\Delta_f C_p°$ J/(mol K)	Ref.
H_2O_{liquid}	-237.18	-285.9	69.9	75	[1]
OH^-	-157.27	-230.0	-10.7	-136	[1]
Ca^{2+}	-552.79	-543.1	-56.5	-31	[1]
$Al(OH)_4^-$	-1301.85	-1497.3	110	102	[1]
CrO_4^{2-}	-731.36	-882.5	57.7	-261	[2]
$CaCrO_4^0$	-1299.96	-142.8	45.1	-91	[3]

Solids	$\log K_{s0}$	$\Delta_f G°$ kJmol^{-1}	$\Delta_f H°$ kJmol^{-1}	$\Delta_f S°$ kJmol^{-1}K^{-1}	$\Delta_f C_p°$ kJmol^{-1}K^{-1}	a_0	a_1	a_2	Ref.
CrO_4-ettringite	-40.2 ± 0.4	-15139.8 ± 2.3	-17283 ± 30	2500 ± 100	2215	2112	0.6	-6.8E+06	[4]
SO_4-ettringite	-44.9 ± 0.7	-15205.9	-17535	1900	2174	1939	0.79		[5]
$CaSO_4$ (Anhydrite)	4.4	-1322.1	-1435	107	99.7	70	0.099		[1]
$CaCrO_4$		-1299.2 ± 10	-1402 ± 10	130.9 ±1.9	113.1	128	0.036	-2.3E+06	[6]

(1) GEMS-TDB as given in Thoenen, T.; Kulik, D. Nagra/PSI chemical thermodynamic database 01/01 for the GEM-Selektor (V.2-PSI) geochemical modeling code, **2003**. Available at http://les.web.psi.ch/Software/GEMS-PSI/doc/pdf/TM-44-03-04-web.pdf.
(2) Shock, E. L.; Sassani, D. C.; Willis, M.; Sverjensky, D. Inorganic species in geologic fluids: correlation among standard molal thermodynamic properties of aqueous ions and hydroxide complexes. Geochim. Cosmochim. Acta **1997**, *61*, 907-950.
(3) calculated from the log K_{S0} = 2.77 from Perkins, R.B., C.D. Palmer Solubility of $Ca_6(Al(OH)_6)_2(CrO_4)_3*26 H_2O$, the chromate analog of ettringite; 5-75 °C. Applied Geochemistry **2000**, *15*, 1203-1218 and $\Delta_f C_p^0$ and $\Delta_f S^0$ estimated from $CaCrO_4$ (solid) (6), $CaSO_4$ (solid) (1) and $CaSO_4^0$ (1).
(4) this study
(5) Lothenbach, B., Matschei, Th., Möschner, G., Glasser, F.P.   Thermodynamic modeling of the effect of temperature on the hydration and porosity of Portland cement. Cement and Concrete Research **2008**, *38*, 1-18.
(6) Lee, Y.M., Nassaralla, C.L. Standard free energy of formation of calcium chromate. Materials Science and Engineering **2006**, *A437*, 334-339.
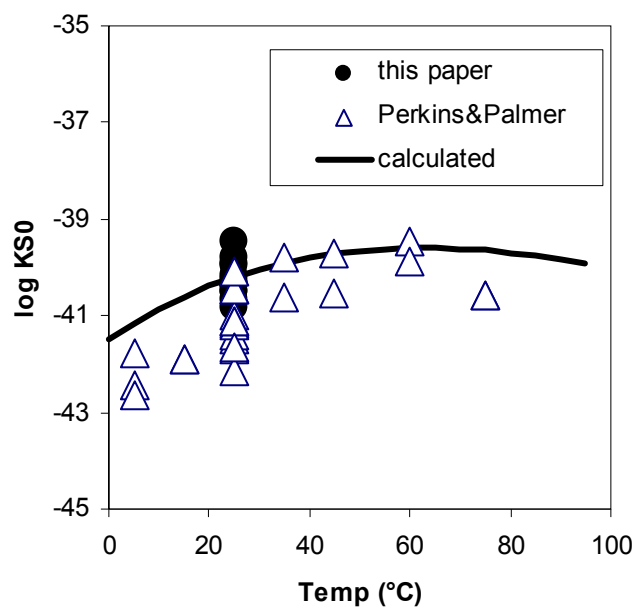
Figure S1 Temperature dependent solubility products of CrO_4-ettringite in the range between 0-100 °C.

Figure S2 SEM picture shows the typical acicular morphology of a solid solution ettringite with $XCrO_4 = 0.3$.

Chapter 3

Thermodynamic modeling of solid solutions between monosulfate and monochromate
3CaO • Al$_2$O$_3$ • Ca[(CrO$_4$)$_x$(SO$_4$)$_{1-x}$] • nH$_2$O

Sabine M. Leisinger, Barbara Lothenbach, Gwenn Le Saout and C. Annette Johnson

Abstract

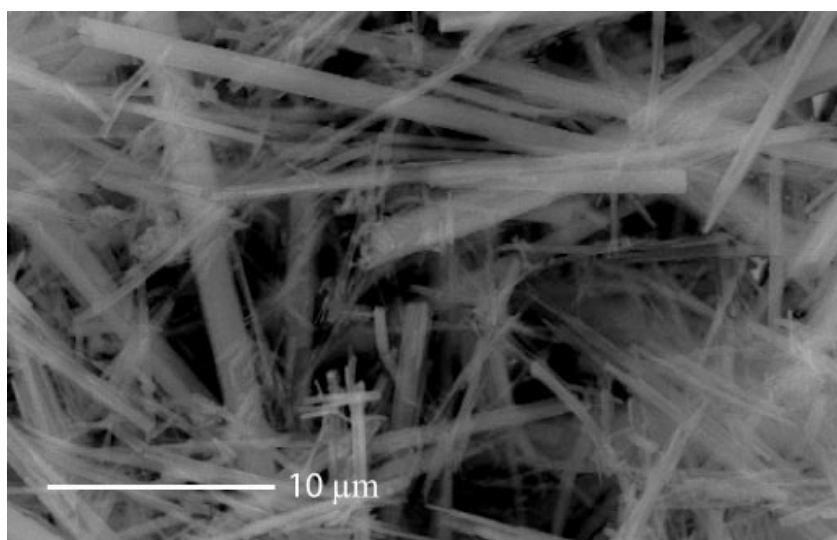In hydrated cement paste AFm-phases are regarded to play an important role in the binding of the toxic contaminant chromate through isomorphic substitution with sulfate. Solid solutions formation can lower the solubility of the solids, thus reducing chromate leaching concentrations.

Solid solutions between monosulfate and monochromate were synthesized and characterized by X-ray diffraction (XRD), thermogravimetric analysis (TGA), scanning electron microscopy (SEM), energy dispersive x-ray spectroscopy (EDX) and inductive coupled plasma optical emission spectroscopy (ICP-OES). Based on the measured ion concentrations in solution total solubility products of the solid solution series was determined.

For pure monochromate a logK= -28.4 ±0.7 was determined. Results from solid and solution analysis showed that limited solid solutions exist. Based on XRD diffractograms a solid solution with a miscibility gap $0.15 < XCrO_4 < 0.85$ with a dimensionless Guggenheim parameter of 2.43 was proposed.

3.1 Introduction

Chromium is a common contaminant in chromate ore processing wastes or wastes from stainless steel production. Chromium, mostly in the form of the trivalent Cr(III) cation, is present also in the earth crust and thus in different cementitious materials such as Portland cement, slag or fly ash. Cr(III) can substitute for Al in most calcium aluminate hydrate phases or precipitate as chromium hydroxide, $Cr(OH)_3$ [1]. Oxidizing conditions and high temperatures as present during clinker manufacturing lead to an oxidation of Cr(III) to Cr(VI), chromate. Ordinary Portland cements (OPC) contain approximately 60 ppm chromate from geogenic sources [2]. Chromate is toxic, in alkaline environment present as oxyanion (CrO_4^{2-}), well soluble and poses thus a significant leaching potential [3, 4] and due to its high toxicity a health risk [3].

For the immobilization of the highly mobile chromate, incorporation into mineral phases becomes the relevant binding mechanism. Among others, AFt- and AFm-minerals have a high anion immobilization potential due to their structures and due to the ease of formation from a wide range of starting materials [5-8]. AFt is shorthand for Alumino-Ferrite-tri phases like ettringite $3CaO \cdot Al_2O_3 \cdot 3CaSO_4 \cdot 32H_2O$ whereas AFm stands for Alumino-Ferrite-mono phases such as monosulfate $3CaO \cdot Al_2O_3 \cdot CaSO_4 \cdot 12H_2O$. The identical charge and comparable radii of SO_4^{2-} and CrO_4^{2-} ions suggest that chromate should readily substitute in the crystal structure of ettringite and monosulfate to form solid solution [Zhang- PhD]. The formation of solid solutions can lower the solubility of the solids, thus reducing chromate leaching concentrations. The solid solutions between CrO_4-and SO_4 ettringite has been previously investigated [Leisinger, 2010] but no data are available concerning the possible solid solution formation between CrO_4- and SO_4-AFm. AFm phases belongs to the double layered hydroxide family (LDH) and consist of a layered crystal structure built by periodical stacking of positively charged $[Ca_2Al(OH)_6 \cdot 2H_2O]^+$

octahedral layers and negatively charged interlayers consisting of anions and water molecules. The structures of the two end members SO_4-AFm and CrO_4 AFm have been described by Allmann [Allmann, 1977] and Segni [Segni, phD] respectively. The layer staking and arrangement of the anions in the interlayer lead to symmetry $R\bar{3}$ for SO_4-AFm and $P\bar{3}$ for CrO_4 AFm. The size of the CrO_4^{2-} (distances Cr-O around 1.69 Å) anion is larger than of the SO_4^{2-} (S-O distances from 1.42 to 1.46 Å) but the main difference is in the position of the anion. The SO_4^{2-} tetrahedral anion, located in the middle of the interlayer, has a pyramidal configuration with the three oxygen atoms closed to the hydroxyl groups in the brucite-like layer and the fourth one pointing toward the opposite hydroxide plane. In the case of the CrO_4^{2-} anion, the configuration is similar but the seventh coordination position of the Ca atoms is occupied statistically either by a water molecule or the fourth oxygen of the CrO_4^{2-} anion. The structure can be described by a stacking of two kinds of layer, one negatively charged $[Ca_2Al(OH)_6\ CrO_4\ H_2O]^-$ and the other positively charged $[Ca_2Al(OH)_6\ 2H_2O]^+$ plus interlayer free water molecules [9]. This grafting reaction in which a layer OH group is replaced by the oxygen of the interlayer anion has also been observed in other AFm structure as CO_3-AFm [10] and NO_3-AFm [11] and may explain why solid solution have been observed between OH and SO_4-AFm while between SO_4 and CO_3 –AFm no solid solution are formed [12]. In this study, we have investigated the solid solution between CrO_4-AFm and SO_4-AFm as for the prediction of long-term chromate leaching potential, the knowledge of the solid solution formation and its stabilising influence are crucial.

3.2   Experimental

3.2.1   Materials

All chemicals were at least of pro analysis (p.a.) grade; $CaCrO_4$, $CaCO_3$, $CaSO_4 \cdot 2H_2O$ and Al_2O_3- powder, KOH solution (1M, Titrisol), HNO_3 Suprapur 65%, ICP-OES multi-elements standard solution IV and SO_4-anion standard solution were used.

All handling of material, sampling and pH measurements were carried out in a glovebox (Mecaplex) equipped with a CO_2 scrubber (pCO_2 < 1ppm, DMP Ltd., Switzerland) to prevent possible CO_2 contamination. Ultrapure water (resistivity >18MΩ.cm) was used for the preparation of solutions and rinsing processes. All polyethylene bottles, tubes and glassware were leached in acid solutions (0.3 M HCl, Merck) for at least 24 h and rinsed three times with ultrapure water.

3.2.2   Synthesis of solid phases

End members: pure SO_4- and CrO_4-AFm. Pure monochromate $3CaO \cdot Al_2O_3 \cdot CaCrO_4 \cdot nH_2O$ was synthesized in triplicate in precipitation experiments at varying pH values from 11 to 14 (n stands for the different possible hydration states). Stoichiometric amounts of freshly burned tricalcium aluminate clinker (C_3A) (4 mmol), and $CaCrO_4$ (4 mmol) were added to 0.001M - 1M KOH solution (50 ml). C_3A was prepared by burning $CaCO_3$ and Al_2O_3 at 1450 °C for 24 hours [13]. The liquid/solid ratio was held constant at 20. The mixtures were equilibrated for 3 months in sealed HDPE bottles (50 ml) at 25 °C on a rotary shaker at 125 rpm. The samples were then centrifuged for 20 min at 4000 rpm. An aliquot of the supernatant (6 ml) was directly used for the measurement of pH and the rest was filtered through 0.45 μm nylon membrane

filters (Titan), and acidified with concentrated HNO_3 Suprapur at a ratio of acid:water equal to 1:100 for ICP-OES.

Synthesis of pure monosulfate $3CaO \cdot Al_2O_3 \cdot CaSO_4 \cdot nH_2O$ was only carried out at a pH of 11. Experimental setup and procedure was accordingly to the synthesis of pure monochromate. The solid residues were washed with acetone, dried and stored in desiccators over silica gel (H_2O absorbent) and soda lime (CO_2 absorbent).

Solid solutions between monosulfate and monochromate. The mixed phases of the series were synthesized according to the following precipitation reaction:

$$(1) \quad \begin{array}{l} C_3A + xCaCrO_4 + (1-x)CaSO_4 \cdot 2H_2O + (10+2x)H_2O = \\ Ca_4[Al(OH)_6]_2(CrO_4)_x(SO_4)_{1-x} \cdot 6H_2O \end{array}$$
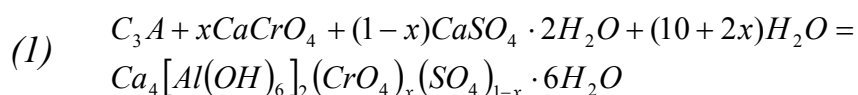
Stoichiometric amounts of freshly burned C_3A (4 mmol), $CaCrO_4$ and/or $CaSO_4 \cdot 2H_2O$ (totally 4 mmol) were mixed with 0.001M KOH solution (50 ml) to obtain different total chromate mole fractions ($XCrO_{4, \text{ TOT}} = [CrO_4^{2-}]$ / ($[CrO_4^{2-}] + [SO_4^{2-}] = 0$, 0.1, 0.2, 0.4, 0.6, 0.8 and 1). While $XCrO_{4, \text{ TOT}}$ represents total chromate mole fractions added to the system, $XCrO_4$ is the chromate mole fraction of the solids that precipitated. Samples are named $Cr[XCrO_4]$ such as Cr0 for pure monosulfate $4CaO \cdot Al_2O_3 \cdot CaSO_4 \cdot 12H_2O$ and Cr1 for pure monochromate $4CaO \cdot Al_2O_3 \cdot CaCrO_4 \cdot 12H_2O$.

Since equilibration of solid solutions may take longer than for pure phases [14], the mixtures were stored for 6 month. Then the solid residues were also washed with acetone, dried and stored in desiccators over silica gel (H_2O absorbent) and soda lime (CO_2 absorbent).

3.2.3   Characterization of the solid phases

After drying, the samples were ground by hand with an agate mortar to <63 μm and analyzed by X-ray diffraction (XRD), thermogravimetric analysis (TGA), scanning electron microscopy (SEM), energy dispersive x-ray spectroscopy (EDX) and inductive coupled plasma optical emission spectroscopy (ICP-OES).

SEM was used to control the morphology of the solid phases. The measurements were done with a Nova Nano SEM 230 FEI at high vacuum mode. Solid stoichiometry was determined using ICP-OES. 0.1 g of a solid sample was dissolved in 500 μl HNO_3 Suprapur in a 50 ml HDPE bottle and filled with ultrapure water to 50 ml. Samples were diluted 1:10 and 1:100 prior to measurement. TGA was carried out on a TGA/SDTA 851 apparatus by Mettler Toledo. The samples (8 - 12 mg) were heated under N_2 over a temperature range of 30 - 980 °C at a rate of 20 °C/min. TGA was carried out to observe mass changes in relation to changes in temperature and time. The determined mass losses were used to determine the water content of the solids and to estimate fractions of the solid that was CO_2. Measurements were carried out in triplicate. The purity, crystallinity and the solid solution examination of the products were analyzed by X-ray diffraction (XRD) using a PANalytical X'Pert PRO XRD system with CuKα radiation. Elemental silicon was mixed to the powder samples as internal standard for the determination of the unit cell parameters. The evaluation software X'Pert HighScore Plus was used for phase identification and solid solution examinations. The unit cell parameters for monosulfate were determined using Rietveld refinement of the structure proposed by Allmann et al [15] and for monochromate a Le Bail fit was carried out [16]. At 98% rh, the unit cell parameters of the monochromate phase deduced by a Le Bail fit a= 5.74 Å and c=30.72 Å (interlayer distance 10.2 Å) correspond well to those given in the PDF file 00-052-0654 (a= 5.75 Å and c=30.73 Å, interlayer distance 10.2 Å) [17]. The unit cell length along the z axis

differs from the value obtained by Segni [18] (a= 5.75 Å and c=20.16 Å, interlayer distance 10.1 Å) and attempts to perform Rietveld analysis based on the structure proposed in [18] were not successful. This difference may be explained by the existence of different positions of the CrO_4^{2-} anion in the interlayer depending on the way of synthesis. Unfortunately, strong preferred orientation and broad peaks of the pattern do not permit a structure refinement of our sample.

To study the effect of relative humidity on AFm phases, a climatic chamber (Anton Paar THC) specially designed for the X-ray diffractometer was used in order to control both temperature and relative humidity. The relative humidity was increased up to 98 % and stabilized at a temperature of about 20 °C.

3.2.4   Characterization of the liquid phase

The pH measurement was carried out with an Aquatrode Plus, Pt 1000 electrode from Metrohm.   Prior to the measurements the pH electrode was calibrated by titration with fresh KOH-solutions (0.001-1 M) to minimize the alkali error, i.e. the error in the pH measurements caused by the presence of high concentrations of alkalis such as potassium or sodium. Alkali ions interfere with the H^+ resulting in a measured pH value that is lower than the actual pH. The alkali error increases with increasing pH values, higher alkali concentrations and increasing temperatures. The voltage reading was correlated to the calculated target pH-value of the respective KOH-solution considering ionic strength as well as the measured temperature of the solution. Dissolved concentrations of Ca, Al, K, Cr and SO_4, were determined by ICP-OES according to the method described for solid phases. Charge balance errors of all samples were <10 %.

3.2.5   Thermodynamic modeling

GEMS is a broad purpose geochemical modeling code. The principle of GEMS is the minimization of the Gibbs energy of a complex chemical system. It computes mass balances, based on equilibrium phase assemblages and speciation in a complex chemical system from its total bulk elemental composition. Chemical interactions involving solids, solid solutions, gas mixture and aqueous electrolyte are considered simultaneously [19]. A built-in thermodynamic database [20] is provided. This database can easy be extended and fitted to the user-defined projects. The thermodynamic data used are compiled in Table 1.

Activity coefficients of aqueous species y_i were then computed with the built-in expanded extended Debye-Hückel equation in Truesdell-Jones form (equation 2).

$$(2) \quad \log \gamma_i = \frac{-A_y z_i^2 \sqrt{I}}{1 + B_y a_i \sqrt{I}} + b_y I$$

where z_i denotes the charge of species i, I the effective molal ionic strength, a_i is a parameter dependent on the size of ion i, b_y is a semi-empirical parameter (0.64 at 25°C), and A_y and B_y are P,T-dependent Debye-Hückel solvent parameters. This activity correction should be applicable up to 1-2 m ionic strength [19, 20]. The measured ion concentrations were used as input in GEMS for the calculation of the solubility product (log K). Based on the calculated ion activities (using the extended Debye-Hückel equation), the solubility products of pure CrO_4- and SO_4-AFm were calculated. All calculated solubility products were converted to zero ionic strength.

Table 1 Thermodynamic data used for speciation calculations.

Reaction	log K_{S0}	Ref.
Aqueous Species		
$H_2O = OH^- + H^+$	-14 .0	[20]
$K^+ + H_2O = KOH^0 + H^+$	-14.46	[20]
$Ca^{2+} + H_2O = CaOH^+ + H^+$	12.78	[20]
$Ca^{2+} + HCO_3^- = CaHCO_3^+$	1.11	[20]
$Ca^{2+} + HCO_3^- = CaCO_3 + H^+$	-7.11	[20]
$SO_4^{2-} + H^+ = HSO_4^-$	1.99	[20]
$Ca^{2+} + SO_4^{2-} = CaSO_4^0$	2.3	[20]
$K^+ + SO_4^{2-} = KSO_4^-$	0.85	[21]
$CrO_4^{2-} + 2H^+ = H_2CrO_4^0$	6.31	[22]
$CrO_4^{2-} + H^+ = HCrO_4^-$	6.55	[22]
$2CrO_4^{2-} + 2H^+ - H_2O = Cr_2O_7^{2-}$	4.7	[22]
$Ca^{2+} + CrO_4^{2-} = CaCrO_4^0$	2.77	[23]
$K^+ + CrO_4^{2-} = KCrO_4^-$	0.78	[21]
$Al^{3+} H_2O = AlOH^{2+} + H^+$	-4.96	[20]
$Al^{3+} + 2H_2O = Al(OH)^+_2 + 2H^+$	-10.59	[20]
$Al^{3+} + 3H_2O = Al(OH)_3^0 + 3H^+$	-16.43	[20]
$Al^{3+} + 4H_2O = Al(OH)_4^- + 4H^+$	-22.88	[20]
$Al^{3+} + SO_4^{2-} = AlSO_4^+$	3.9	[20]
$Al^{3+} + 2SO_4^{2-} = Al(SO_4)_2^-$	5.9	[20]
Solid phases		
Portlandite $Ca(OH)_2 + 2H^+ = Ca^{2+} + 2H_2O$ -	22.8	[20]
Gypsum $CaSO_4 * 2H_2O = Ca^{2+} + SO_4 + 2H_2O$	-4.58	[20]
Calcite $CaCO3(s) + H^+ = CaHCO^{3+}$	1.85	[20]
Al-hydroxide am. $Al(OH)_{3, amph} + OH^- = Al(OH)_4^-$	0.24	[20]
calcium chromate $CaCrO_4 = Ca^{2+} + CrO_4^{2-}$	-2.77	[24]
CrO$_4$-AFm $Ca_4(Al(OH)_6)_2(SO_4)*6H_2O =$		
$4Ca^{2+} + 2Al(OH)_4^- + SO_4^{2-} + 4OH^- + 6H_2O$	-29.7 $_{+/- 04}$	this study
SO$_4$-AFm $Ca_4(Al(OH)_6)_2(CrO_4)*6H_2O =$		
$4Ca^{2+} + 2Al(OH)_4^- + CrO_4^{2-} + 4OH^- + 6H_2O$	-28.4	$_{+/-0.7}$

this study

3.3 Experimental results and discussion

3.3.1 Solid analysis

SEM. The two pure phases, monosulfate and monochromate, exhibited a different morphology both in size and shape (Figure 1 top left and top right). While pure monosulfate crystallized to a euhedral hexagonal platelets shape with diameters of around 20 μm, monochromate crystallites precipitated as subhedral platelets with a diameter around a few micrometers. Crystallites in the mixtures formed at different sizes and morphologies. Some crystallites showed clear hexagonal platelets corresponding to monosulfate, while at others only layered platelets without sharp borders were observed (Figure 1, at the bottom). Samples looked as if they were a mechanical mixture of both end members SO_4- and CrO_4-AFm. Additionally, traces of ettringite-needles were observed in all samples with increased amounts the higher the $XCrO_4$ of the solids.

Chemical composition by ICP-OES. Measured chromate mole fractions of the solid ($XCrO_4$) agreed with total chromate mole fractions ($XCrO_{4,\,TOT}$) of the prepared experiments for samples $0<XCrO_{4,TOT}<0.4$ (Table 2).

At higher $XCrO_{4,\,TOT,}$ precipitated solids contained a lower $XCrO_4$ than expected. The chemical analyses give the composition of the bulk samples. However, as no other chromate of sulfate containing solids than the AFm-phases were detected (with exception of traces of ettringite in the pure and high sulfate samples), the bulk composition was assumed to correspond to the AFm-composition. The differences between the precipitated $XCrO_4$ in the solids and the $XCrO_{4,\,TOT}$ in the system is due to the around 10 times lower solubility product (~1 log unit) of pure SO_4-AFm (logK = -29.6) compared to pure CrO_4-AFm (logK = -28.4), see results below, indicating a higher stability of the SO_4-AFm. Thus the solid samples prepared at a higher $XCrO_{4,TOT}$ were more enriched in SO_4 than the corresponding solutions. This observation is

comparable to the findings of other solid solution precipitation experiments [8, 25]. In the present paper, all samples are labelled according to the precipitated $XCrO_4$ (nomenclature in the last column of table 2).

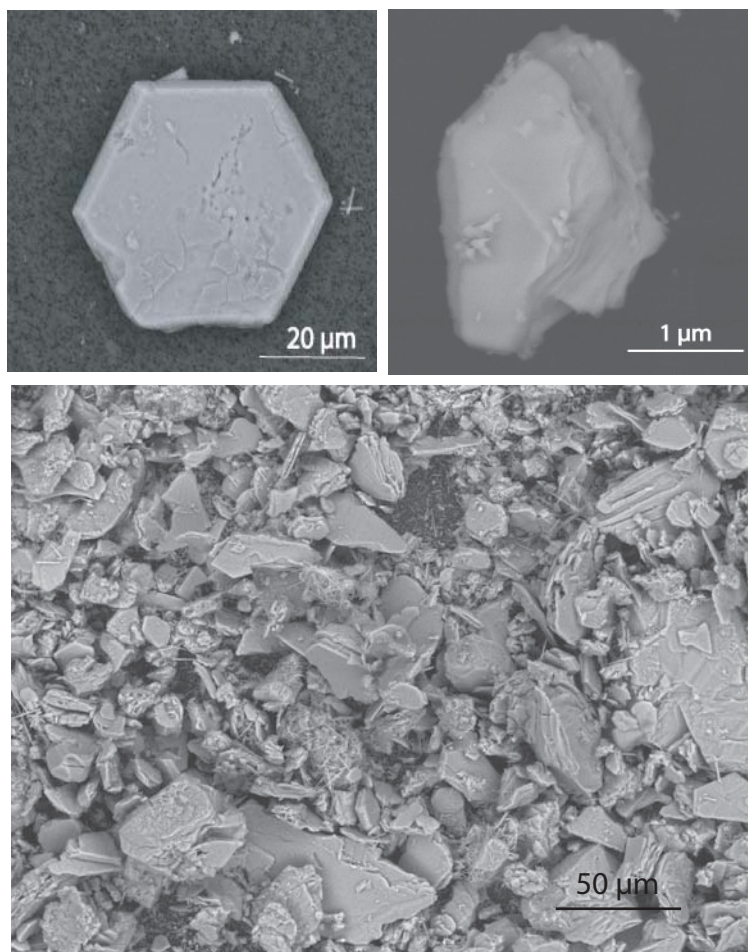**Figure 1** SEM pictures showed pure SO_4-AFm (top left) and pure CrO_4-AFm (top right). The crystals of sample Cr0.5 varied both in size and shape (at the bottom). Traces of ettringite were observed especially in samples with increased $XCrO_4$ content.

Table 2 Results of solid digest analyses of synthesized $Ca_4(Al(OH)_6)_2(CrO_4)_x(SO_4)_{1-x} \cdot n\ H_2O$.

[a]$XCrO_{4,TOT}$	Ca	Al	CrO_4	SO_4	Ca	Al	CrO_4	SO_4	$XCrO_4$[b]
	mg/g solid				normalized to 4 Ca				
0	261.5	103.7		210.0	4	2.4	0.0	1.3	**0**
0.1	248.2	101.5	10.4	180.0	4	2.4	0.1	1.2	**0.1**
0.2	230.1	94.3	18.7	150.0	4	2.4	0.3	1.1	**0.2**
0.4	242.9	99.0	41.2	125.0	4	2.4	0.5	0.9	**0.4**
0.6	250.0	103.3	60.9	95.0	4	2.4	0.7	0.6	**0.5**
0.8	247.2	101.3	75.3	85.0	4	2.4	0.9	0.6	**0.6**
1	231.9	92.3	108.9	0.0	4	2.4	1.4	0.0	**1**

[a] chromate mole fractions = $[CrO_4]/ ([CrO_4] +[SO_4])$ present in the system
[b] chromate mole fraction of solids precipitated

TGA. Thermogravimetric analysis showed that total mass lost of the samples with $0< XCrO_4 <0.5$ and dried over silica gel was between 30.4 - 30.8 weight %. This corresponds to a stable hydration state of 10 ±0.4 water molecules per mole substance $3CaO \cdot Al_2O_3 \cdot Ca[(SO_4)_{1-x},(CrO_4)_x] \cdot \mathbf{10}H_2O$. Pure CrO_4-AFm showed a smaller mass lost of 29.4 weight % corresponding to a hydration state of 9 ±0.1 (Figure 2). The dehydration behavior between 50 and 250 °C where the loosely bound water from the interlayer is lost, depends on the drying method which determines the hydration states of the samples; AFm phases may have several different water contents [26]. At a temperature higher than 250 °C water loss of the main layer is observed. An additional peak between 700 -750 °C belongs to mass lost from volatile CO_2. However the CO_2 contaminations were very small (<1 weight %) and only observed in CrO_4-AFm and the sample Cr0.6.
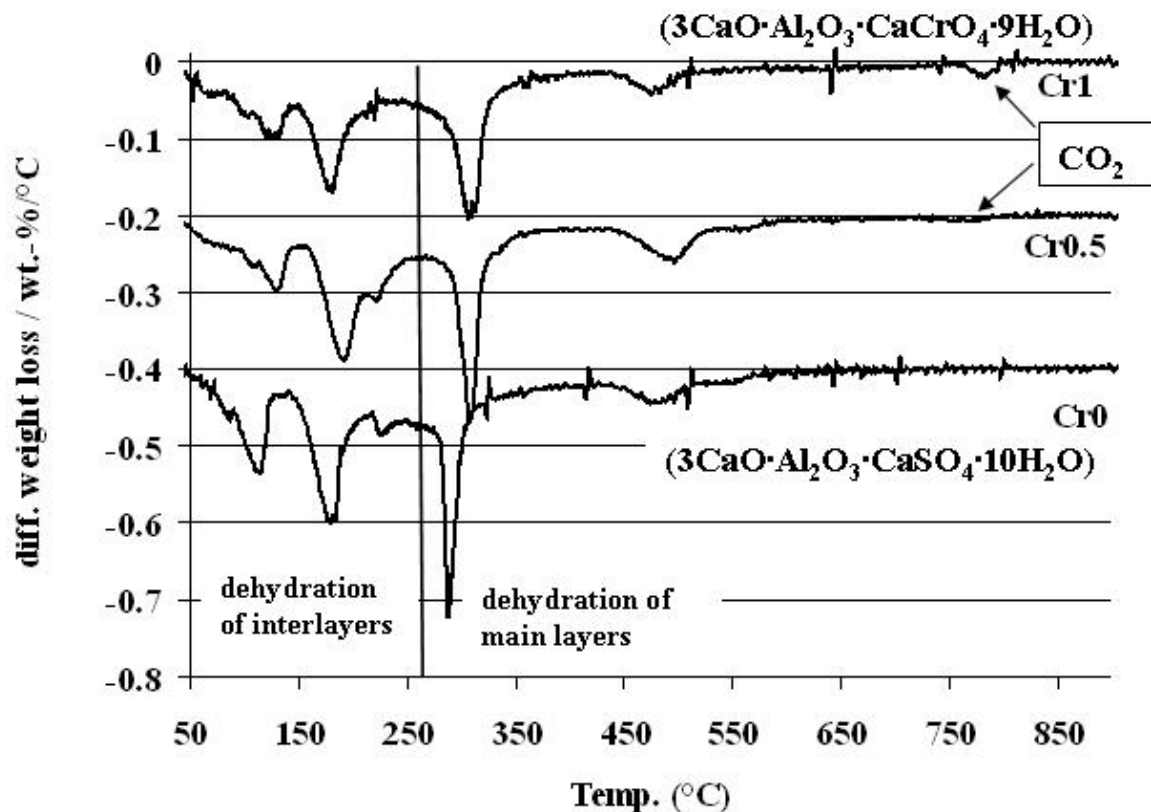
Figure 2 DTGA measurements of monosulfate (Cr0) and monochromate (Cr1) and the solid solution sample (Cr0.5) showed the dehydration steps of the interlayers (50-250 °C) and the main weight loss of the main layers (at 290-300 °C). The dehydration of the main layer moved to higher temperatures for samples with higher $XCrO_4$ content. Traces of CO_2 ingress (~ 760 °C) is observed in Cr1 and the solid solution sample Cr0.5.

XRD of pure CrO_4-AFm. First XRD analyses of pure CrO_4-AFm phases were carried out at increasing relative humidity (r.h.) (Figure 3). Starting at an ambient r.h. of approximately 35 % the peak (009) corresponded well to the CrO_4-AFm with a hydration state of 9 compared to the database file (PDF 00-042-0063) of the International Center for Diffraction Data (ICDD). With increasing r.h. the peak shifted to lower 2θ values and hydration states of 12 and 14 could be identified (PDF files 00-041-0478 and 00-052-0654 respectively). These results are in good agreement with previous results [17, 27-29]. When

fully hydrated samples were subjected to lower humidity's, water molecules were released quickly released again and the peak shifted back to higher 2θ values (Figure 3). The peak shifting can be explained by the increased amount of water molecules present in the interlayers causing a swelling at high r.h. and the release of the water molecules from the interlayers resulting in a shrinking. This shows that SO_4- and CrO_4-AFm phases are extremely sensitive to relative humidity and that the process of water uptake and release is reversible.
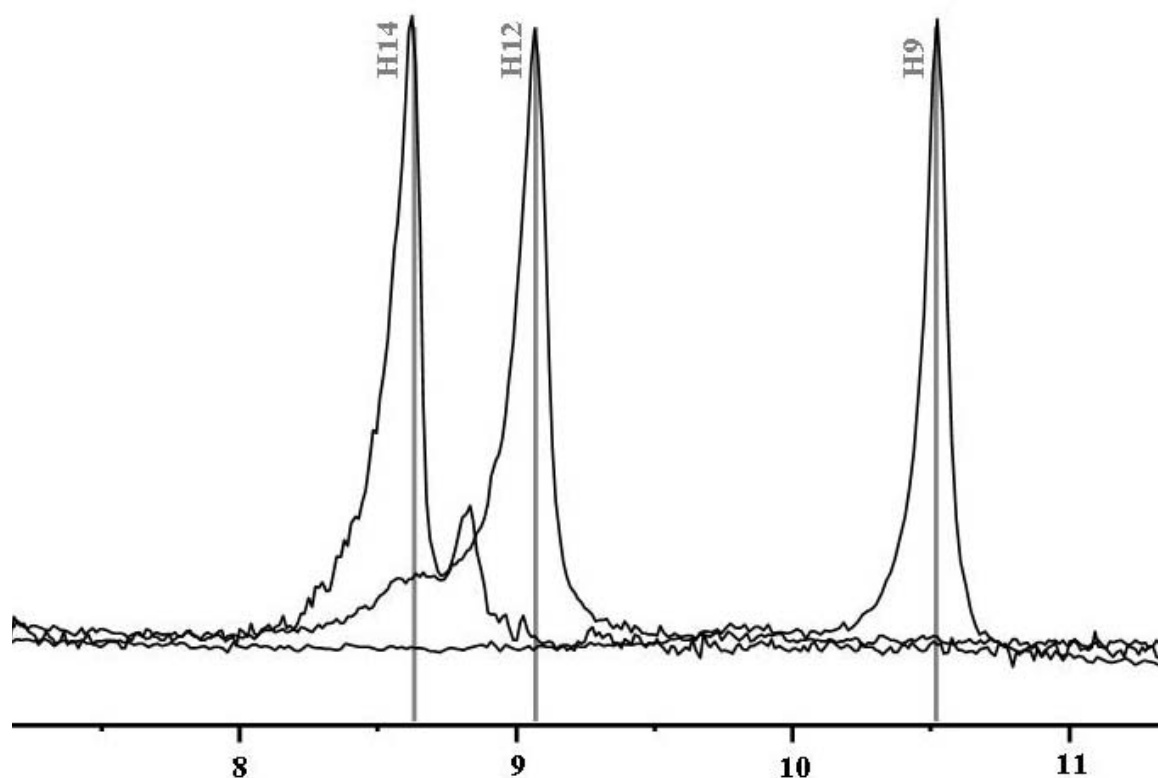
Figure 3 Monochromate peak (003) from XRD measurements show the shifts to higher 2 Theta values with decreasing relative humidity (rh). Starting at 98 % rh monochromate with a hydration state of 14 was observed (Cr14). At lower rh hydration states of 12 and 9 (ambient rh) are shown. Water uptake and release according to the humidity conditions was a reversible process and occurred within a few minutes. The following PDF files correspond to the grey lines: Cr14 to 00-052-0654, Cr12 to 00-041-0478 and Cr9 to 00-042-0063.

XRD of mixed phases. Beside the several existing hydration states a peak shift occurs also through possible ion exchange with different ionic radius (Cr^{6+} =0.4 Å, S^{6+} =0.26 Å) [30]. The chromium radius is larger than the sulfur radius. Thus, with increasing $XCrO_4$ in the sample the more CrO_4 is present in the interlayer and the larger the interlayer distance becomes - causing a peak shift to lower 2 θ values.

The freshly prepared mixed samples were measured at ambient r.h. (~35). The diffractograms showed well crystallized phases (Figure 4). The CrO_4-AFm end member correlated well to monochromate with $3CaO \cdot Al_2O_3 \cdot CaCrO_4 \cdot \mathbf{9}H_2O$ as illustrated above. For monosulfate dried at ambient r.h. a peak was observed at 2< theta> =10.5° (d-spacings 8.42 Å). This corresponds to $3CaO \cdot Al_2O_3 \cdot CaSO_4 \cdot \mathbf{10.5}$ H_2O according to Pöllmann [26] and to $3CaO \cdot Al_2O_3 \cdot CaSO_4 \cdot \mathbf{10}H_2O$ according to Dosch [31].

The analysis of the solid solution series shows that clear peak shifting occurs except for sample Cr0.1 (Figure 4). Starting at pure CrO_4-AFm the peak shifts more and more to higher 2<theta> values with decreasing $XCrO_4$ in the sample. Only in sample Cr0.1 the peak is not visible any more. Starting at the bottom at the SO_4-AFm end member the peak as well shifts with increasing $XCrO_4$ to lower 2<theta> values as expected. These peak shifts are due to the anion exchange between SO_4 and CrO_4 indicating that solid solution forms. However, since in all the samples (again except Cr0.1) we observe 2 distinct peaks instead of one, two mixed phases SO_4-CrO_4 AFm phases are present. One of these phases is mainly composed of CrO_4 while the other one mainly contains SO_4 anions. The presence of two peaks is not obvious in the sample Cr0.6. The small picture to the right of figure 4 reveals a small but not insignificant second peak close to the SO_4-AFm end member.
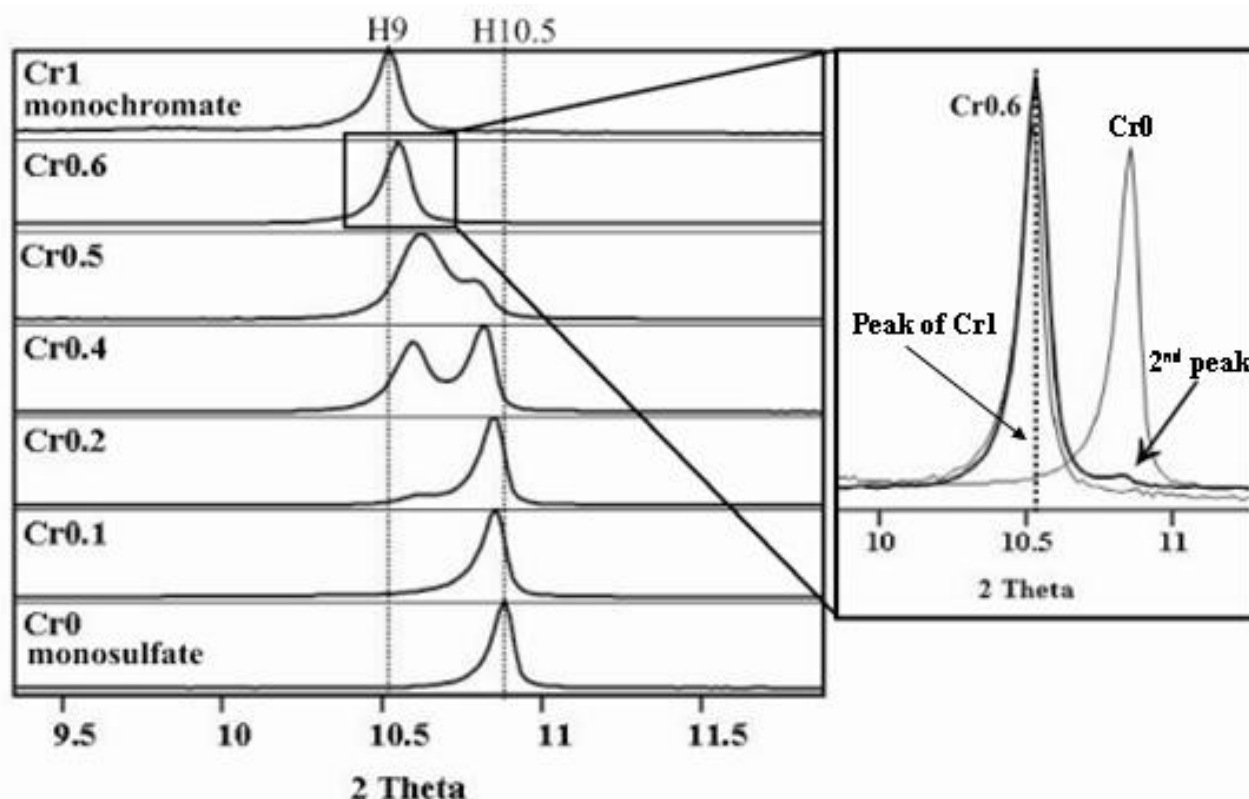
Figure 4 Peak (003) of freshly dried mixture samples between monochromate (Cr1) and monosulfate (Cr0) were measured at a relative humidity ~30% Cr1 had a hydration state of 9 (H9 in figure) corresponding to PDF 00-042-0063). Monosulfate corresponds to a hydration state of 10.5 according to Pöllmann [26] and 10 after Dosch [31]. Except sample Cr0.1 where only one slightly shifted peak was observed, all other mixtures showed a small shift and peak splitting. The picture of the zoomed Cr0.6 sample reveals as well a second peak - peak splitting.

Due to the observed strong preferred orientation of the crystals, the quality of the peaks was too poor to carry out Rietveld refinements except for pure SO_4-AFm samples. Further investigations on better crystallized samples would be needed to investigate the influence of the positions of the anions in the interlayer on the ability to form solid solutions. Since the SO_4-AFm crystals were large (see figure 1) compared to mixed phases and pure CrO_4-AFm, there were enough counts for all peaks to carry out a Rietveld refinement. Unit cell parameters a and c of 5.76 Å and 26.86 Å were determined. For all other

samples the d-spacing values are determined with a reasonable accuracy (Figure 5). For the two end members values of 8.12 Å and 8.40 Å for SO_4- and CrO_4-AFm respectively were determined. Figure 5 shows the two values for each sample except for Cr0.1 indicating the peak splitting.

The peak shifts observed in the XRD analysis show the formation of a solid solution between SO_4-and CrO_4-AFm, the peak splitting at $XCrO_4 \geq 0.2$ the existence of a miscibility gap. The lower boundary of the gap lies between $0.1 < XCrO_4 > 0.2$, thus a value of 0.15 was estimated. Since no samples between $0.6 < XCrO_4 > 1$ have been measured, an exact upper miscibility boundary cannot be set. Due to this lack of data, the most simple model, i.e. the presence of a regular solid solution, is assumed corresponding to a symmetric miscibility gap between $0.15 \leq XCrO_4 \leq 0.85$ (Figure 5). Additional investigations would be needed to verify or reject this upper limit of the miscibility gap.

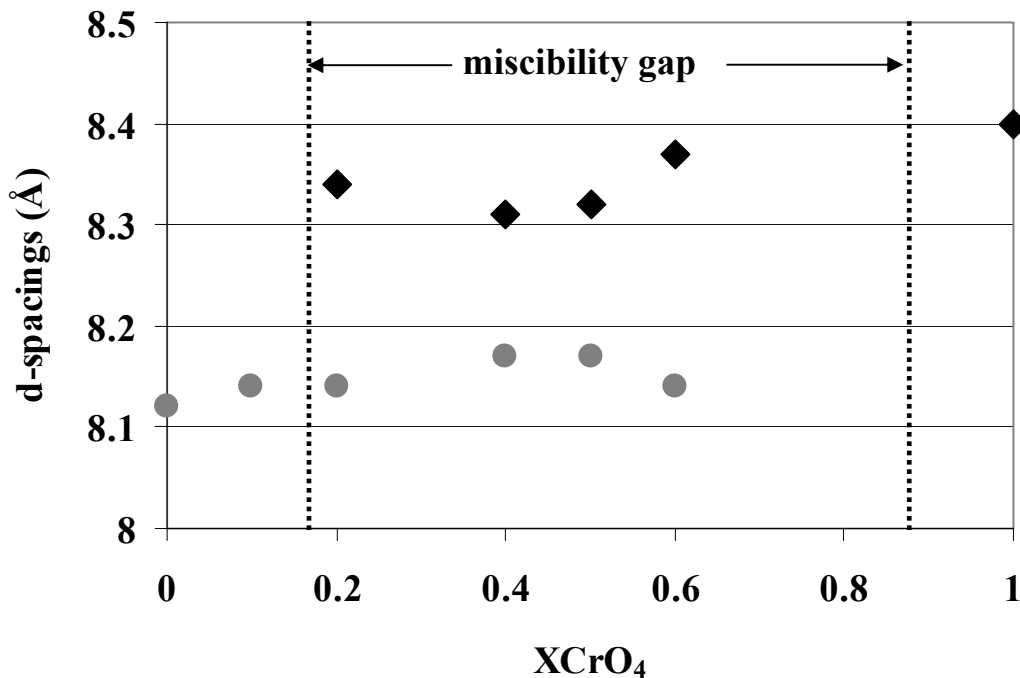**Figure 5** Observed d-spacings of the mixture samples including pure monosulfate ($XCrO_4$ =0) and monochromate ($XCrO_4$ =1). The black dotted lines indicate a miscibility gap between $0.15 \leq XCrO_4 \leq 0.85$.

3.3.2 Solution analysis and thermodynamic modeling

Measured ion concentrations in solution show that with increasing XCrO4 of the sample higher concentrations are present in solution. This is expected since pure SO_4-AFm has a lower solubility than CrO_4-AFm. Since traces of ettringites were observed in samples with higher XCrO4 content small shifts in the determined bulk concentrations occure for AFm phases. However, since no ettringite was observed in the XRD pattern, the amount of ettringite must be <1 weight%. Additionally, the presence of a secondary phase does not disturb solubility calculations as long as thermodynamic equilibrium has reached.

Solubility product of pure CrO_4- and SO_4-AFm. Based on measured ion concentrations from the pH dependent precipitation experiments, modeled ion activities, denoted by { }, were used to calculate the solubility products (logK) of CrO_4-AFm according to equation 3:

(3) $\quad \log K_{CrO_4-AFm} = 4\log\{Ca^{2+}\} + 2\log\{Al(OH)_4^-\} + \log\{CrO_4^{2-}\} + 4\log\{OH^-\} + 6\log\{H_2O\}$

A mean $logK_{CrO4-AFm}$ = -28.4 ± 0.7 was determined (Figure 6, Table 3). No trend of the CrO_4-AFm solubility product with pH was observed. This value is somewhat lower than the published value of Perkins [7] with a $logK_{CrO4-AFm}$ = -30.4 ±0.3. Recalculation of the data using the published concentrations of Perkins and Palmers [7, 32] gave a $logK_{CrO4-AFm}$ = -30.0 ±0.5. The solubilities measured by Zhang [33] gave $logK_{CrO4-AFm}$ = -29.4 ±0.3.

The solubility product of pure SO_4-AFm was determined according to equation 3 (with SO_4 instead of CrO_4) resulting in a $logK_{SO4-AFm}$ = -29.7 ±0.4. This corresponds well to the $logK_{SO4-AFm}$ = -29.3 published by Matschei [34].

Table 3 CrO$_4$-AFm solubility (at I = 0) was determined by precipitation experiments between pH 11 and 14. Measured ion concentrations are listed.

| Sample_pH	KOH (mM)	Ca (mmol/l)	Al (mmol/l)	Cr (mmol/l)	logK CrO$_4$-Afm
Cr1_14	1000	0.4	2.9	5.1	-28.5
Cr1_14	1000	0.4	3.2	4.7	-28.6
Cr1_14	1000	0.3	1.7	4.8	-29.7
Cr1_13.75	560	0.5	3.2	1.5	-28.5
Cr1_13.75	560	0.7	1.3	7.4	-28.2
Cr1_13.75	560	0.4	1.2	5.5	-29.5
Cr1_13.5	320	0.3	2.5	1.2	-29.7
Cr1_13.5	320	0.9	0.6	2.6	-28.8
Cr1_13.25	180	3.0	0.03	6.9	-29.3
Cr1_13.25	180	3.1	0.04	5.2	-29.0
Cr1_13	100	6.7	0.1	0.6	-27.8
Cr1_13	100	0.1	2.9	0.3	-28.1
Cr1_12.75	60	3.9	0.1	3.2	-28.5
Cr1_12.5	30	10.1	0.02	2.2	-28.7
Cr1_12.5	30	5.4	0.1	0.3	-29.3
Cr1_12.25	20	3.4	1.7	0.03	-28.7
Cr1_12.25	20	3.5	1.6	0.03	-28.8
Cr1_12.25	20	3.3	0.6	0.2	-28.8
Cr1_12	10	4.7	1.1	0.1	-28.4
Cr1_12	10	4.3	1.4	0.3	-27.9
Cr1_12	10	4.3	1.9	0.1	-28.5
Cr1_11.75	6	8.1	0.4	3.8	-27.8
Cr1_11.5	3	6.7	1.6	0.1	-27.7
Cr1_11.5	3	7.9	0.2	2.8	-28.5
Cr1_11.5	3	11.5	0.04	6.0	-29.2
Cr1_11.25	2	8.5	2.8	0.01	-28.0
Cr1_11.25	2	6.6	1.5	0.3	-27.6
Cr1_11.25	2	8.0	2.6	0.4	-26.7
Cr1_11	1	6.6	2.1	1.7	-27.4
Cr1_11	1	7.3	2.1	1.9	-27.1
Cr1_11	1	6.4	1.9	0.1	-28.3
Average					**-28.4**
stand. dev.					**0.7**
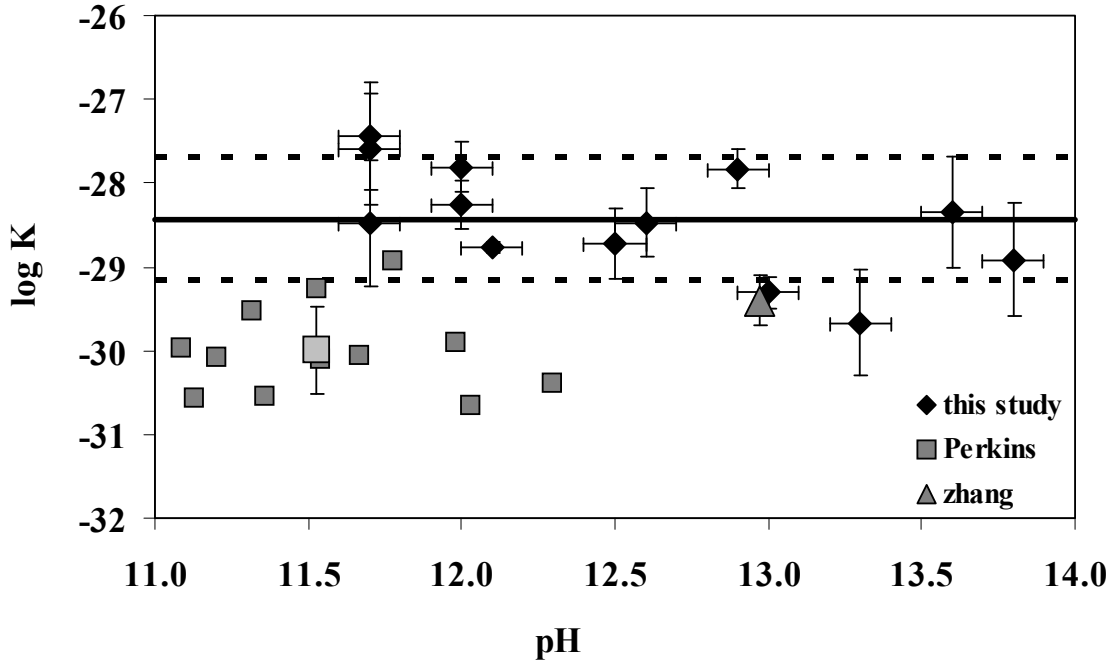
Figure 6 Solubility products of monochromate determined from precipitation experiments at 25 °C between the pH range 11 and 14 resulted in a mean of logK -28.4 +/-0.7 at I=0. Solubility products recalculated from the data given by Perkins and Palmer [7, 32] and Zhang [33] have a lower solubility.

3.2.2 Monosulfate-monochromate solid solutions.

Solubility data of the binary solid solution system are plotted in the frequently used Lippmann diagram using the total solubility product (Figure 7) [35, 36]. The total solubility product ($\sum\Pi$) of solid solutions equals the sum of the partial solubility products (equation 4 and 5) of each end member, if the system has reached thermodynamic equilibrium. Adding up the left side of equation 4 and 5 results in equation 6 and equation 7 is the sum of the right side of equation 4 and 5 leading to the following definitions of the total solubility products $\sum\Pi$.

$$(4)\quad K_{SO4-AFm} \cdot X_{SO4-AFm} \cdot \gamma_{SO4-AFm} = \{Ca^{2+}\}^4 \cdot \{Al(OH)_4^-\}^2 \cdot \{SO_4^{2-}\} \cdot \{OH^-\}^4 \cdot \{H_2O\}^6$$

$$(5)\quad K_{CrO4-AFm} \cdot X_{CrO4-AFm} \cdot \gamma_{CrO4-AFm} = \{Ca^{2+}\}^4 \cdot \{Al(OH)_4^-\}^2 \cdot \{CrO_4^{2-}\} \cdot \{OH^-\}^4 \cdot \{H_2O\}^6$$

$$(6)\quad \Sigma\Pi = K_{CrO4-AFm} \cdot X_{CrO4-AFm} \cdot \gamma_{CrO4-AFm} + K_{SO4-AFm} \cdot X_{SO4-AFm} \cdot \gamma_{SO4-AFm}$$

$$(7)\quad \Sigma\Pi = \{Ca^{2+}\}^4 \cdot \{Al(OH)_4^-\}^2 \cdot [\{CrO_4^{2-}\} + \{SO_4^{2-}\}] \cdot \{OH^-\}^4 \cdot \{H_2O\}^6$$

67

The waved brackets indicate ion activites, $K_{CrO4\text{-}AFm}$ and $K_{SO4\text{-}AFm}$ represent the solubility products of pure CrO_4- and pure SO_4-AFm, $X_{CrO4\text{-}AFm, \, SO4\text{-}AFm}$ are the chromate and sulfate mole fractions of the solid solution ($X_{CrO4\text{-}AFm}$ +$X_{SO4\text{-}AFm}$ =1) and $\gamma_{CrO4\text{-}AFm,}$, $\gamma_{SO4\text{-}AFm}$ are the solid activity coefficient (with f=1 for ideal solid solutions). Solid activity coefficients are needed since the solid phase composition in a solid solution system changes according to variations in solution composition. The solid activity in a regular solid solution is no longer 1 as it is per definition for pure solids and in ideal solid solutions [14]. The solid activity coefficients can be expressed by the Guggenheim expansion series modified by Redlich and Kister expressions (equation 8 and 9) [37].

(8) $\ln \gamma_{CrO4-AFm} = X^2_{SO_4-AFm} \left[a_0 - a_1 \left(3X_{CrO_4-AFm} - X_{SO_4-AFm} \right) + a_2 (...) \right]$

(9) $\ln \gamma_{SO4-AFm} = X^2_{CrO_4-AFm} \left[a_0 - a_1 \left(3X_{SO_4-AFm} - X_{CrO_4-AFm} \right) + a_2 (...) \right]$

A regular solid solution series (with a symmetric miscibility gap) only needs one Guggenheim fitting parameter (a_0) which was determined by the MBSSAS code [38] based on the observed miscibility gap between 0.15<XCrO$_4$>0.85. A value of a_0=2.43 resulted and was used to calculate the SO_4- and CrO_4-AFm end member activity coefficients.

Calculated total solubility products are illustrated in Figure 7 (black points). Three different calculation models were compared to the experimentally determined points of log$\sum\Pi$. The first model does not consider any solid solution formation, but assumes the presence of two solids. This means for the solubility products to be constant as indicated by the two doted lines at -29.6 for SO_4-AFm and -28.4 for pure CrO_4-AFm. Secondly, an ideal solid solution model was used, illustrated as by the grey line in Figure 7. An ideal solid solution model (activity coefficient=1) could have been used if no peak splitting and thus no miscibility gap would have been observed. The third and most realistic solid solution model included a miscibility gap, 0.15<XCrO$_4$>0.85

(black line). However, based on the determined $\sum \Pi$, it cannot be decided whether and which kind of solid solution is present due to the relatively large error associated with the total solubility products (Figure 7) and due to the small difference between the solubility products of pure SO_4- and CrO_4-AFm phases. The presence of a solid solution with a miscibility gap is concluded from the peak shifts observed in the XRD patterns and from the observation that the solubility products of the SO_4- and CrO_4-AFm end-members (see the last two columns in table 4) vary systematically with increasing sulfate content.
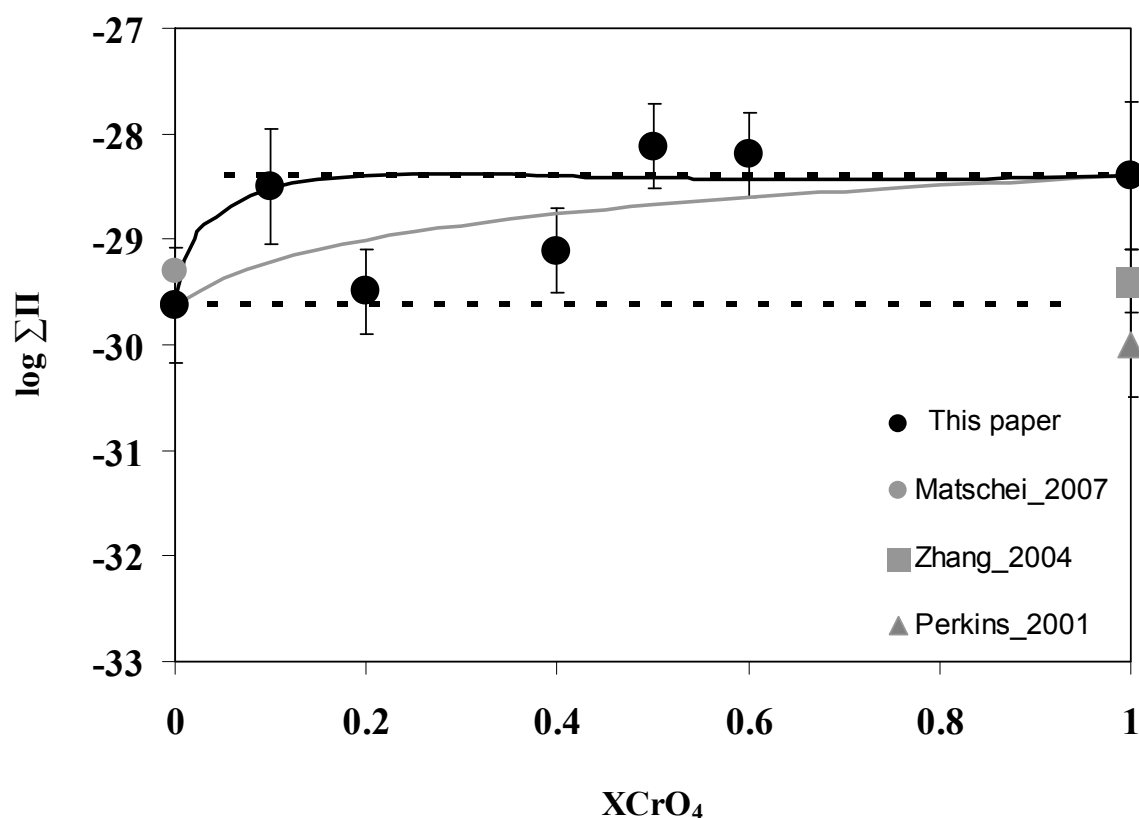
Figure 7 The variation of the solubility product of SO_4- and CrO_4-AFm as well as the total solubility products (this paper) of mixed phases were determined at 25 °C and I=0. The calculated curves indicate no solid solution formation (black dotted lines), ideal solid solutions (light grey line) and solid solution including a miscibility gap between $0.15 \leq XCrO_4 \leq 0.85$ (black line). Solubility products of published pure SO_4- and CrO_4-AFm end-members are given.

Table 4 Measured ion concentrations of the solid solution series are listed together with calculated total solubility products and solubility products of pure CrO_4- and SO_4-AFm (at I = 0). All prepared in 0.001 M KOH solution.

sample XCrO$_4$	pH	Ca (mmol/l)	Al (mmol/l)	SO$_4$ (mmol/l)	CrO$_4$ (mmol/l)	log∑Π	logK CrO$_4$-AFm	logK SO$_4$-AFm
Cr1		see table 3					-28.4	
Cr0.6_1	12.0	6.5	2.0	0.022	0.062	-28.0	-28.2	-28.5
Cr0.6_2	12.0	6.4	2.6	0.018	0.022	-28.2	-28.6	-28.5
Cr0.6_3	11.6	6.2	2.2	0.018	0.023	-28.4	-28.7	-28.6
Cr0.5_1	11.9	5.7	2.7	0.114	0.029	-27.9	-28.8	-28.0
Cr0.5_2	11.9	5.7	2.7	0.084	0.018	-28.1	-29.0	-28.2
Cr0.5_3	11.9	6.0	2.7	0.023	0.021	-28.3	-28.8	-28.5
Cr0.4_1	11.9	5.3	1.9	0.015	0.007	-29.1	-29.6	-29.3
Cr0.4_2	11.9	5.3	2.5	0.014	0.005	-29.0	-29.5	-29.2
Cr0.4_3	11.9	5.0	2.1	0.014	0.008	-29.2	-29.7	-29.4
Cr0.2_1	11.8	4.8	2.2	0.013	0.003	-29.5	-30.4	-29.5
Cr0.2_2	11.8	4.7	2.0	0.017	0.005	-29.5	-30.2	-29.5
Cr0.2_3	11.9	4.7	2.0	0.012	0.003	-29.5	-30.3	-29.6
Cr0.1_1	11.9	4.9	1.8	0.034	0.004	-29.1	-30.2	-29.2
Cr0.1_2	11.9	5.3	2.3	0.140	0.005	-28.2	-29.9	-28.3
Cr0.1_3	11.9	5.3	2.0	0.223	0.011	-28.1	-29.6	-28.1
Cr0_1	11.9	5.0	1.6	0.017				-29.4
Cr0_2	11.9	4.9	0.9	0.014				-29.6
Cr0_3	11.9	4.6	1.6	0.013				-29.9

3.4   Conclusion

In this study the solid solution series between SO_4- and CrO_4-AFm was investigated. The solubility product of pure CrO_4-AFm was determined at different pH values from precipitation experiments resulting in a $logK_{CrO4-AFm}$ = -28.4 ±0.7. The solubility product of the other end member SO_4-AFm was found to be $logK_{SO4-AFm}$ = -29.7 ±0.4. In experiments, where both CrO_4 and SO_4 have been present, a peak shifts in the XRD diffractograms and varying solubility products of CrO_4-AFm and SO_4-AFm have been observed, indicating the formation of a solid solution. Based on the results a solid solution including a miscibility gap between 0.15<XCrO$_4$<0.85 is proposed.

This study shows that the investigation of SO_4- and CrO_4-AFm solid solutions is complex and that the combination of different techniques is needed for the investigation and additional experiments would be needed to support the results presented here.

3.5 Acknowledgments

3.6 References

[1] Kindness, A., A. Macias, and F.P. Glasser, Immobilization of chromium in cement matrices. Waste Management, 1994. **14**(1): p. 3-11.

[2] Stephan, D., et al., High intakes of Cr, Ni, and Zn in clinker: Part I. Influence on burning process and formation of phases. Cement and Concrete Research, 1999. **29**(12): p. 1949-1957.

[3] Langard, S. and M. Costa, eds. Chromium. Handbook on the Toxicology of Metals, ed. G. Nordberg, et al. 2007, Academic Press, Inc. 1024.

[4] Nriagu, J.O. and E. Nieboer, eds. Chromium in the natural and human environments. 1 ed. Advances in Environmental Science and Technology, ed. J.O. Nriagu. Vol. 20. 1988, John Wiley & Sons, Inc. 571.

[5] Chrysochoou, M. and D. Dermatas, Evaluation of ettringite and hydrocalumite formation for heavy metal immobilization: Literature review and experimental study. Journal of Hazardous Materials, 2006. **136**(1): p. 20-33.

[6] Palmer, C.D., Precipitates in a Cr(VI)-contaminated concrete. Environ. Sci. Technol., 2000. **34**(19): p. 4185-4192.

[7]   Perkins, R.B. and C.D. Palmer, Solubility of chromate hydrocalumite $(3CaO \cdot Al_2O_3 \cdot CaCrO_4 \cdot nH_2O)$ 5-75°C. Cement and Concrete Research, 2001. **31**(7): p. 983-992.

[8]   Perkins, R.B. and C.D. Palmer, Solubility of ettringite $(Ca_6[Al(OH)_6]_2(SO_4)_3 \cdot 26H_2O)$ at 5-75°C. Geochimica et Cosmochimica Acta, 1999. **63**(13-14): p. 1969-1980.

[9]   Segni, R., et al., Hydrocalumite- type materials: 1. Interest in hazardous waste immobilization. J. Phys. Chem. Sol., 2006. **67**: p. 1037-1042.

[10] Francois, M., G. Renaudin, and O. Evrard, A cementitous compound with composition 3CaO*Al2O3*CaCO3*11H2O. Acta Cryst., 1998. **C54**: p. 1214-1217.

[11] Renaudin, G. and M. Francois, The lamellar double-hydroxide (LDH) compound with composition 3CaO*Al2O3*Ca(NO3)2*10H2O. Acta Cryst., 1999. **C55**: p. 835-838.

[12] Matschei, T., B. Lothenbach, and F.P. Glasser, Thermodynamic properties of Portland cement hydrates in the system CaO-Al2O3-SiO2-CaSO4-CaCO3-H2O. Cement and Concrete Research, 2007. **37**(10): p. 1379-1410.

[13] Atkins, M., F.P. Glasser, and A. Kindness, Cement hydrate phases. Solubility at 25°C. Cement and Concrete Research, 1992. **22**(2-3): p. 241-246.

[14] Prieto, M., Thermodynamics of solid solution-aqueous solution systems, in Thermodynamics and Kinetics of Water-Rock Interaction, E.H. Oelkers and J. Schott, Editors. 2009, Mineralogical Society of America and Geochemical Society. p. 47-85.

[15] Allmann, R., Refinement of the hybrid layer structure. Neues Jahrbuch für Mineralogie-Monatshefte, 1977: p. 136-143.

[16] Le Bail, A., Monte Carlo indexing with McMaille. Powder Diffraction, 2004. **19**(3): p. 249-254.

[17] Goeske, J., U. König, and H. Pöllmann, Kinetical investigations on lamellar calcium-aluminate chromate hydrates with high speed detector. Mat. Sci. For., 2004. **43-44**: p. 299-302.

[18]   Segni, R., Caractérisation structurale, propriétés d'échanges et stabilité de matériaux de type hydrocalumite $[Ca_2M(OH)_6]^+[X^{n1/n}*xH_2O]^-$ avec M=Al, Fe et Sc et X= SO_4, CrO_4, V_2O_7 et SiO_3., in Physique des Matériaux. 2005, Université Blaise Pascal: Clermon-Ferrand.

[19]   Kulik, D.A., U. Berner, and E. Curti, Modelling chemical equilibrium partitioning with the GEMS-PSI code, in PSI Scientific Report. 2003, PSI: Villigen. p. 109-122.

[20]   Hummel, W., et al., Nagra/PSI Chemical Thermodynamic Data Base 01/01. 2002, Parkland, Florida, USA: Universal Publishers/uPUBLISH.com.

[21]   Allison, J.D., D.S. Brown, and K.J. Novo-Gradac, MINTEQA2/PRODEFA2, a geochemical assessment model for environmental systems: version 3.0, U.S.E.P. Agency, Editor. 1990.

[22]   Ball, J.W. and D.K. Nordstrom, Critical evaluation and selection of standard state thermodynamic properties for chromium metal and its aqueous ions, hydrolysis species, oxides, and hydroxides. J. Chem. Eng. Data, 1998. **43**(6): p. 895-918.

[23]   Perkins, R.B. and C.D. Palmer, Solubility of $Ca_6[Al(OH)_6]_2(CrO_4)_3 \cdot 26H_2O$, the chromate analog of ettringite; 5-75°C. Applied Geochemistry, 2000. **15**(8): p. 1203-1218.

[24]   Lee, Y.M. and C.L. Nassaralla, Standard free energy of formation of calcium chromate. Materials Science and Engineering, 2006. **A 437**(2): p. 334-339.

[25]   Leisinger, S.M., et al., Solid solutions between CrO_4- and SO_4-ettringite $Ca_6(Al(OH)_6)_2[(CrO_4)_x(SO_4)_{1-x}]_3*26$ H_2O. Environ. Sci. Technol., 2010. **44**(23): p. 8983-8988.

[26]   Poellmann, H., Die Kristallchemie der Neubildungen bei Einwirkung von Schadstoffen auf hydraulische Bindemittel, in Naturwissenschaftliche Fakultät. 1984, Friedrich-Alexander-Universität: Erlangen-Nürnberg. p. 332.

[27]   Poellmann, H., H.J. Kuzel, and S. Auer, ICDD Grant-in-Aid: Calcium aluminum chromium oxide hydrate 00-042-0063 in Mineralogical Institute. 1990, University of Erlangen: Erlangen.

[28]   Goske, J., et al., ICDD Grant-in-aid: Calcium aluminum oxide chromium hydrate. 2001, Martin-Luther-University: Halle.

[29]   Poellmann, H. and S. Auer, ICDD Grant-in-aid: Calcium aluminum chromium oxide hydrate 00-041-0478, in Mineralogica Institute. 1990, University of Erlangen: Erlangen.

[30]   Shannon, R.D., Revised effective ionic radii and systematic studies of interatomic distances in halides and chalcogenides. Acta Cryst., 1976. **A32**: p. 751.

[31]   Dosch, W. and H. Zur Strassen, Untersuchungen in den Alkali enthaltenen Systemen, gebildet aus den Komponenten CaO, Al2O3, Fe2O3, SiO2, SO3, Na2O, K2O H2O. 1962, University of Mainz: Mainz (GER).

[32]   Perkins, R.B., The solubility and thermodynamic properties of ettringite, its chromium analogs and calcium aluminum monochromate, in Environmental science and resources. 2000, Portland State University: Portland, USA. p. 200.

[33]   Zhang, M., Incorporation of oxyanionic B, Cr, Mo and Se into hydrocalumite and ettringite: application to cementitious systems, in Earth Science. 2000, University of Waterloo Ontario, Canada. p. 172.

[34]   Matschei, T., B. Lothenbach, and F.P. Glasser, The AFm phase in Portland cement. Cement and Concrete Research, 2007. **37**(2): p. 118-130.

[35]   Lippmann, F., Phase diagrams depicting aqueous solubility of binary mineral systems. N.JB.Miner.Abh., 1980. **139**(1): p. 1-25.

[36]   Glynn, P.D. and E.J. Reardon, Solid-Solution Aqueous-Solution Equilibria - Thermodynamic theory and representation. American Journal of Science, 1990. **290**(2): p. 164-201.

[37]   Redlich, O. and A.T. Kister, Algebraic representation of the thermodynamic properties and the classification of solutions. Ind. Eng. Chem., 1948. **40**: p. 345-348.

[38]   Glynn, P.D., MBSSAS: A code for the computation of Margules parameters and equilibrium relations in binary solid-solution aqueous-solution systems. Computers and Geoscience, 1991. **17**(7): p. 907-966.

75

Chapter 4

Solubility of chromate in a hydrated OPC

Sabine M. Leisinger, Amit Bhatnagar, Petra Braun, Barbara Lothenbach, C. Annette Johnson

Abstract

The knowledge of the chromate binding mechanisms is essential for the prediction of the long-term leachability of cement-based solidified waste containing increased chromate concentrations because of its toxicity and high mobility. In this paper pore water concentrations from OPC doped with varying $CaCrO_4$ concentrations (0.01-0.8 mol/kg), equilibrated for 28 days were measured. Additionally, pH dependent leaching tests were carried out on the same doped OPC samples. Experimental results were compared to modeled data. Solid solution formation between monosulfate and ettringite as well as between $CaCrO_4$ and $CaSO_4 \cdot 2H_2O$ were considered in the thermodynamic database. It could be shown, that the cementitous matrix can bind chromate concentrations up to 0.1 mol/kg and that the chromate solubility limiting phase were solid solutions with ettringite. Measured chromium leaching concentrations were lower than the predicted data indicating that an additional chromate binding process takes place. Lowest chromate leaching concentrations were found between pH 11 and 13. Compared to AFt phases chromate containing AFm phases were not formed.

4.1   Introduction

The stabilization/solidification of wastes by cement can greatly reduce the potential risk of contaminant release to the environment. In the long-term, however, as the cementitious matrix is leached and weathers, contaminant species may be released [1, 2]. Negatively charged species are particularly susceptible to leaching from alkaline and neutral matrices, as found in ashes and cementitious matrices, because they sorb weakly to surfaces. The solubility of oxyanions is generally controlled by the precipitation of calcium metallates but may be bound to cement phases in highly alkaline systems [1, 3]. Chromate, CrO_4^{2-}, is toxic, very soluble and ubiquitous in cementitious systems. It results from the oxidation of chromium(III), present in raw meal, during cement production and waste incineration as well as being a common contaminant in wastes [4]. It is therefore of great importance to be able to predict CrO_4 (charges are omitted for simplicity from hereon) porewater concentrations in a hydrated cement paste. Two approaches to assess leachability of CrO_4 from cement-waste mixtures exist: 1) by testing each material using standard tests [5-7] and 2) by geochemical modeling. For the latter, knowledge of CrO_4 binding mechanisms in the cementitious matrix [8] as well as the availability of a complete thermodynamic database for CrO_4-containing phases are essential [9]. Apart from being economical, geochemical modeling is applicable to many systems. Parameter variations are also possible to predict the hydrated cement composition and porewater concentrations under different conditions as well as the extrapolation to longer time scales [10].

Hydrated ordinary Portland cement (OPC) pastes consist primarily of C-S-H (Calcium silicate hydrates), portlandite, ettringite (in cement nomenclature an AFt-phase meaning Al_2O_3 - Fe_2O_3 -tri), monosulfate and monocarbonate (AFm-phases meaning Al_2O_3 - Fe_2O_3 -mono). Together theses minerals make

up around 90 wt %. Unreacted clinker, pore solution as well as minor components make up the residual 10 wt % [11]. Cement formulations that contain other components, such as coal fly ash, blast furnace slag and additional limestone, when hydrated, have a different mineralogical composition [12-14]. To date, C-S-H, AFt- and AFm-phases have been demonstrated to be important for heavy metal and metalloid binding [1].

It is well known that ettringite and monosulfate are available for the exchange of a variety of anions with SO_4, including CrO_4 [15-17]. Investigations on CrO_4-doped cement samples appear to find substitution into both phases. Analysis of CrO_4-doped cement samples using X-ray diffraction (XRD), scanning electron microscopy (SEM) and X-ray absorption spectroscopy (XAS) have shown that nearly pure CrO_4-AFm and CrO_4-enriched ettringite exist [18, 19].

Several investigations were carried out on CrO_4 uptake and release from hydrated cement pastes, recycled concrete aggregate samples and ordinary Portland cement mortars. The authors showed that the CrO_4 release was strongly pH dependent. Solid solution formation between SO_4 and CrO_4-ettringite was identified as the dominant binding process controlling CrO_4 solubility [3, 20-22]. Other authors [15, 23] suggested that CrO_4-AFm formation was more stable over a broader pH range than CrO_4-ettringite and that the AFm-phase was limiting CrO_4 concentrations in leaching experiments. The different results were mainly based on differences in the thermodynamic databases especially in solubility products of CrO_4-ettringite and monochromate such as the implementation of solid solution formation for these phases. The solubility of CrO_4-ettringite and monochromate has been studied experimentally in pure CaO-CrO_4-Al_2O_3-H_2O systems [23-26], and the derived solubility products indicated the formation of very stable monochromate compared to monosulfate, while the CrO_4-ettringite was less stable than the SO_4-ettringite. For both phases the formation of CrO_4 and SO_4 solid solutions has been observed [25, 26]. The

formation of solid solutions can stabilise CrO_4 in the SO_4 phase and thus lower the CrO_4 concentrations.

The sorption of CrO_4 onto C-S-H was investigated by several authors [27-29]. These studies showed that an increase of Na uptake by C-S-H (over-)compensated the negative charge of the silanol surfaces leading to an increased CrO_4 uptake by C-S-H. The possibility of overcharging C-S-H was also discussed by Park and Bachelor [30] and Labbez et al. [31].

While hydration minerals are only stable at the alkaline pH (e.g. [15]) range CrO_4 binding must also be considered at lower pH since environmentally exposed cementitous systems may alter through CO_2 diffusion and thus leading to lower pH values. At such conditions CrO_4 will be released from the deteriorating hydration minerals.

This project validated thermodynamic data of the CrO_4- SO_4 solid solutions in ettringite and monosulfate [25, 26] and it also explored potential solid solution formation with the deterioration product $CaCrO_4$ - $CaSO_4 \cdot 2H_2O$ at low pH. These thermodynamic data were applied to hydrated OPC systems doped with $CaCrO_4$. The existence of these thermodynamic data is crucial for the safe management of CrO_4 contaminated cementitious systems.

4.2   Materials and methods

4.2.1   Investigation of the solid solutions between CaSO₄ and CaCrO₄

Synthesized solids were characterized by X-ray diffraction (XRD) and thermogravimetric analysis (TGA). Ion concentrations in solution were measured by Inductive coupled plasma optical emission spectroscopy (ICP-OES). These concentrations were then used to calculate solubility products of the pure phases $CaCrO_4$ and $CaSO_4$ as well as total solubility products for mixed phases.

Synthesis of the solids. Solid solution phases were synthesized according to the following precipitation reaction:

1) $Ca^{2+} + x(CrO_4^{2-})   + (1-x)SO_4^{2-} = Ca[(CrO_4)_x, (SO_4)_{1-x}]$
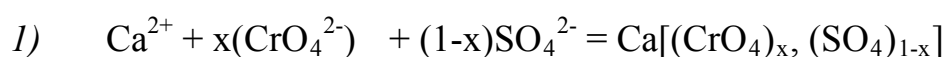
0.1 mol $CaCl_2$ and stoichiometric amounts of Na_2CrO_4 and Na_2SO_4 (0-0.1 mol) were added to ultrapure water (50 ml) to obtain different chromate mole fractions ($XCrO_4 = [CrO_4^{2-}]/([CrO_4^{2-}]+[SO_4^{2-}]) = 0$, 0.2, 0.4, 0.6, 0.8 and 1 with Cr0 and Cr1 as the end members $CaSO_4$ and $CaCrO_4$ respectively. The samples were equilibrated for 2 month on a rotary shaker at 125 rpm at 25 °C. The samples were then centrifuged for 20 min at 4000 rpm. About 6 ml of the supernatant was used for pH measurement. The rest was filtered with 0.45 μm nylon membrane filters (Titan), and acidified with concentrated HNO_3 Suprapur (1:100). All samples were stored at 4 °C. Solid phases were washed with ultrapure water and stored in petri dishs placed in a clean box.

Characterization of the solid and liquid phase. After drying the samples were ground by hand with an agate mortar to <63 μm and analyzed by X-ray diffraction (XRD) and thermogravimetric analysis (TGA). XRD analysis was used to determine the purity and crystallinity of the phases using CuKα radiation.

Elemental silicon was mixed to the powder samples as internal standard. Raw data were evaluated by X'Pert HighScore Plus. TGA was carried out on a TGA/SDTA 851 apparatus by Mettler Toledo. The samples (8 - 12 mg) were heated under N_2 over a temperature range of 30 - 980 °C at a rate of 20 °C/min. TGA was carried out to observe mass changes in relation to change in temperature/time.

Part of the liquid phase was used for pH-measurement. Dissolved concentrations of Ca, Cr and SO_4, were determined by ICP-OES. Multi-element standard solution was used for calibration of Ca, and Cr. Anion standard solution was used for the SO_4 calibration.

4.2.2 Porewater and leaching experiments with $CaCrO_4$ doped OPC

Experiments were carried out with an ordinary Portland cement (OPC), type CEM I 42.5 N. The composition of the cement was determined by X-ray fluorescence analysis (XRF) and the calculated amount of the clinker phases in the unhydrated cement was determined using modified Bogue calculations [11, 32] (Table 1).

Cement pastes were doped with varying concentrations of $CaCrO_4$ at a water : cement (w/c) ratio of 0.4. Between 0 - 0.8 mol $CaCrO_4$/kg cement were dissolved in nanopure water (400 ml) and mixed with 1 kg of cement. The cement pastes were poured into 500 ml plastic bottles and stored at 20 °C and hydrated for 28 days.

Table 1 Composition of the Ordinary Portland Cement (CEM I 42.5)

Chemical analysis		Normative phase composition[a]		
	g/100 g		g/100g	mmol/100g
$SiO2$	19.8	C_3S	55.0	241
Al_2O_3	4.60	C_2S	15.3	89
Fe_2O_3	2.50	C_3A	7.96	29
CaO	63.5	C_4AF	7.61	16
MgO	1.80	$CaSO_4$	4.18	31
Na_2O	0.10	K_2SO_4	1.48	8.5
K_2O	0.89	Na_2SO_4	0.10	0.7
CaO frei	0.46	K_2O	0.09	0.9
CO_2	1.87	Na_2O	0.06	0.9
SO_3	3.30	CaO	0.46	8.2
TiO_2	0.27	$CaCO_3$	4.25	43
P_2O_5	0.35	MgO	1.80	45
Mn_2O_3	0.04	SO_3	0.08	1
SrO	0.07			

readily soluble alkalis

K2O	0.8
Na2O	0.05

[a] calculated from the chemical analysis

Influence of $CaCrO_4$-doped OPC on CrO_4 content in porewater. The CrO_4-doped cement samples were cut out of the plastic and the porewater of the hardened samples was extracted using the steel die method with pressure up to 1000 kN [33, 34]. The first 3 ml of the pore fluid was discarded. Part of the liquid phase was used for pH-measurement, which was carried out with an Aquatrode Plus Pt 1000 electrode from Metrohm. Prior to the measurements the pH electrode was calibrated by titration with fresh KOH-solutions (0.001-1 M) to minimize the alkali error. The voltage reading was correlated to the calculated target pH value of the respective KOH-solution considering ionic strength as well as the measured temperature of the solution. After pH measurement, the porewater was filtered with a 0.45 μm nylon filter and acidified with 65 %-HNO_3 suprapur (diluted 1:100) and stored at 4 °C. Porewater ion concentrations were analyzed by inductive coupled plasma optical emission spectroscopy (ICP-OES) for Na, K, Mg, Ca, Cl, SO_4, Al, Si and Cr. Chromium

concentrations measured by ICP-OES were identical to determined CrO_4 concentrations carried out by photometry on a UV/VIS spectrometry using a colorimetric complexation method with Diphenylcarbazide as ligand (Table 4). Further Cr measurements were carried out only by ICP-OES.

Cr-leaching in diluted OPC as a function of pH. The cement samples doped with 0.01-0.1 mol $CaCrO_4$/kg were dried, crushed to <0.5 mm and re-equilibrated for 14 days at a w/c = 10 (10 ml water : 1 g ground cement) in solutions adjusted with 2 M HNO_3 to pH values between 8 - 13.4. The samples were then filtered using 0.45 µm nylon filters and the filtrate was analyzed for pH, and major ion concentrations were determined.

4.2.3 Thermodynamic modeling

The broad-purpose geochemical modeling code GEMS-PSI (Gibbs Energy Minimization Selector) was used to model ion porewater concentrations and mineralogical cement composition after an equilibration time of 28 days. The principle of the GEM method is the minimization of the Gibbs energy of a complex chemical system. Chemical interactions involving solids, solid solutions, gas mixture and aqueous electrolyte are considered simultaneously [35]. A built-in thermodynamic database is provided [36]. This database was expanded with cement specific data Cemdata07 [37]. The formulation of siliceous hydrogarnet was excluded due to kinetic reasons; also strätlingite was excluded.

Activity coefficients of aqueous species y_i were computed with the built-in expanded extended Debye-Hückel equation in Truesdell-Jones form (equation 1).

$$\text{(1)} \quad \log \gamma_i = \frac{-A_y z_i^2 \sqrt{I}}{1 + B_y a_i \sqrt{I}} + b_y I$$

where z_i denotes the charge of species i, I the effective molal ionic strength, a_i is a parameter   dependent on the size of ion i, b_y is a semi-empirical parameter (~ 0.064 at 25°C), and A_y and B_y are P,T-dependent Debye-Hückel solvent parameters. This activity correction should be applicable up to 1-2 M ionic strength [35],[36].

Thermodynamic information of CrO_4-relevant solid-solution systems, such as CrO_4-SO_4-ettringite [38], CrO_4-SO_4-AFm [39] and $CaCrO_4$ and $CaSO_4$ were included into the database (Table 2). Results of the solid solution investigation between $CaCrO_4$ and $CaSO_4$ are described and illustrated in the appendix.

The prediction of porewater concentrations are based on the thermodynamic hydration model developed by Lothenbach and Winnefeld [10]. The calculated composition of the porewater and the hydrate assemblage after hydration times of 28 and 42 days were used as input parameters in the porewater experiments and pH dependent leaching experiments respectively. The uptake of alkalis by C-S-H was approached by using an ideal solid solution model between jennite, tobermorite, $[(KOH)_{2.5} \, SiO_2 \, H_2O]_{0.2}$ and $[(NaOH)_{2.5} \, SiO_2 \, H_2O]_{0.2}$ as proposed by Kulik et al. [40].

Table 2 Chemical reactions used for simulation of chromate solubility.

Reaction	$log\ K_{298}$	Ref.
Aqueous Species		
$CrO_4^{2-} + 2H^+ = H_2CrO_4^0$	6.31	[36]
$CrO_4^{2-} + H^+ = HCrO_4^-$	6.55	[36]
$2CrO_4^{2-} + 2H^+ - H_2O = Cr_2O_7^{2-}$	14.7	[36]
$K^+ + CrO_4^{2-} = KCrO_4^-$	0.57	[41]
$Ca^{2+} + CrO_4^{2-} = CaCrO_4^0$	2.77	[24]
Solid phases		
Gypsum* $\quad CaSO_4 \cdot 2H_2O = Ca^{2+} + SO_4^{2-} + 2H_2O$	-4.58	[36]
CaCrO$_4$* $\quad CaCrO_4 = Ca^{2+} + CrO_4^{2-}$	-3.69$_{+/- 0.04}$	(this paper)
SO$_4$-ettringite$^-$ $\quad Ca_6(Al(OH)_6)_2(SO_4)_3 \cdot 26H_2O =$ $6Ca^{2+} + 2Al(OH)_4^- + SO_4^{2-} + 4OH^- + 26H_2O$	-44.9 $_{+/- 0.7}$	[37]
CrO$_4$-ettringite$^-$ $\quad Ca_6(Al(OH)_6)_2(CrO_4)_3 \cdot 26H_2O =$ $6Ca^{2+} + 2Al(OH)_4^- + CrO_4^{2-} + 4OH^- + 26H_2O$	-40.2 $_{+/-0.4}$	[38]
monosulfate$^+$ $\quad Ca_4(Al(OH)_6)_2SO_4 \cdot 6H_2O =$ $4Ca^{2+} + 2Al(OH)_4^- + SO_4^{2-} + 4OH^- + 6H_2O$	-29.7 $_{+/-0.3}$	[39]
monochromate$^+$ $\quad Ca_4(Al(OH)_6)_2CrO_4 \cdot 6H_2O =$ $4Ca^{2+} + 2Al(OH)_4^- + CrO_4^{2-} + 4OH^- + 6H_2O$	-28.4. $_{+/-0.7}$	[39]

* ideal solid solution
$^-$/$^+$ non ideal solid solutions with miscibility gap

4.3   Results and Discussion

4.3.1   Investigation of the solid solutions CaSO$_4$ - CaCrO$_4$

Characterization of the solids. TGA measurements showed that for all samples except pure CaCrO$_4$ a total weight loss of 20.4 -20.6 % was measured. This corresponds to 2 H$_2$O in the samples and indicates that the synthesized sulfate end member is gypsum and that mixed phases between CaCrO$_4$ and gypsum (CaSO$_4$·2H$_2$O) were formed. Pure CaCrO4 samples showed that no crystal water was present (weight loss <2.5 %). Peak positions of CaCrO$_4$ and CaSO$_4$·2H$_2$O in the XRD diffractograms were consistent to the PDF files 008-0458 and 021-0816 in the database of the International Center for

Diffraction Data (ICDD). Clear peak shift to higher 2 Theta values (lower d-spacings) for samples with decreasing $XCrO_4$ was observed in all mixed samples indicating that solid solutions were formed (Figure 1). The peak shift is caused by the larger ionic radius of CrO_4 with 2.4 Å compared to SO_4 with 2.3 Å [42].
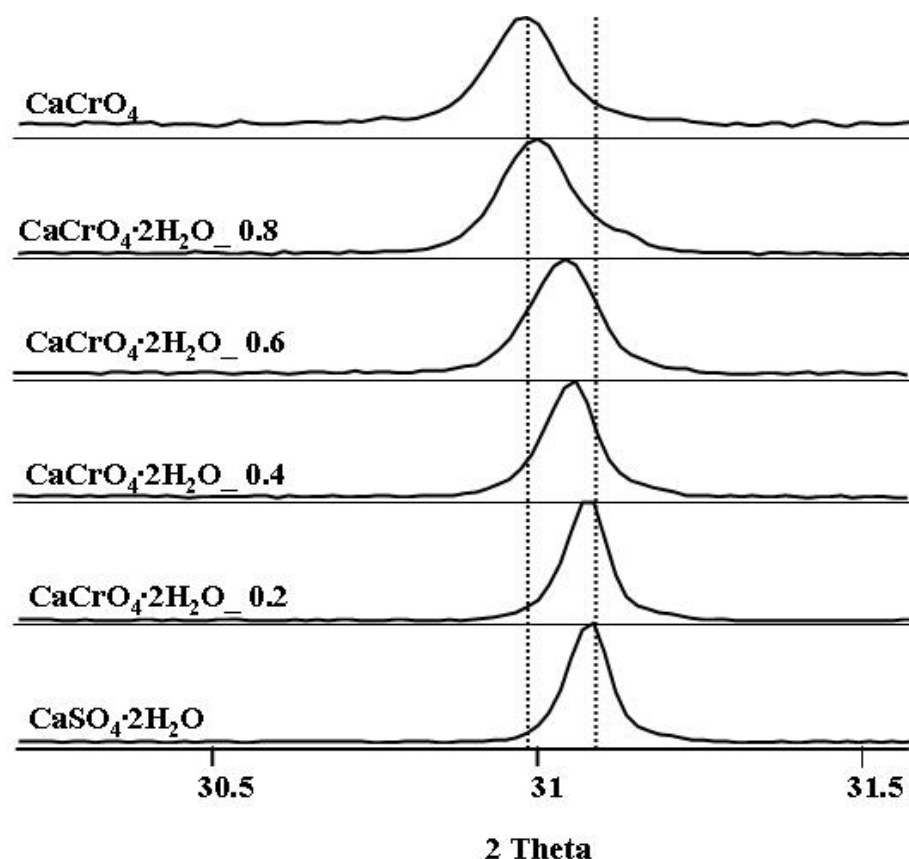
Figure 1 Clear peak shifts were observed in the solid solution series between $CaCrO_4$ and $CaSO_4 \cdot 2H_2O$ for all mixed phases indicating that solid solution formation existed. With increasing $XCrO_4$ (last number in the sample nomenclature) a peak shift to lower 2 Theta values (higher d-spacings) was observed.

Solubility calculations. Solubility products of pure $CaCrO_4$ and $CaSO_4 \cdot 2H_2O$ were determined in all solid solution samples based on measured ion concentrations and pH (Table 3). The solubility product of pure $CaCrO_4$ was

determined to be -3.65 ± 0.04. Wang determined $\Delta_f G°$ of $CaCrO_4$ which results in a logK = -3.15. The gypsum solubility resulted in a logK = -4.48 ±0.04. This value corresponds well to the published value of logK = -4.58 [10].

Table 3 Measured pH and solute concentrations are listed in **mmol/l**.

sample	$XCrO_4$	pH	Ca	SO_4	CrO_4	log $\sum\Pi^a$	$CaCrO_4$ log K	$CaSO_4*2H_2O$ log K
$CaCrO_4$	1						-3.15^b	
$CaCrO_4$	1	8.8	160	0	294		-3.69 ±0.04	
	0.8	8.9	145	15.1	226	-3.79 ±0.01	-3.83 ±0.01	-4.99 ±0.01
	0.6	8.9	123	17.0	161	-3.91 ±0.04	-3.81 ±0.03	-4.92 ±0.01
	0.4	9.1	164	17.0	227	-3.77 ±0.03	-3.78 ±0.03	-4.91 ±0.03
	0.2	8.7	120	23.3	123	-4.08 ±0.03	-4.05 ±0.03	-4.77 ±0.04
$CaSO_4·2H_2O$	0	8.3	51.8	57.1	0			-4.44 ±0.04
$CaSO_4·2H_2O$	0							-4.58^c

[a] $\log\sum\Pi = \log\{Ca^{2+}\} + \log[\{SO_4^{2-}\} + \{CrO_4^{2-}\}] + 2\log\{H_2O\}$.
[b] Wang [43].
c Lothenbach and Winnefeld [10].

An indication that solid solution formation occurs were the varying end member solubilities in the solid solution samples. $CaSO_4·2H_2O$ solubility showed a clear trend to lower logK values with increasing $XCrO_4$ and the $CaCrO_4$ solubility product increased to higher solubility with decreasing $XCrO_4$. If no solid solutions existed the solubility products of pure $CaCrO_4$ and $CaSO_4·2H_2O$ would stay constant. This is clearly not the case. Determined total solubility products ($\sum\Pi$) [44] fell between the end member solubilities of $CaCrO_4$ and $CaSO_4·2H_2O$. The ionic strength of the solution was about 4 M in all samples and the used built-in expanded Debye-Hückel equation should be applicable up to a ionic strength of 2 (see Chapter 2, thermodynamic modeling).

Based on the result from solid analysis it can be concluded that solid solutions between $CaCrO_4$ and $CaSO_4 \cdot 2H_2O$ exists and that the model of an ideal solid solution can be assumed.

Solid solution formation between $CaCrO_4$ and $CaSO_4 \cdot 2H_2O$ was implemented into the thermodynamic database and regarded in the modeling projects of this paper.

4.3.2 Influence of CaCrO$_4$-doped OPC on Cr content in pore water

In cements containing no chromate reducing agents, the chromium concentrations during the first hours were in the range of 0.4 to 1.4 mmol/l [10, 13]. European cements contain now generally a chromate reducing agent such as $Fe_2(SO_4)_3$ to reduce the soluble chromate content and thus to reduce dermatitis. However, the cement investigated was free of chromate reducing agents. After 1 day and longer chromium concentrations have been observed to decrease to 0.07 to 0.22 mmol/l [10, 13]. These values were comparable to the 0.14 mmol/l chromium observed in the pore solution of the undoped OPC after a hydration time of 28 days (Table 4). At doping concentrations between 0.01-0.1 mol/kg OPC between 89 – 95 % of total CrO_4 in the cement was bound to the cement matrix, while a significant decrease of CrO_4 binding was observed at doses higher than 0.1 mol/kg. In the latter samples the pH decreased from 13.8 to 13.5.

Comparable porewater concentrations were found by Kindness ea [45] (Figure 2). The reason for the lower degree of binding at high concentrations is probably related to the exhaustion of ions available for the formation of AFt and/or AFm phases.

Table 4 Measured pH and pore water concentrations of undoped and doped cements.

	CaCrO$_4$ (mmol/l)	pH	I	OH^b	Na	K	Ca	Al	Si	SO$_4$	Cr$_{tot}$	CrO$_4$^{c}
							mmol/l					
OPC	undoped	13.8	0.63	630	26	162	3.33	0.127	0.209	9.4	0.14	0.06
OPC_001	25	13.7	0.61	610	24	280	3.29	0.124	0.199	7.3	1.39	1.4
OPC_002	50	13.8	0.63	630	23	460	3.17	0.126	0.264	7.3	2.63	2.8
OPC_005	125	13.8	0.63	630	16	520	3.10	0.131	0.204	7.0	5.88	5.5
OPC_01	250	13.8	0.65	650	13	600	2.84	0.120	0.178	8.7	27.6	
OPC_02	500	13.8	0.64	640	16	800	2.17	0.033	0.157	58	127	
OPC_04	1000	13.5	0.35	350	20	1130	1.16	0.026	n.a.^{a}	63	498	
OPC_06	1500	13.3	0.2	190	20	1190	3.75	0.034	n.a.	39	779	
OPC_08	2000	13.3	0.22	210	27	1450	4.56	0.036	n.a.	22	1075	

^{a} n.a. = not analyzed

^{b} the values for OH- refer to the free concentrations measured in the pore solutions

^{c} measured by UV/VIS spectrometry using a colorimetric complexation method
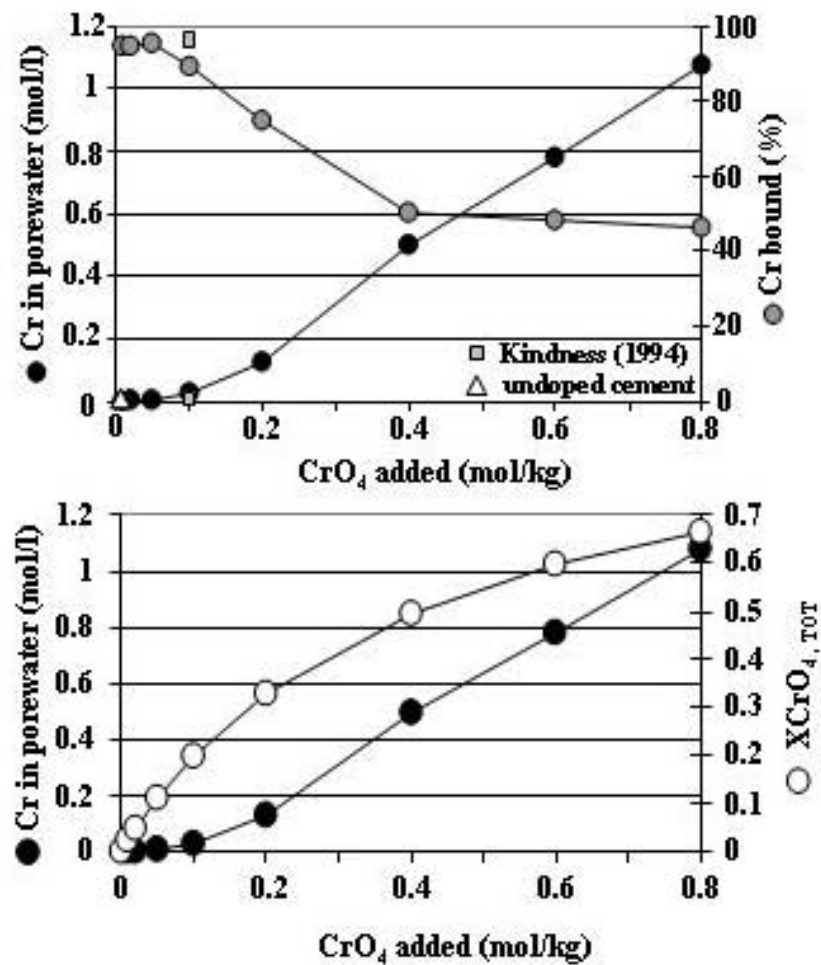
Figure 2 Measured porewater concentrations show that between 89-95 % of the added chromium was bound in the cement matrix for OPC doped with max. 0.1 mol $CaCrO_4$ / kg. At higher doping concentrations chromium porewater concentrations increased dramatically.

Modeled solute concentration in porewater. Experimentally derived porewater concentrations were compared with modeled concentrations (Figure 3). The calculations included solid solution formation between CrO_4 and SO_4 in AFt and AFm as well as solid solution formation between $CaCrO_4$ and $CaSO_4 \cdot 2H_2O$ phases [38, 39]. A discrepancy of half an order of magnitude between modeled and measured concentrations was considered as an adequate match. In the absence of additional $CaCrO_4$, the modeled concentrations agreed

with the experimental data (Figure 3, top). Upon addition of increasing amounts of $CaCrO_4$, the dissolved Cr was present in increasing concentrations (shown in Figure 2), while the OH concentrations decreased. The increase of CrO_4 was accompanied by a, however less distinct, increase in SO_4, as both CrO_4 and SO_4 were bound mainly in AFt and AFm phases. As the pH decreased, calcium concentrations which were mainly limited by the presence of portlandite, increased. It is interesting to note that the measured K concentrations increased. The sorption of K on C-S-H decreased with decreasing pH, as at lower pH values the C-S-H is less negatively charged and less cations were needed to counteract the negative C-S-H surface. In contrast to K, measured Na concentrations were not significantly affected. Generally the trends in the modeled data agreed with the experimental data. Good matches were obtained for K and Ca, while Na and OH matched up to 0.4 mol $CaCrO_4$/kg added. Most CrO_4 data points were found to be within half a log unit of difference. Some differences were observed for SO_4 in the samples doped with 0.2 and 0.4 mol $CaCrO_4$/kg. The Na concentrations were overestimated and pH was underestimated at high $CaCrO_4$ concentrations leading to a corresponding overestimation of Ca concentration in the model. It also showed that at low $CaCrO_4$ concentrations the model overestimated chromate and at the same time underestimated SO_4 porewater concentrations indicating that an additional uptake process must take place.

Modeled phase assemblage. Modeling the solid phase composition predicted that the undoped cement was mainly composed of C-S-H, portlandite, SO_4-ettringite and monocarbonate (making up 80 vol%) and smaller amounts of calcite, OH-hydrotalcite and some unhydrated clinker phases (Figure 3c). This mineral assemblage agreed with experimental observations in similar systems [10, 13]. Additions of $CaCrO_4$ only caused changes in AFt and AFm phases.

91

The more $CaCrO_4$ added to the cement the more CrO_4-rich ettringite was formed at the expense of monocarbonate. At 0.42 mol $CaCrO_4$/kg all of the monocarbonate was finally dissolved. Above a concentration of 0.3 $CaCrO_4$ added to the system, the solid solution composition converted from a SO_4-rich ettringite to a CrO_4-rich ettringite indicated with step in the solid solution composition. At very high $CaCrO_4$ concentrations (>0.6 mol/kg) the formation of solid solutions between $CaSO_4 \cdot 2H_2O$ and $CaCrO_4$ startet to form. The solid solutions contained a chromate mole fraction of about 30 %. The formation of a second CrO_4 binding phase initially caused a second step in the solid solution composition of the SO_4-CrO_4 ettringite. The occurence of solid solutions between $CaSO_4 \cdot 2H_2O$ and $CaCrO_4$ correlated to the observations of Laforest and Duchesne [46] who equilibrated OPC in CrO_4-concentrated solutions and identified chromatite ($CaCrO_4$) by XRD above concentrations of 0.4 mol/kg.
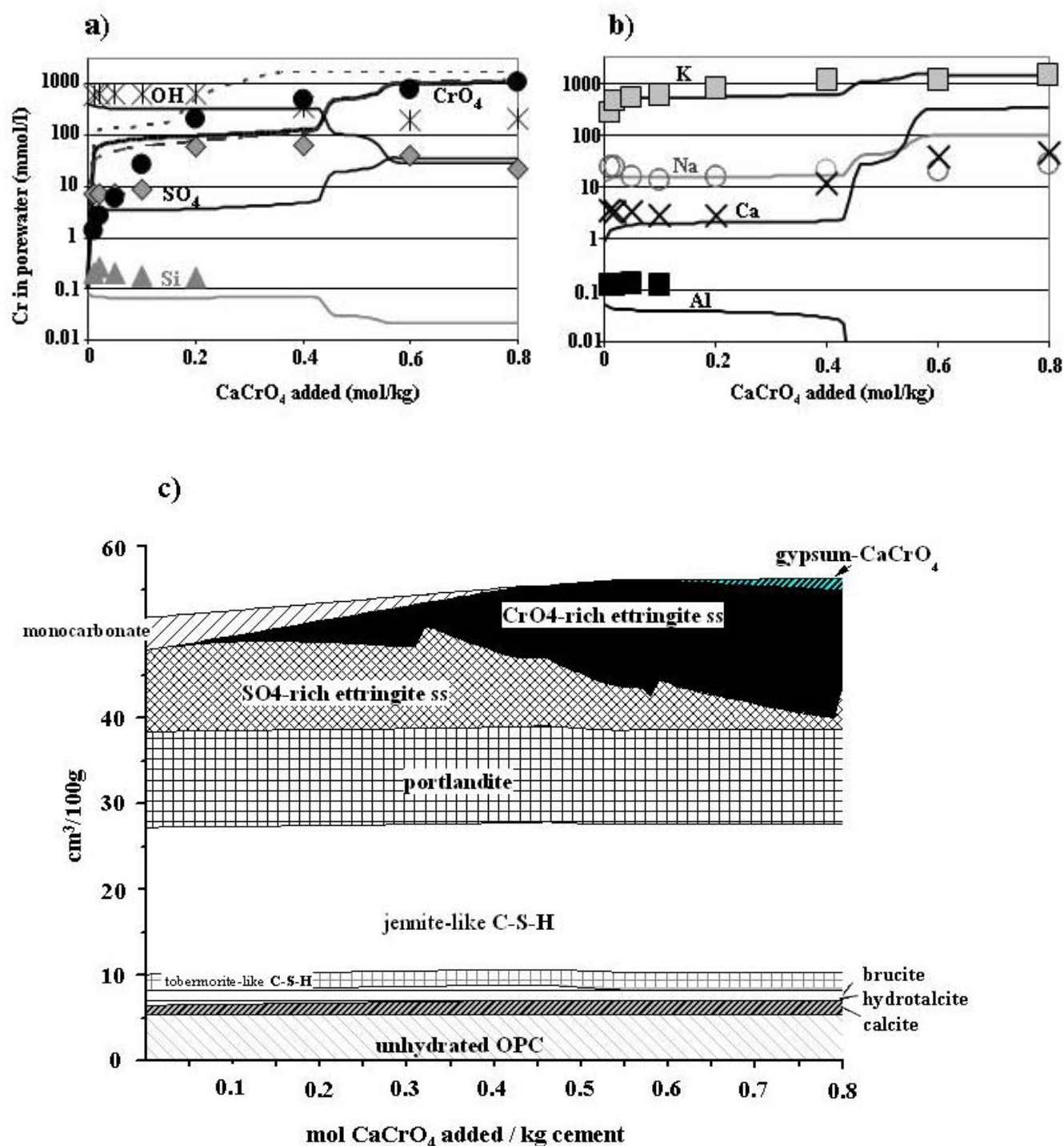
Figure 3 Measured (symbols) and modeled (lines) porewater concentrations of OPC doped with 0-0.8 mol $CaCrO_4$ /kg cement (**a, b**) were compared. The development of the mineral assemblages (**c**) showed that CrO_4 solubility was mainly controlled by ettringite solid solutions and at high CrO_4 concentrations additionally solid solution formation with gypsum became important.

The modeled result showed that chromate solubility was mainly controlled by the formation of CrO_4-SO_4 ettringite solid solutions and at very high CrO_4 solution also by solid solution formation between $CaCrO_4$ and $CaSO_4 \cdot 2H_2O$. Since experimental CrO_4 porewater concentrations were lower than the modeled data an additional CrO_4 uptake mechanism that was not considered must take place.

This experiment showed that about 95 % of the added CrO_4 was bound in the hydrated cement paste for doping concentrations up to 0.1 mol $CaCrO_4$/kg. At higher $CaCrO_4$ added concentrations only around 50 % was bound. Chromate concentrations in the porewater were mainly controlled by solid solution formation with ettringite and at high concentrations also by solid solution formation between $CaCrO_4$ and $CaSO_4 \cdot 2H_2O$.

4.3.3 Cr-leaching in diluted OPC as a function of pH

Experimental CrO_4 leaching concentrations. The influence of the pH on the CrO_4 leaching was studied using hydrated samples immersed in $NaOH$ or HNO_3 solutions at a w/c = 10. In these more diluted experiments 10 to 30 times lower chromium concentrations were observed than in the pore solution experiments described above (see Table 5). Also the measured concentrations of sulfate and silicate were lower.

Measured CrO_4 leaching concentrations as a function of pH were split into 4 different sectors (I-IV in Figure 4). At a pH up to 10 (**I**) 95 % of added CrO_4 was in solution thus not bound by the cement matrix. Chromate binding started at pH >10 (**II**) and was most efficient between pH 11 and 13 (**III**). At higher pH 13-14 chromate binding decreased significantly (**IV**). Dissolved Cr concentrations

increased when more Cr was added to the doped to the cement over the entire pH range (**I to IV** indicated with a black arrow, Figure 4).

Table 5 Measured pH and chromium concentrations (in mmol/l) of pH dependent leaching experiments (w/s = 10) in samples doped with 0.01-0.1 mol $CaCrO_4$ per kg cement were compiled together with additional solutes measured in sample OPC_0.02.

	pH	6.7	9.4	10	10	10.6	11.1	11.5	12	12.2	12.3	12.7	13.2	13.4	13.8[b]
OPC undoped															0.14
OPC_0.01	**Cr**	-[a]	-	-	-	0.06	0.02	0.02	0.02	0.02	0.02	0.01	0.05	0.11	1.4
OPC_0.02		1.49	1.54	1.46	0.80	0.10	0.03	0.05	0.04	0.06	0.04	0.01	0.09	0.18	1.6
OPC_0.05		3.69	4.04	3.85	1.86	0.51	0.06	0.11	0.13	0.13	0.09	0.05	0.26	0.52	5.9
OPC_0.1		7.32	7.91	7.73	5.26	2.01	0.13	0.17	0.22	0.25	0.20	0.12	0.59	0.9	28

	pH	6.7	9.4	10	10.2	10.6	11.1	11.5	12	12.2	12.3	12.7	13.2	13.4	13.8[b]
	Ca	882	819	778	712	661	608	549	483	381	263	40.4	12.2	8.22	3.1
OPC_0.02	**Si**	0.53	0.71	0.74	0.6	0.27	0.12	0.05	0.01	0.01	0.01	0.01	0.02	0.04	0.26
	SO4	5.68	5.97	5.98	0.2	0.1	0.09	0.09	0.08	0.07	0.04	0.02	0.16	0.49	9.4

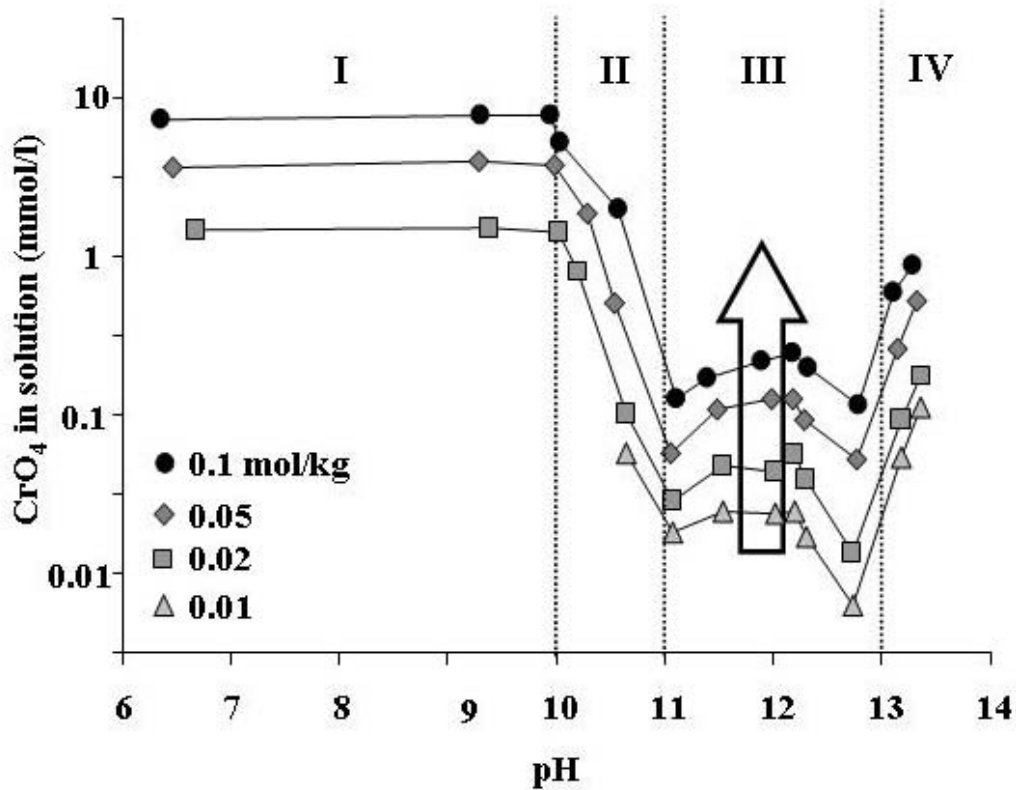[a] - not analyzed

[b] unleached OPC (w/c = 0.4)

Figure 4 The development of Cr pore water concentrations from pH dependent leaching experiments can be explained in 4 pH ranges. At low pH (**I**) most added chromate is in solution thus not bound by the cement matrix. Chromate binding began at pH of 10 (**II**) and was most efficient between pH 11 and 13 (**III**). At higher pH >13 a step increase in chromate concentration occured (**IV**). With increasing chromate added to the system increasing chromium concentrations were found in solution (indicated by the black arrow).

Modeled phase assemblage. The influence of pH on the chromate binding is exemplified for the OPC specimens containing originally 0.02 mol $CaCrO_4$ /kg cement (see Figure 5 , Table 5). The composition of the solid phases changed drastically from pH 14 to 7. At pH values near 14, ettringite becomes less stable (Figure 5, bottom). This decrease of ettringite stability at very high pH values was consistent with observations of e.g. Perkins and Palmers [47] in this pH range.

In the pH range 13 to 12.5 C-S-H, ettringite, monocarbonate and portlandite were stable, at pH below 12.5, portlandite became unstable and C-S-H with a low Ca/Si was formed. In contrast to the changes observed for C-S-H, no or very little change was calculated in the composition of the AFt and AFm phases. As discussed above, AFt phases had a significant ability to take up chromate. In the pH range between 11 to 10 thermodynamic modeling indicated that monocarbonate became unstable. Also the solubility of ettringite increased again at this pH range, leading to an increase of sulfate concentrations (Figure 5, top). CrO_4-ettringite was calculated to be unstable at a pH of approx. 10, while SO_4-ettringite was predicted to persist down to a pH value of roughly 9.5. The C-S-H present decalcified progressively with decreasing pH. At pH <9 amorphous silica gel, $Al(OH)_3$, $Fe(OH)_3$, calcite and solid solution formation of CrO_4 in gypsum were predicted to be [48, 49].

Modeled solute concentrations. These drastic changes are also visible in the aqueous concentrations as shown in top part of (Figure 5). At pH values near 14, Ca concentrations are low as they are controlled by the presence of portlandite. In contrast, the concentrations of CrO_4, sulfate and also silicate increased strongly. This is due to the lower Ca concentrations but also due to the very high pH that starts to destabilize ettringite.

Thermodynamic modeling indicated that the formation of solid solutions between CrO_4- and SO_4-ettringite and also between $CaCrO_4$ and $CaSO_4 \cdot 2H_2O$, increased the uptake of CrO_4 and thus lowered the CrO_4-concentration considerably (see dotted line in next chapter)
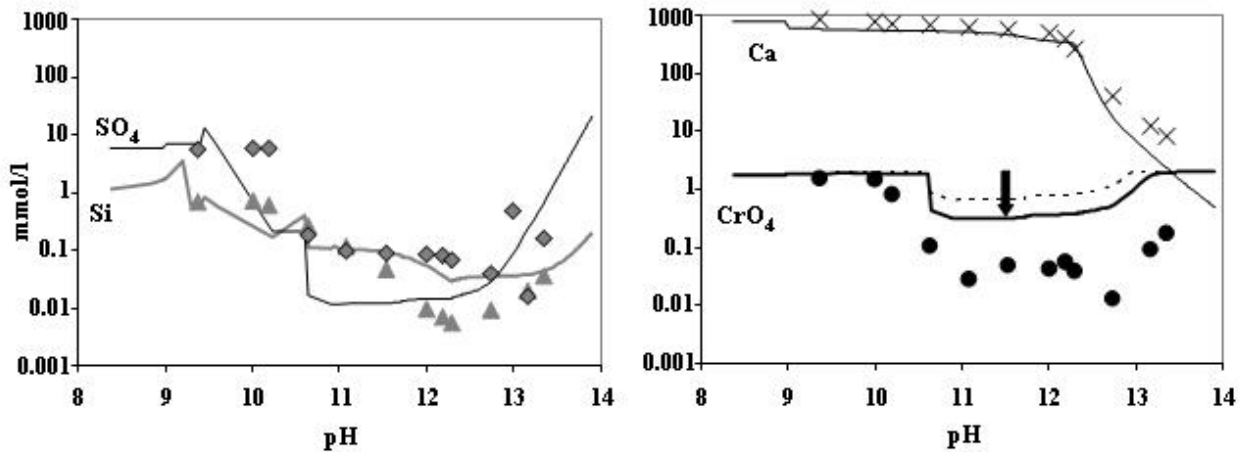
Figure 5 Measured solute concentrations of an OPC doped with 0.02 mol CaCrO$_4$ /kg were compared to the modeled data in the pH range of 8.5 to 13.5 (top); phase assemblages at the same pH range illustrated (bottom) that CrO$_4$ solubility was controlled by CrO$_4$-AFt solid solution. Solid solution formation lowered CrO$_4$ solubility (indicated by the black arrow -top right).

At pH between 13 and 11, the lowest concentrations not only of chromate but also of sulfate and silicate were observed (Figure 5, top). In this pH region drastic changes in the C-S-H composition occurred, while AFt and AFm phases were stable. The measured minimum in CrO$_4$ concentrations at this pH region was thus consistent with the assumption that AFm and Aft phases are mainly responsible for CrO$_4$ binding. At pH below 11, first chromate and at lower pH values also sulfate concentrations increased as CrO$_4$- and SO$_4$-ettringite started to become unstable. At pH values <10 approx. 95 % of the added CaCrO$_4$ was leached to the pore water. Also the measured concentration of sulfate and silicates concentrations were constantly high. At these low pH values, a small fraction (2.5 %) of the chromate is calculated to be taken up by the gypsum, due to solid solution formation. The residual 2.5 % was probably taken up by Al- and Fe-hydroxides [20, 22].

Discrepancy between modeled and experimental data. While at low pH Cr leaching concentration was controlled by the solid solution formation between $CaCrO_4$ and $CaSO_4 \cdot 2H_2O$, above a pH >10 solid solutions with ettringite represented the limiting phases. Modeled concentrations fitted well for Ca over the entire pH range with decreased concentrations at high pH due to the portlandite formation. Discrepancies existed in the pH range between 11 and 13. Even though the trend of increased Cr leaching concentrations with increasing $CaCrO_4$ doped to the cement correlated well and the influence of solid solution formation was nicely shown, modeled Cr leaching concentrations were about 10 times (one log unit) higher than the measured values (Figure 6). At the same time the SO_4 solubility was underestimated by one log unit. Since ettringite solid solutions determined Cr leaching concentration, the solubility product of CrO_4-ettringite is important and the indicated standard deviation of the published solubility product of $logK = -40.2 \pm 0.4$ [25], caused a difference in Cr concentration in solution of 0.13 log units or 0.15 mmol/l. This was not sufficient to explain the discrepancy and indicates the presence of an additional Cr uptake process which was not considered. An additional CrO_4 uptake mechanism must exist (e.g. solid solution formation with hydrotalcite). Also CrO_4 uptake might occur since a high Ca/Si ratio of the C-S-H and high SO_4 concentrations can lead to significant SO_4 uptake by C-S-H [50]; SO_4/Si ratios of up to 0.03 have been observed. For chromate a similar uptake by C-S-H can be suspected. Bobirica et al. [28] showed that an increase of Na uptake by C-S-H, which (over-)compensated for the negative charge of the silanol surfaces led to an increased CrO_4 uptake by C-S-H. CrO_4 adsorption on C-S-H might therefore play an important role in the CrO_4 binding mechanism and the development of a thermodynamic model to describe chromate uptake by C-S-H would be needed.
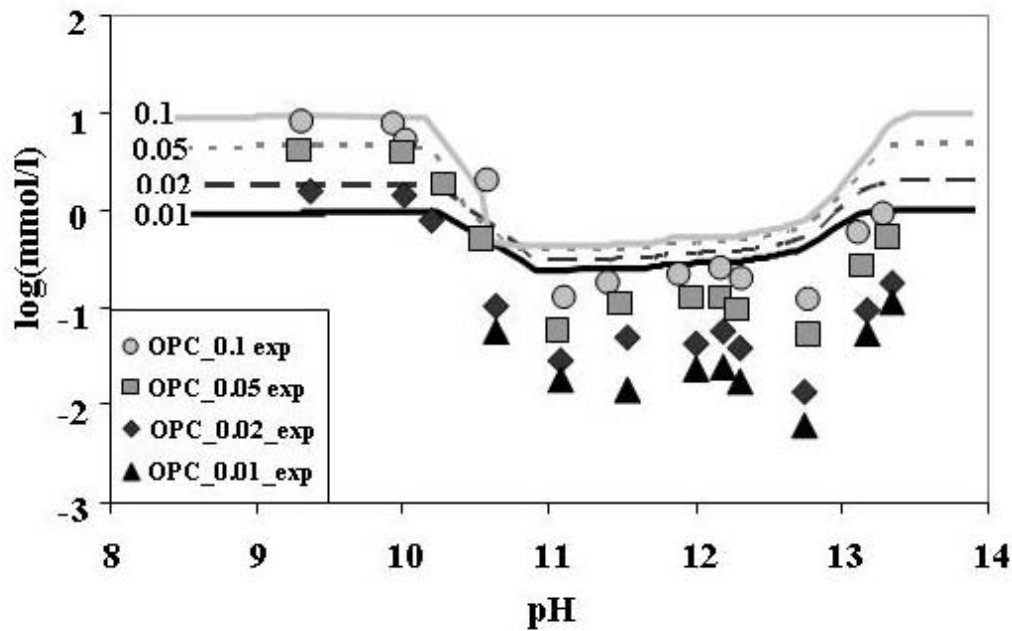
Figure 6 Modeled (lines) and measured (symbols) CrO$_4$ concentrations generally match well. The trend of increased CrO$_4$ concentration in solution with increasing CrO$_4$ doped to the cement in the pH range between 11 and 13 differed from the modeling result.

The pH experiments showed that at low pH values, AFt- and AFm phases were not stable and thus high chromate concentrations were leached. The pH between 11 and 13 is most favorable for chromate binding into ettringite and an additional uptake process. Several authors have identified the same pH interval of 11 and 13 being most favorable for CrO$_4$ uptake resulting in the lowest CrO$_4$ leaching concentrations [15, 18, 20, 22, 51]. However, whether AFm or AFt are the chromate solubility controlling phase is controversially discussed in literature [15, 22]. The thermodynamic calculations indicated that the exact determination of the solubility products of both monochromate and CrO$_4$-ettringite was crucial. If, e.g. the solubility product of monochromate was lowered 1.9 log units from -28.4 ±0.7 [39] to logK = -30.3, corresponding to the solubility product of monochromate as determined by Perkins and Palmer [23], monochromate was more stable than the ettringite solid solutions at lower (<0.1

mol/kg) $CaCrO_4$ concentrations. At higher concentrations, the ettringite solid solution was more stable even using the lower solubility product for monochromate. The same observations were made if the solubility product of CrO_4-ettringite was increased accordingly. Additionally, the trend of increasing Cr concentrations in solution when more $CaCrO_4$ added to the cement was well reflected. Differences in the solubility products of the key hydrated minerals for chromate binding used for modeling may explain the different published results.

4.4   Conclusion

Hydrated OPC can immobilize CrO_4 up to 0.1 mol/kg and modeling results suggest that this is mainly due to the solid-solution formation with ettringite. The model is quite sensitive to the thermodynamic data of ettringite and monochromate and whether CrO_4-ettringite or monochromate are formed depends on the exact values of the solubility products of these phases.

The leaching experiments illustrated the importance of the kind of hydrates present for lowering ion pore water concentrations. In addition to the uptake by ettringite, an additional chromate binding process must take place since measured concentrations were lower than the predicted ones in all samples in the pH range 11 to 13.

With regards to the development of a porewater prediction tool, it will be necessary to understand the discrepancies between porewater measurements and predictions. It may be necessary to explore other possibilities, particularly the role of C-S-H as a sorbent for chromate. Chromate porewater predictions must also be possible for cement-waste mixtures (e.g with fly ash, bottom ash or with residues from chromite ore processing operations) and for other cement types e.g. calcium sulfoaluminate cements which are more sustainable in production and

also have a better ion binding capacity. Another important topic concerns the carbonation of samples. Kinetic information about carbonation of cement-waste mixtures is important for improved release estimations.

Besides the lack of additional thermodynamic data on chromate binding phases there is certainly a need for investigation of other potential contaminant species. Our understanding of binding mechanisms is still qualitative for most potential contaminants. A holistic attitude is crucial and should be promoted.

4.5   Acknowledgements

4.6   References

[1] Johnson, A., Cement stabilization of heavy-metal-containing wastes, in Energy, waste and the environment: a geochemical perspecitve, R. Grieré and P. Stille, Editors. 2004, The Geological Society: London. p. 595-606.

[2] van der Sloot, H.A. and H.A.v.d.S.a.T.G.A. J.J.J.M. Goumans, Systematic Leaching Behaviour of Trace Elements from Construction Materials and Waste Materials, in Studies in Environmental Science. 1991, Elsevier. p. 19-36.

[3] van der Sloot, H.A., Characterization of the leaching behaviour of concrete mortars and of cement-stabilized wastes with different waste loading for long term environmental assessment. Waste Management, 2002. **22**(2): p. 181-186.

[4] Environmental effects of concrete. fib Bulletin. Vol. 23. 2003, Lausanne: Federal Institute of Technology Lausanne (EPFL). 68.

[5]   van der Sloot, H.A., Comparison of the characteristic leaching behavior of cements using standard (EN 196-1) cement mortar and an assessment of their long-term environmental behavior in construction products during service life and recycling. Cement and Concrete Research, 2000. **30**(7): p. 1079-1096.

[6]   van der Sloot, H.A., Quick techniques for evaluating the leaching properties of waste materials: their relation to decisions on utilization and disposal. TrAC Trends in Analytical Chemistry, 1998. **17**(5): p. 298-310.

[7]   Andac, M. and F.P. Glasser, The effect of test conditions on the leaching of stabilised MSWI-fly ash in Portland cement. Waste Management, 1998. **18**(5): p. 309-319.

[8]   Spence, R.D., Chemistry and microstructure of solidified waste forms. 1993, Boca Raton, Florida: Lewis Publishers. 276.

[9]   Matschei, T., B. Lothenbach, and F.P. Glasser, Thermodynamic properties of Portland cement hydrates in the system CaO-Al2O3-SiO2-CaSO4-CaCO3-H2O. Cement and Concrete Research, 2007. **37**(10): p. 1379-1410.

[10]   Lothenbach, B. and F. Winnefeld, Thermodynamic modelling of the hydration of Portland cement. Cement and Concrete Research, 2006. **36**(2): p. 209-226.

[11]   Taylor, H.F.W., Cement Chemistry. Vol. 1. 1997, London: Thomas Telford Publishing. 459.

[12]   Gruskovnjak, A., et al., Hydration mechanisms of super sulphated slag cement. Cement and Concrete Research, 2008. **38**(7): p. 983-992.

[13]   Lothenbach, B., et al., Influence of limestone on the hydration of Portland cements. Cement and Concrete Research, 2008. **38**(6): p. 848-860.

[14]   Duchesne, J. and G. Laforest, Evaluation of the degree of Cr ions immobilization by different binders. Cement and Concrete Research, 2004. **34**(7): p. 1173-1177.

[15]   Chrysochoou, M. and D. Dermatas, Evaluation of ettringite and hydrocalumite formation for heavy metal immobilization: Literature review and experimental study. Journal of Hazardous Materials, 2006. **136**(1): p. 20-33.

[16]   Klemm, W.A., Ettringite and oxyanion-substituted ettringites - their characterization and applications in the fixation of heavy metals: a synthesis of the literature. 1998, Portland Cement Association Skokie, Illinois (USA). p. 68.

[17]   Zhang, M., Incorporation of oxyanionic B, Cr, Mo and Se into hydrocalumite and ettringite: application to cementitous systems, in Earth Science. 2000, University of Waterloo Ontario, Canada. p. 172.

[18]   Palmer, C.D., Precipitates in a Cr(VI)-contaminated concrete. Environ. Sci. Technol., 2000. **34**(19): p. 4185-4192.

[19]   Rose, J., et al., X-ray absorption spectroscopy study of immobilization processes for heavy metals in calcium silicate hydrates: 1. Case of lead. Langmuir, 2000. **16**(25): p. 9900-9906.

[20]   Park, J.-Y., W.-H. Kang, and I. Hwang, Hexavalent chromium uptake and release in cement pastes. Environmental Engineering Science, 2005. **23**(1): p. 133-140.

[21]   Karamalidis, A.K. and E.A. Voudrias, Release of Zn, Ni, Cu, SO_4^{2-} and CrO_4^{2-} as a function of pH from cement-based stabilized/solidified refinery oily sludge and ash from incineration of oily sludge. Journal of Hazardous Materials, 2007. **141**: p. 591-606.

[22]   Engelsen, C.J., et al., Leaching characterisation and geochemical modelling of minor and trace elements released from recycled concrete aggregates. Cement and Concrete Research, 2010. **40**(12): p. 1639-1649.

[23]   Perkins, R.B. and C.D. Palmer, Solubility of chromate hydrocalumite ($3CaO \cdot Al_2O_3 \cdot CaCrO_4 \cdot nH_2O$) 5-75°C. Cement and Concrete Research, 2001. **31**(7): p. 983-992.

[24]   Perkins, R.B. and C.D. Palmer, Solubility of $Ca_6[Al(OH)_6]_2(CrO_4)_3 \cdot 26H_2O$, the chromate analog of ettringite; 5-75°C. Applied Geochemistry, 2000. **15**(8): p. 1203-1218.

[25]   Leisinger, S.M., et al., Solid Solutions between CrO_4- and SO_4-Ettringite $Ca_6(Al(OH)_6)_2[(CrO_4)_x(SO_4)_{1-x}]_3*26 H_2O$. Environmental Science & Technology, 2010. **44**(23): p. 8983-8988.

[26]   Leisinger, S.M., et al., Solid solution between monosulfate and monochromate. Cem. Concr. Res., 2011. **accepted**.

[27]   Park, J.-Y. and B. Batchelor, Prediction of chemical speciation in stabilized/solidified wastes using a general chemical equilibrium model II: Doped waste contaminants in cement porewaters. Cement and Concrete Research, 1999. **29**(1): p. 99-105.

[28]   Bobirica, C., et al., Immobilization mechanisms of chromium in cement-based solidified waste. Environmental Engineering and Management Journal, 2009. **8**(4): p. 759-763.

[29]   Halim, C.E., et al., Implications of the structure of cementitous wastes containing Pb(II), Cd(II), As(V), and Cr(VI) on the leaching of metals. Cement and Concrete Research, 2004. **34**: p. 1093-1102.

[30]   Park, J.-Y. and B. Batchelor, Prediction of chemical speciation in stabilized/solidified wastes using a general chemical equilibrium model Part I. Chemical representation of cementitious binders. Cement and Concrete Research, 1999. **29**(3): p. 361-368.

[31]   Labbez, C., et al., Experimental and theoretical evidence of overcharging of calcium silicate hydrate. Journal of Colloid and Interface Science, 2007. **309**: p. 303-307.

[32]   Bogue, R.H., Calculation of the compounds in Portland cement. Ind. Eng. Chem., 1929. **1**(4): p. 192.

[33]   Barneyback Jr, R.S. and S. Diamond, Expression and analysis of pore fluids from hardened cement pastes and mortars. Cement and Concrete Research, 1981. **11**(2): p. 279-285.

[34]   Longuet, L.B. and A. Zelwer, La phase liquide du ciment hydraté. Revue des mateériaux de costruction. Revue des matériaux de construction, 1973. **676**: p. 35-41.

[35]   Kulik, D.A., U. Berner, and E. Curti, Modelling chemical equilibrium partitioning with the GEMS-PSI code, in PSI Scientific Report. 2003, PSI: Villigen. p. 109-122.

[36]   Hummel, W., et al., Nagra/PSI Chemical Thermodynamic Data Base 01/01. 2002, Parkland, Florida, USA: Universal Publishers/uPUBLISH.com.

[37]   Lothenbach, B., et al., Thermodynamic modelling of the effect of temperature on the hydration and porosity of Portland cement. Cement and Concrete Research, 2008. **38**(1): p. 1-18.

[38]   Leisinger, S.M., et al., Solid solutions between CrO_4- and SO_4-ettringite $Ca_6(Al(OH)_6)_2[(CrO_4)_x(SO_4)_{1-x}]_3*26\ H_2O$. Environ. Sci. Technol., accepted October 2010. **accepted**.

[39]   Leisinger, S.M., et al., Solid solution between monosulfate and monochromate. Cem. Concr. Res., submitted October, 2010.

[40] Kulik, D., J. Tits, and E. Wieland, Aqueous-solid solution model of strontium uptake in C-S-H phases. . Geochim. Cosmochim. Acta, 2007. **71** (12, Supplement 1): p. A530.

[41] Allison, J.D., D.S. Brown, and K.J. Novo-Gradac, MINTEQA2/PRODEFA2, a geochemical assessment model for environmental systems: version 3.0, U.S.E.P. Agency, Editor. 1990.

[42] Waddington, T.C. and H.J.E.a.A.G. Sharpe, Lattice Energies and their Significance in Inorganic Chemistry, in Advances in Inorganic Chemistry. 1959, Academic Press. p. 157-221.

[43] Wang, T. and Z. Li, Some thermodynamic properties of calcium chromate. J. Chem. Eng. Data, 2004. **49**: p. 1300-1302.

[44] Lippmann, F., Phase diagrams depicting aqueous solubility of binary mineral systems. N.JB.Miner.Abh., 1980. **139**(1): p. 1-25.

[45] Kindness, A., A. Macias, and F.P. Glasser, Immobilization of chromium in cement matrices. Waste Management, 1994. **14**(1): p. 3-11.

[46] Laforest, G. and J. Duchesne, Immobilization of chromium (VI) evaluated by binding isotherms for ground granulated blast furnace slag and ordinary Portland cement. Cement and Concrete Research, 2005. **35**(12): p. 2322-2332.

[47] Perkins, R.B. and C.D. Palmer, Solubility of ettringite $(Ca_6[Al(OH)_6]_2(SO_4)_3 \cdot 26H_2O)$ at 5-75°C. Geochimica et Cosmochimica Acta, 1999. **63**(13-14): p. 1969-1980.

[48] Berner, U., Modelling porewater chemistry in hydrated portland cement. Mat. Res. Soc. Symp. Proc., 1987. **84**: p. 319-330.

[49] Berner, U.R., Evolution of pore water chemistry during degradation of cement in a radioactive waste repository environment. Waste Management, 1992. **12**(2-3): p. 201-219.

[50] Barbarulo, R., H. Peycelon, and S. Prene, Experimental study and modelling of sulfate sorption on calcium silicate hydates. Ann. Chim. Sci. Mat. , 2003. **28**((Suppl. 1)): p. 5-10.

[51] Trezza, M.A. and M.F. Ferraiuelo, Hydration study of limestone blended cement in the presence of hazardous wastes containing Cr(VI). Cement and Concrete Research, 2003. **33**(7): p. 1039-1045.

Chapter 5

Conclusion and Outlook

5.1 Conclusion

Research on heavy-metal binding mechanisms in cement-waste mixtures has progressed since the early 1980's, when investigations on cement-stabilized wastes, cements and mortars containing elevated heavy metal concentrations began. Initial research focused on performance and made use of various leaching tests. Greater insight into the complex binding behavior was provided by investigations of heavy metal binding to single cement minerals. The past work has shown that each ion has very individual geochemical properties in cementitous systems. However, it can briefly be generalized that cations either precipitate as hydroxides and/or sorb to cement hydration minerals, especially to C-S-H, due to its high concentration of surface sites. The adsorption of (oxy)anions to cement minerals is generally low due to the competition with hydroxide ions. Precipitation as Ca metallates and/or incorporation into ettringite and monosulfate are reported to be important anion-binding mechanisms. Different binding mechanisms predominate, depending on parameters such as pH, heavy metal concentration, cement type and water:cement ratio (w/c). With an understanding of the binding mechanism and the availability of thermodynamic data, the long-term leaching behavior of waste materials from bulk chemical composition can be predicted. However, the prime challenge is obtaining thermodynamic data. While it is possible to identify and quantify precipitation products, it is difficult to discern between adsorption, surface precipitation and isomorphic substitution (solid solution) on/in cement minerals. Part of the reason is that cement minerals are generally in the submicrometer size range. C-S-H is particularly X-ray amorphous with very small crystalline domains. Hydrated cement minerals are also very sensitive to environmental conditions; e.g. modification in morphology can occur due to a change in humidity, or CO_2 contamination may alter the minerals. The

thermodynamic stabilities of AFm and AFt phases are quite close and an interchange between the two types of minerals is quite easily achieved.

Sorption isotherms determined by wet-chemical experiments can be used to identify binding mechanisms. However, the distinction between solid solution formation and adsorption can be difficult, especially if addition of a particular ion can affect the stability of the mineral phase under examination. This study showed that the use of microscopic and spectroscopic techniques were crucial to the identification of mineral phases. With the combination of techniques including wet-chemical experiments and spectroscopic/microscopic investigations sorption mechanisms in a solid solution-aqueous solution (SSAS) systems can best be identified. The following points should be considered in the experimental design:

I) Equilibration time. The equilibration time of precipitation experiments of solid solutions varied between several weeks and half a year in the case of ettringite and monosulfate solid solutions. In the case of iron-containing AFm-phases and selenate-AFt phases it has been shown that between 1 and 4 years are needed to reach equilibrium. The longer equilibration times are due to high supersaturated solutions in precipitation experiments when initial precipitates need to be rearranged by dissolution and precipitation of new phases to reach equilibrium.

II) Set up of experiments. The question of the number of mixed samples that should be synthesized must be decided separately for each case. Especially in SSAS systems with a possible miscibility gap it is helpful to have a large number of mixed samples with varying mole fractions of exchanged ions in order to be able to determine the limits of the miscibility gaps. The same goes for the end members having identical solubility products. Additionally, the quantity of produced solid phases must be set so that several analysis methods can be carried out.

IV) Solid analysis. The use of XRD analysis has proven to be a practical tool for the characterization of the solid solutions (e.g crystallinity and possible secondary phases can be determined straight forwardly). With specific information of peak shifts in the case of a solid solution and peak splittings in the case of two separate phases instead of one mixed phase, solid solutions could be identified. Distinctions in the unit cell parameters could then support the findings and specific crystal information was determined. Together with thermogravimetric analysis (TGA) and scanning electron microscope (SEM), water content of the samples and information of the morphology was given. The different combined allow a complete characterization of the solid solution phases.

V) Solubility products. Since the end of the 1970's several models have been developed describing solubility calculations of mixed phases. The right choice of the adequate model for calculation is important and the illustration of the solubilities in a Lippman diagram has proved to be a practical tool since both, the solubility of solid phases as well as the composition of the corresponding solution can be shown in one graph.

When modeling the hydration of a cementitious system one must be aware that the model is a very simplified version of reality. During cement hydration a completely new mineral assemblage forms. Clinker phases dissolve, hydrated minerals precipitate and contaminants have the possibility of binding in different ways. In addition it takes more than a year to reach a thermodynamic state close to equilibrium and experiments are usually carried out over a much shorter time span. Thus, predicted mineral assemblages can differ from experimental ones. Another issue is heterogeneity. The cementitous matrix is very inhomogeneous and several processes are taking place in varying locations. This cannot be accounted for by thermodynamic modeling. Another factor that plays an important role is weathering. Stabilized wastes are exposed to a changing

environment leading to carbonation and destabilization of cement minerals due to a lowering of pH. At pH values below 10 hydrated cement minerals such as ettringite and monosulfate become unstable and dissolve. Bound contaminants are released leading to increased porewater concentrations.

The challenges are illustrated by the modeling of CrO_4-doped hydrated ordinary portland cement (OPC) using the thermodynamic data of the AFt and AFm solid-solution systems. My findings agreed with the reported observations that solid solutions with AFt phases contribute to the solubility control of CrO_4 in these systems. However, dissolved concentrations were lower than predicted, indicating that additional processes control CrO_4 solubility. The observed correlation between solid and aqueous-phase concentrations provided a strong indication of either solid-solution formation (e.g. with hydrotalcite) or the adsorption to mineral surfaces, such as C-S-H, the main hydration product. The discrepancy between the model and measurements shows how complex the cementitious system is. Nevertheless, the improvement of the available thermodynamic database of a cementitious system and the continuing development of the geochemical modeling codes provides essential tools for waste management purposes.

5.2 Outlook

The goal of this work was to take a step towards determining porewater composition from knowledge of bulk chemistry. The reported significance of solid solutions for CrO_4 binding was explored and verified. Unfortunately there are few similar investigations to compare these findings with.

With regards to the development of a porewater prediction tool, it will be necessary to understand the discrepancies between porewater measurements and

predictions. It may be necessary to explore other possibilities, particularly the role of C-S-H as a sorbent for chromate. Chromate porewater predictions must also be possible for cement-waste mixtures (e.g with fly ash, bottom ash or with residues from chromite ore processing operations) and for other cement types e.g. calcium sulfoaluminate cements which are more sustainable in production and also have a better ion binding capacity. Another important topic concerns the carbonation of samples. Kinetic information about carbonation of cement-waste mixtures is important for improved release estimations.

Besides the lack of additional thermodynamic data on chromate binding phases there is certainly a need for investigation of other potential contaminant species. Our understanding of binding mechanisms is still qualitative for most potential contaminants. A holistic attitude is crucial and should be promoted. While a potential contaminant may not be mobile, its potential as a resource is not forgotten.

Curriculum Vitae

Sabine Melanie Leisinger (- Schlapbach)

born 17th of April 1977 in Winterthur, Switzerland
married, two children

1984 - 1993	Primary and Secondary School at Zofingen and Strengelbach / AG
1993 - 1997	Gymnasium (Matura Typus C, Science of Nature) at Zofingen / AG
1994 - 1995	Exchange student in McRae High School, Arkansas/USA
1997 - 1999	Sport studies at the ETH
1999 - 2004	Study of Earth Science at the University of Berne in Switzerland, Diploma in Earth Sciences (dipl.geol.)
2001 - 2002	Study of Hydrology and Geophysics at the at the University of Rennes in France
2004 - 2005	Project assistant at Dr. Heinrich Jäckli AG, Geology, Geotechnics and Groundwater
2006 - 2010	PhD Thesis in the Department of Environmental Sciences, Swiss Federal Institute of Technology of Zurich (ETHZ) and in the Department of Water Resources and Drinking Water, Swiss Federal Institute for Aquatic Science and Technology (Eawag)